Universidad de La Frontera

Facultad de Ingeniería y Ciencias

Doctorado en Ciencias de Recursos Naturales

“HYBRID FORWARD OSMOSIS FOR ACID MINE DRAINAGE WASTEWATER TREATMENT AND REUSE”

DOCTORAL THESIS IN FULFILLMENT OF THE REQUIREMENTS FOR THE DEGREE: DOCTOR IN SCIENCES OF NATURAL RESOURCES

ERIK HUGO CABRERA CASTILLO

TEMUCO-CHILE

2020

“Hybrid forward osmosis for acid mine drainage wastewater treatment and reuse.”

Esta tesis fue realizada bajo la supervisión del Dr. Gustavo Ciudad perteneciente al Departamento de Ciencias Químicas y Recursos Naturales de la Universidad de La Frontera y es presentada para su revisión por los miembros de la comisión examinadora.

ERIK HUGO CABRERA CASTILLO

……
Dr. Andrés Quiroz Cortez
Director Programa de Doctorado en Ciencias de Recursos Naturales.

……
Dra. Mónica Rubilar Díaz
Directora Académica de Postgrado
Universidad de La Frontera.

……
Gustavo Ciudad

……
Rodrigo Navia

……
Germán Aroca

……
David Jeison

……
Laura Azocar

……
Christian Antileo

Acknowledgments

The most profound thankfulness goes to my family members, my parents, my sisters and grandparents, for supporting me either in my decision to study overseas and their constant support during my Ph.D. journey. Thanks to Barbara for her company during this rollercoaster ride that has been the doctorate. A special thanks to may two Chilean families, the Soto-Candia´s and Raposo-Mendez´s, for opening your arms and hearts to me. I would also like to thanks my old and new friends I have made in these four years.

Special gratitude goes to my official and non-official Thesis supervisor, Dr. Gustavo Ciudad and Dr. Juan Carlos Ortega, for their confidence, motivation, understanding and constant support.

I also want to thanks my friends and colleagues in the Environmental Institute (IMA) and the Center of Water Management and Technologies (CEGTco).

I would also want to thanks to the members of the evaluation committee Dr. David Jeison, Dra. Laura Azocar, Dr. Rodrigo Navia, Dr. Germán Aroca and Dr. Christian Antileo for their useful comments and suggestions in each Thesis Advance.

Besides, I am grateful to the Scientific and Technological Bioresource Nucleus of the Universidad de La Frontera (BIOREN-UFRO) and to the Center of Waste Management and Bioenergy for their collaboration and assistance in my experimental work.

Finally, the author wishes to express his thanks for the financial support provided by CONICYT/FONDECYT project Nº 3160398, FONDECYT project Nº 1191230 and for the scholarship grant of CONICYT Nº 21160046. The author also thanks the support provided by CRHIAM center (ANID/FONDAP/15130015). In addition, thanks to the Scientific and Technological Bioresource Nucleus of the Universidad de La Frontera (BIOREN-UFRO) for funding my overseas scholarship for English development.

Table of Contents

CHAPTER I:

General Introduction.

Chapter I: General Introduction.

Water is the source of all living creatures on the planet. Unfortunately, this vital natural resource is unequally distributed worldwide. Fresh available water only occupied 0.5% of global water volume, and this percentage is irregularly dispersed all over the planet [1]. Global water use has been tripled over the last 50 years, and with global warming and its related environmental consequences, freshwater sources are being continuously endangered [2]. The growing scarcity of freshwater is driving the implementation of reuse and recycling on an increasingly large scale [3]. Recycling water strategies and technologies will be an essential aspect of future water and environment management policies, ensuring reliable alternative water resources and reducing environmental pollution [2]

Since the industrial revolution, industry development and growth of the human population, high salinity wastewater is being produced every day [4]. Contamination of water bodies and groundwater sources by high concentrated wastewater is an essential factor that affects freshwater availability [5]. Sources of salinized wastewater are numerous, such as seawater and brackish desalination [6], agriculture, pharmaceutical industry, landfills, among others [4]. Otherwise, municipal sewage, oil-gas produced water, mine acid drainage are some of the most saline wastewaters [7].

Acid mine drainage (AMD) is a generated solution from mine tailings, which has a highly acid characteristic, rich in dissolved ferrous, non-ferrous metal sulfates and salts. The final composition of AMD will be highly dependent on the minerals and heavy metals presented in the original geology [8]. The primary responsible agent for AMD is the oxidation of sulfide minerals present in minerals at a natural state such as pyrite (FeS_2), which in contact with atmosphere and water produces sulphuric acid and iron [9]. Due to its high acidity, toxicity (toxic metals), and sulfate compound contents, AMD becomes a major environmental concern in this industry. These characteristics make AMD very dangerous if it reaches water resources or aquatic communities; soil could be severely affected too, damaging the health of plants, humans and wildlife.

In Chile, the mining industry began in 1904 in El Teniente (the largest underground copper mine in the whole world) and soon became the main economic activity in the country [10]. Chilean mining industry represents 55% of the total country exports and about 37% of the

total mined copper in the world [11]. Over the years, in northern Chile, mining operations increased without environmental controls. This resulted in numerous mine-tailing deposits, containing about 50% of the total solid residues generated in mine operations [12]. In the first trimester of 2017, the Chilean mining industry produced approximately 1,191,000 tons [13]. Taking into account that about 50% of the productions go to mine tailings, a considerable AMD volume is produced by the mining industry.

This kind of wastewater tends to have high concentrations of organic and inorganic compounds, making it difficult to treat as conventional treatment methods and technologies have low salt-tolerance and fail to bring good processing results [7]. Membrane desalination technology offers a very promising response to this challenge. A very high effluent quality could be achieved by desalination systems, accomplishing strict discharge regulations. The produced effluents can be reused for industrial applications, irrigation, and even as a source of potable drinking water [14].

Forward osmosis (FO) is an emerging membrane technology for clean water production, which is gaining strength against conventional desalination processes like reverse osmosis (RO) because of its lower water production costs (energy consumption and pre and post-treatment costs) [15]. Opposite to RO, where it is necessary to apply a high pressure to overcome the solution osmotic pressure, FO needs no external pressure, because its driving force is the difference in chemical potential between a concentrated draw and the feed solution [16], meaning there is no need of high hydraulic pressure. The FO technology has been successfully applied to municipal sewage [17–20], mine acid drainage [21] and oil-gas produced water [22]. This wide range of applications demonstrates the versatility of FO as a treatment alternative for organic and inorganic high concentrated wastewaters.

Membrane distillation (MD) is a low-temperature distillation process that involves water evaporation in the pores of a hydrophobic microporous [6]. In this coupled heat and mass transfer process, water vapor circulates through the membrane from a hot feed solution to cold liquid water [23]. Unlike FO, the driving force of MD is the temperature gradient, rather than the concentration gradient [24]. This temperature gradient provokes a vapor pressure difference across the membrane and it is slightly affected by high concentrations of dissolved salts [6]. For these characteristics, MD could be used as a recovery process for high

concentrated FO draw solutions or be used as a single treatment process for high concentrated brines.

The FO−MD configuration is a less explored membrane-based hybrid technology, consisting of in a FO module for extracting clean water from wastewater feed solution and an MD process. The MD section reconcentrates the diluted draw solution for the FO module and at the same time, produces high-purity water from its permeate side. This FO-MD configuration combines the strengths of both processes: high product water quality, low fouling and high draw solution recovery [25].

Although FO and MD have relatively low fouling behavior, membrane fouling is still the main setback of all desalination strategies. Membrane fouling occurs when unwanted particles are absorbed inside membrane pores or adhere to the membrane surface [26]. This particle accumulation affects membrane performance increasingly, reducing filtration fluxes. Either for FO or MD, membrane fouling is a result of several aspects such as operating conditions, hydrodynamics, membrane and fouling agent characteristics, feed solution chemistry, and draw solution properties (for FO) [27]. Managing factors as operating conditions, hydrodynamics and selecting a proper draw solution (for FO) are critical for achieving the best possible system performance.

Both FO and MD are relatively new technologies and scarcely studied. With recent development in membrane materials (less fouling and better fluxes), these technologies are matching and surpassing traditional treatment options as reverse osmosis and full thermal processes in terms of treated water flows and efficiency.

Mineral exploitation consumes high quantities of freshwater, whose sources are groundwater, superficial water bodies and seawater. In Chile, mining activity consumes about 12.5 m^3/s (1,080,000 m^3/day) of freshwater. This enormous water consumption and AMD production exacerbate the water scarcity in northern Chile´s ecosystem and communities, highlighting the need for an efficient way to treat and reuse this wastewater. Membrane technologies like FO and MD have the potential for been used with AMD, and the goal of this research is to confirm this potential.

Some innovative aspects of this research are:

- FO-MD has not been used with acid mine drainage before. This research will be a pioneer in this application.
- In the literature, only a few studies have performed a technical-economic analysis for an FO-MD setup, especially with these two technologies.
- These technologies will help to reduce the increasing wastewater volume produced by the mining industry and will allow reusing the treated water in mining processes.

Hypothesis:

Taking into account these previous considerations:

- Long-time mineral extraction in Chilean territory has been producing high volumes of acid mine drainage for decades, menacing the environment with its high toxicity.
- A considerable freshwater volume is used in the mining industry; therefore, a water recycling system will help to decrease this high demand.
- Forward Osmosis and Membrane distillation are renascent technologies that have shown promising results against high salinity wastewaters.

The following **Hypothesis** was proposed considering the previous statements:

Hybrid Forward Osmosis-Membrane Distillation (FO-MD) setup is a technical-cost effective alternative to reclaim water from acid mine drainage for reusing in mining operations.

Objectives:

In order to evaluate the research hypothesis, a set of **Objectives** were proposed:

General objective

To assess the technical-economical performance of a hybrid FO-MD operation for water recovery from acid mine drainage.

Specific objectives

1. *To evaluate an FO-MD operation for freshwater reclamation from acid mine drainage.*
2. *To address the use of membrane spacers as a strategy for improving flux performance and fouling mitigation.*
3. *To compare an FO-MD and FO-RO plant through a technical-economical assessment for recovering freshwater from acid mine wastewater.*

CHAPTER II:

Forward Osmosis–Membrane Distillation for metal wastewater treatment: An application for acid mine drainage.

Chapter II: Forward Osmosis–Membrane Distillation for metal wastewater treatment: An application for acid mine drainage.

- This chapter presents a section of a submitted research article in the Journal of Membrane Science. Some unpublish results are presented as well in this Chapter.

Abstract

Contamination of water bodies by highly concentrated wastewater affects global freshwater availability, especially in arid zones like northern Chile, where rivers are the main water source. Acid mine drainage (AMD) is a highly acidic wastewater, rich in dissolved metal sulfates and salts, making it very dangerous if it reaches water resources or aquatic communities. A real AMD from a contaminated river in northern Chilean was used in this study. The aim of this work was to show the feasibility of forward osmosis (FO) combined with membrane distillation (MD) as an alternative for treating saline wastewaters, focusing on AMD. Raw AMD was used as FO feed solution and MD was used to concentrate the FO draw solution, a solution of NaCl. Baseline assays were performed with tap-water and AMD at different NaCl concentrations and temperatures to determine the parameter combination that promoted maximum water fluxes. The chosen combination, 1.0 M of NaCl at 60°C, produced a FO flux of 32 LMH with tap-water and 27 LMH with AMD. Three models were used for FO and one model for MD; all of them successfully predicted FO and MD fluxes with a high r coefficient (>0.95). Continuous FO assay was performed with the chosen condition and showed a high initial flux (25 LMH). Nonetheless, continuous flux decay was observed due to membrane fouling, where the fouling cake occupied around 50% of the membrane area due to low wall-shear stress. High ratios of copper and sulfate rejection, of 88% and 96%, were achieved by FO.

***Keywords**: Heavy metal rejection, Flux modeling, Membrane fouling.*

List of abbreviations

AMD	Acid Mine Drainage
CP	Concentration Polarization
DCMD	Direct Contact Membrane Distillation
DS	Draw Solution
ECP	External Concentration Polarization
FO	Forward Osmosis
FS	Feed Solution
ICP	Internal Concentration Polarization
Jw	Membrane water flux (LMH = L*m-2*h-1)
MD	Membrane Distillation
PTFE/PP	Polytetrafluoroethylene and Polypropylene
SEM-EDX	Scanning Electron Microscopy - Energy Dispersive X-ray spectroscopy
TFC	Thin-Film Composite
Δt	Temperature difference
πdraw	Draw solution osmotic pressure
πfeed	Feed solution osmotic pressure

1. Introduction

The mining industry is an essential activity for the Chilean economy, generating around 10% of Chilean gross domestic product [28]. Chile is the number one copper producer in the world, producing around 50% of all the copper used worldwide [29]. Nevertheless, this activity has important associated issues like a large residue generation and a large water demand. Around 50% of the total mining residue production ends in the mine tailing, where the acid mine drainage is generated (AMD) [12]. AMD is highly acidic wastewater, rich in dissolved ferrous and non-ferrous metal sulfates and salts; produced due to the oxidation of mine tailing residues. The principal components in AMD originate from the oxidation of sulfide minerals such as pyrite (FeS_2), which is present in natural state minerals. In contact with the atmosphere and water, pyrite oxidation occurs ($FeS_2 + 7/2\ O_2 + H_2O \rightarrow Fe^{2+} + 2\ SO_4^{2-} + 2\ H^+$) producing sulphuric acid and iron [9]. The AMD mineral composition will be subjected to the residue origin geology (Table 1) [8].

Table 1. Examples of the chemical composition of significant constituents from acid mine drainage.

Location	Iran. [30]	U.S.A. [31]	Romania. [32]	Chile. [33]	Chile. [21]*
Constituents	Concentrations in mg/L, except pH (dimensionless)				
pH	2.0	0.5 – 1	4.4	2.5	3.5
SO_4	>3,000	20–108 $x10^3$	615.6	14,337	6,267
Cu	2,050	120–650	1,012.6	2,298	1,020
Mg	1,310	Not reported	17.3	630.6	436
Ca	100	Not reported	198.6	325.9	313
Al	Not reported	1.4–6.7 $x10^3$	8.5	1,139	293
Mn	740	17–120	1.54	224.5	203
Zn	400	700–2,600	363.4	Not reported	15.3
Fe	3,450	13–19 $x10^3$	11.4	627.5	13.4

* Same AMD as used in our study.

The high water Water consumption by the Chilean mining industry, up to 2.7 million cubic meters in 2018, is intensifying the water scarcity present in northern Chile nowadays [28,34]. This high water demand and the necessity of treating AMD open an opportunity for water reclamation technologies. Forward osmosis (FO) is an emerging membrane technology for clean water production, which is gaining ground against conventional desalination processes like reverse osmosis (RO), because of its ability to face very high concentrated wastewater

[15]. In FO, a feed solution and a highly concentrated solution (draw solution) are separated by a semipermeable membrane. The osmotic difference between both solutions drives water from the feed to the draw solution by the osmosis phenomena [16].

Nevertheless, FO faces a technological barrier, and it is the need to separate the draw solution from the produced water for its reconcentration and recovery. The separation and recovery of the draw solution require an additional processing unit, which can consume energy and still remains a significant challenge for water treatment applications. The FO success will be subject to demonstrated how efficient the draw solute separation process is [35].

Membrane distillation (MD) is a low-temperature distillation process that involves water evaporation in the pores of a hydrophobic microporous membrane. This technology driving force is the vapor pressure difference between a feed and a permeate (freshwater) solution. [6]. Because vapor pressure is only slightly affected by the concentrations of dissolved salts, MD could be used as a successful recovery process for the highly concentrated FO draw solution.

The FO−MD configuration is a hybrid membrane technology consisting of a FO module for extracting clean water from particular wastewater (feed solution) coupled with an MD stage. The MD section reconcentrates the diluted draw solution for the FO module while producing high-purity water on the permeate side. The FO-MD setup combines the strengths of both processes: high product water quality, low fouling and high draw solution recovery [25].

The FO-MD setup has been evaluated in a wide variety of wastewaters: oil industry [36–38], landfill leachate [39], municipal wastewater and urine [40,41], seawater/brackish desalination [42,43] and pharmaceutics industry wastewaters [44]. Nevertheless, this set-up has never been used with an AMD wastewater.

This work aimed to study the feasibility of an FO-MD configuration as an alternative for treating saline wastewaters with an emphasis on water reclamation. The research involved experimental activities for the determination of FO water flux, using real acid mine drainage as feed, and different NaCl solutions as DS.

2. Materials and methods

2.1. Feed and draw solutions

A sample of real AMD was used as FO feed solution. It was obtained from a river located in northern Chile that receives the acid leaching from a nearby copper mine. The AMD was characterized previously by Vital *et al.* (2018) [21] (Table 1). Different concentrations of NaCl as draw solutions were used in FO and MD baseline assays and FO and MD continuous experiments (Tables 2 and 3). All draw solutions were prepared using analytical grade reagents and tap water with a conductivity of 785 µS/cm.

2.2. FO and MD membrane

For the FO process, we used a thin-film composite (TFC) membrane from Porifera Inc. (FOMEM-0415 – Hayward, CA, USA). The water (A_0) and salt (B_0) permeabilities of the membrane are 2.1 L/m^2.h.bar and $1.2 \cdot 10^{-7}$ m/s, respectively. The structural parameter (S_0) was 334 µm, and the zeta potential (ζ) was -13.7 ± 1.9 mV. The structural parameter determines the internal concentration polarization (ICP), and the zeta potential is a measurement of the surface charge of the membrane and impacts the rejection mechanism by electrostatic repulsion [45].

For the MD process, a Hydrophobic Polytetrafluoroethylene and Polypropylene (PTFE/PP) membrane was used in this study. The membrane was provided by Membrane Solutions (2202, No.1759 North Zhongshan Road, Shanghai 200061). Properties of the membrane are thickness 140-190 µm, pore size 1 µm and bubble point in a range of 0.04-0.05 MPa.

2.3. FO and MD setup and experiments

Figure 1 represents the FO and MD setups used in this research. Each consisted of an acrylic module, separated by a FO or MD membrane. In the FO module, the membrane was positioned with the active layer facing the FS Each module had an internal effective membrane area of 33.6 cm^2 with an internal geometry of 86 x 39 x 2 mm (Figure 2). For this study, every FO and MD experiment were performed separately.

No external pressure was applied to any module. FO-feed and MD-permeate solutions were contained in graduated cylinders. Water flux calculation was determined by changes in liquid volume inside the cylinders (Figure 2). A progressive cavity pump (Franklin Electric, Model: 1601007403) was used to circulate the FO-feed, FO-draw, and MD-permeate solutions. The temperature was provided by an electric heater placed in the draw solution.

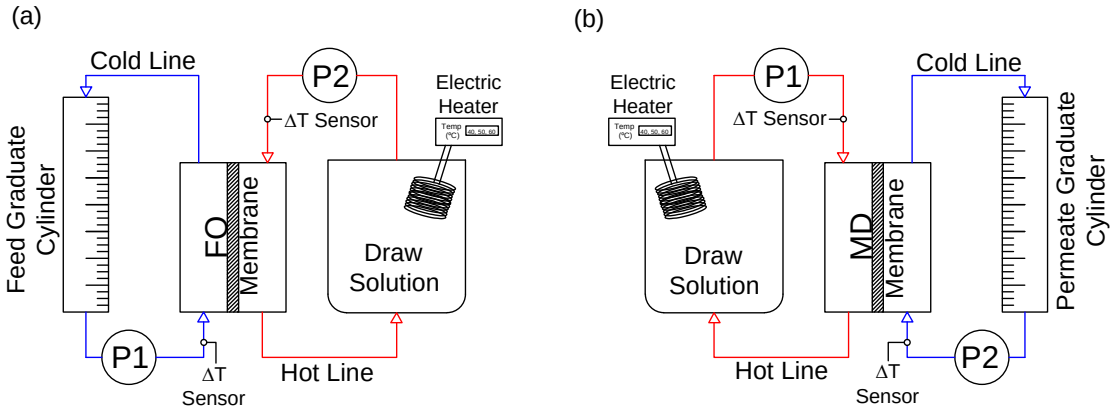

Figure 1. Experimental setup. **(a)** Forward Osmosis and **(b)** Membrane Distillation.

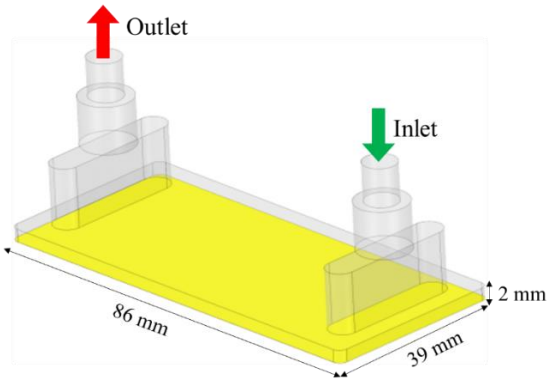

Figure 2. Module internal geometry with the yellow area representing FO and MD membranes.

In order to evaluate the effects of DS temperature and concentration on permeate flux, a series of baseline assays were designed using NaCl solutions of 0.5, 1.0, and 2.0 M at 40, 50, and 60 °C. Baseline assays, FO (Table 2), and MD (Table 3) were designed to achieve maximum water fluxes and to select which combination of DS temperature and concentration will be used in further experiments. The selection criterion was based on choosing the lowest DS temperature and concentration that produced the highest flux. During baseline experiments,

initial FO-feed and MD-permeate volume were 250 mL, and DS volume was 3 L to support a dilution rate less than 5%. All assays were done in triplicate.

For continuous assays (Table 2 and Table 3), the FO-feed volume was 1 L of AMD, and for MD, the feed volume was 0.5 L of tap water. Both assays were performed until 50% recovery was achieved. The DS volume was 12 L to keep the dilution below 5% during continuous running. All assays were done in triplicate.

Table 2. FO experimental design.

Experiment	Feed solution (FS)	T. (°C)	Draw solution (DS)	T. (°C)	Stop Criteria
Baseline	Tap water AMD	20	NaCl [0.5, 1, 2 M]	40, 50, 60	1-hour operation
Continuous	AMD	20-22	NaCl [1 M]	60	50% recovery

Table 3. MD experimental design.

Experiment	Feed solution (FS)	T. (°C)	Permeate (P)	T. (°C)	Stop Criteria
Baseline	NaCl [0.5, 1, 2 M]	40, 50, 60	Tap-water	20-22	1-hour operation
Continuous	NaCl [1 M] with sulfate copper traces	60	Tap-water	20-22	50% recovery

2.4. FO flux modeling

FO water flux was predicted using three theoretical models: Loeb *et al.* (1997) [46], McCutcheon and Elimelech (2006) [47] and Phuntsho *et al.* (2014) [48]. The main difference between Loeb's model [46] and the other two references is the non-inclusion of the effect of external concentration polarization phenomenon, which can produce a significant impact in water flux.

Concentration Polarization (CP) is divided into external and internal concentration polarization, ECP, and ICP, respectively, and both of them are subdivided into concentrative and dilutive, respectively [49,50]. Concentrative ECP and dilutive ICP have the most substantial effects on transmembrane flux. Concentrative ECP occurs as water is transported through the membrane while solutes are retained at the membrane surface, causing an increase in solute fouling on the membrane. The osmotic driving force must overcome the

resulting fouling resistance to bring the water into contact with the membrane [47]. The dilutive ICP effect produces a more severe reduction in water flux in the FO process as water transported from the feed to the draw solution causes dilution of the draw solute within the porous support layer of the membrane. Dilutive ICP causes a considerable reduction in the net osmotic pressure, resulting in a significant reduction in the permeate flux [51].

Loeb *et al.* (1997) [46] estimates water fluxes based on a classic ICP model. McCutcheon and Elimelech (2006) [47] simplified Loeb's model by assuming that salt permeability is negligible, and Phuntsho *et al.* (2014) [48] included the concentrative ECP phenomenon in Loeb's equation.

$$J_{W_{Loeb}} = K_m \ln\left(\frac{A * \pi_{draw} + B}{A * \pi_{feed} + J_W + B}\right) \quad (1)$$

$$J_{W_{Mc\&E}} = A\left[\pi_{draw} * e^{-J_W * K} - \pi_{feed} * e^{J_w/_k}\right] \quad (2)$$

$$J_{W_{\text{Phuntsho}}} = K \ln\left(\frac{A * \pi_{draw} + B}{A * \pi_{feed} * e^{J_W/_k} + J_W + B}\right) \quad (3)$$

Where Jw is the membrane water flux, A is the water permeability coefficient; B is solute permeability coefficient; π_{draw} and π_{feed} are the osmotic pressure of draw and feed solution, and K_m is the mass transfer coefficient.

2.5. MD flux modeling

The water flux during Direct Contact MD is directly related to the difference in water vapor pressure. For distilled water as the permeate flux, MD water flux can be expressed as:

$$J_{w_{MD}} = B_m\left(P^0_{w.f} * \gamma_{w.feed} * x_{w.feed} - P^0_{w.p}\right) \quad (4)$$

Where $P_{w.f}{}^0$ and $P_{w.p}{}^0$ are the vapor pressure of pure water on the feed and permeate sides, respectively, B_m is the membrane permeability parameter, and $\gamma_{w.feed}$, and $\chi_{w.feed}$ are the activity coefficient and the mole fraction of the species [52,53].

The B_m coefficient depends on the features of the membrane and the operating temperature. Various theoretical models have been developed to determine B_m based on the Kinetic Theory of Gases through porous media.

All expression and constants needed for the construction of the MD model and FO models are listed in Appendix Table A1.

2.6. Rejection performance

Rejection performance was determined using copper and sulfate measurement (ions with highest concentration in the AMD sample). Samples were collected at the beginning and end of the continuous assay from the feed and draw solution containers. Concentration of sulfate ions was measured using a spectrophotometer (Hach SulfaVer 4, Method 8051). Copper concentration was measured using the Flame Atomic Absorption Spectrometric Method (Chilean Standard NCh2313/10.Of96).

Membrane removal efficiency for each ion present in the feed solution was calculated using the following expressions:

$$R\ [\%] = \left(1 - \frac{C_p}{C_f}\right) * 100 \qquad (5)$$

Where C_f (mg/L) is the total concentration of ions in the feed solution at the start of the experiment and C_p (mg/L) is the ion concentration of the water that permeates through the membrane to the draw solution. Permeate concentration was determined by:

$$C_p = \frac{C_d * V_d}{V_p} \qquad (6)$$

Where C_d (mg/L) is the ion concentration in the draw solution at the end of the experiment, V_d (L) is the draw solution volume at the end of the assay and V_p (L) is the permeate volume, which is the difference between the initial and final feed solution volumes.

2.7. Membrane fouling-scaling analysis

Sections of the FO membrane were cut off at the end of every continuous assay to measure the fouling layer. The measurement was performed using a SEM-EDX equipment, which provided a semiquantitative analysis of the fouling layer composition and gives an estimate of the foulant ion concentrations

3. Results and discussion

3.1. FO baseline assays and modeling results

Results from FO baseline tests (Figure 3a) show that the increase in water flux is directly linked to the increase of DS concentration and temperature. This behavior is explained by Van't Hoff's equation, which describes a rise in DS osmotic pressure when a higher concentration and/or temperature is used [54]. Nevertheless, when the temperature is increased for a fixed DS concentration, the observed flux is not only explained by Van't Hoff, but also by the Arrhenius equation [55] (Figure 3a). According to the Arrhenius equation [55], a rise in DS temperature produces an increase in DS solute diffusivity. Furthermore, the higher temperature decreases DS viscosity, which reduces the ICP effect and produces an improvement in water flux [56–58].

FO performance using AMD as feed solution was evaluated for only one hour to avoid the formation of critical fouling (Figure 3b). Results show a flux decrease (around 35%) comparing with FO tap-water tests. This flux reduction is related to a smaller osmotic pressure potential between NaCl draw solution and AMD, compared to the osmotic potential between NaCl solution and tap water (Table 3).

Another factor that causes the flux to decline is the concentrative ECP phenomenon. Because AMD is rich in dissolved solids and metal ions, it can cause an accumulation of ions on the active layer of the membrane.

Table 3. Osmotic pressure potential differences, calculated at 20ºC.

Draw solution NaCl (M)	Tap-water $\Delta\pi$ (bar)[1]	AMD $\Delta\pi$ (bar)[2]	$\Delta\pi$ Difference (%)[3]
0.5	22.5	18.8	-16.4
1.0	45.2	41.4	-8.4
2.0	90.5	86.8	-4.1

[1][$\Delta\pi = \pi_{(NaCl)} - \pi_{(Tap\text{-}water)}$], [2][$\Delta\pi = \pi_{(NaCl)} - \pi_{(AMD)}$], [3][$\Delta\pi = (\pi_{(AMD)} / \pi_{(Tap\text{-}water)} - 1) * 100$].

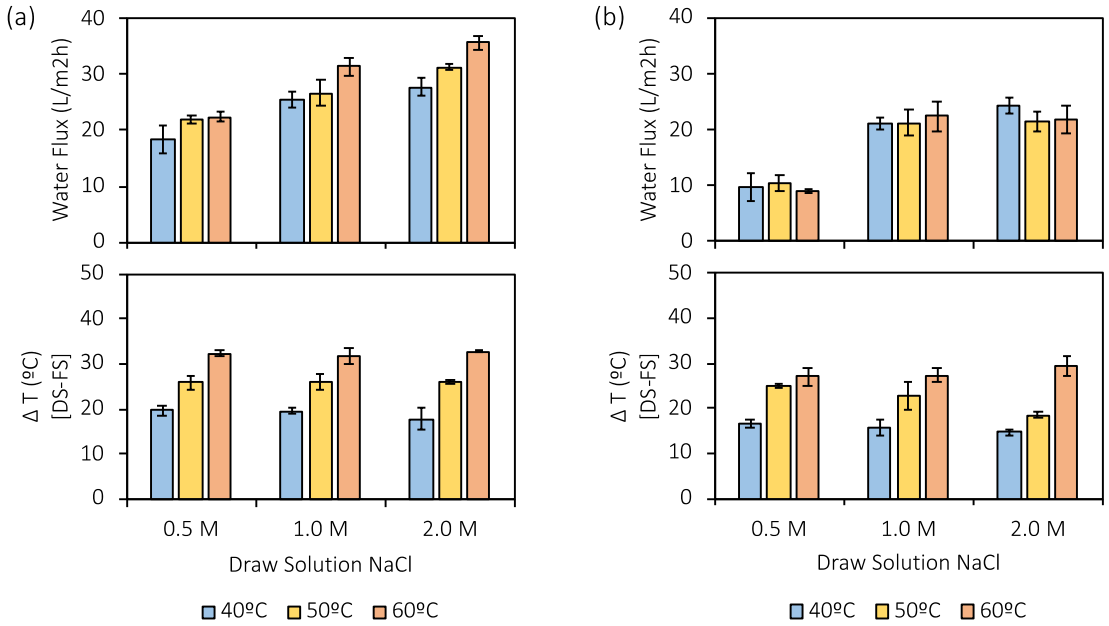

Figure 3. Effect of draw solution concentration on initial water flux (1 hour) during FO operation: **a)** Tap-water baseline test, **b)** AMD baseline test. Error bars represent the standard deviation. Temperatures shown correspond to DS.

Figure 4 shows FO modeling results using Loeb *et al.* (1997) [46], McCutcheon and Elimelech (2006) [47], and Phuntsho *et al.* (2014) [48]. These models were evaluated using tap water as feed and NaCl solution as draw. The modeling considers feed solution at room temperature (22°C) and draw solution at 40, 50, or 60°C. Simulated flux shows good agreement with experimental data (Figure 4d), and no appreciable difference was found between the three models (Figure 4a, b, c). Models were able to predict flux under low ECP when tap water was used. In the absence of a high ECP, the three models had similar results.

Figure 5(a, b, c) showed experimental data and modeling results when AMD was used as feed. With AMD, ECP is expected to play an essential role in system behavior. This was evident in Figure 5d. Models were not able to accurately represent the ECP effect due to AMD complex composition. Model ECP calculation is based on element diffusivities. Nonetheless, when a feed solution is composed of multiple elements, the solution diffusivity coefficient becomes challenging to estimate.

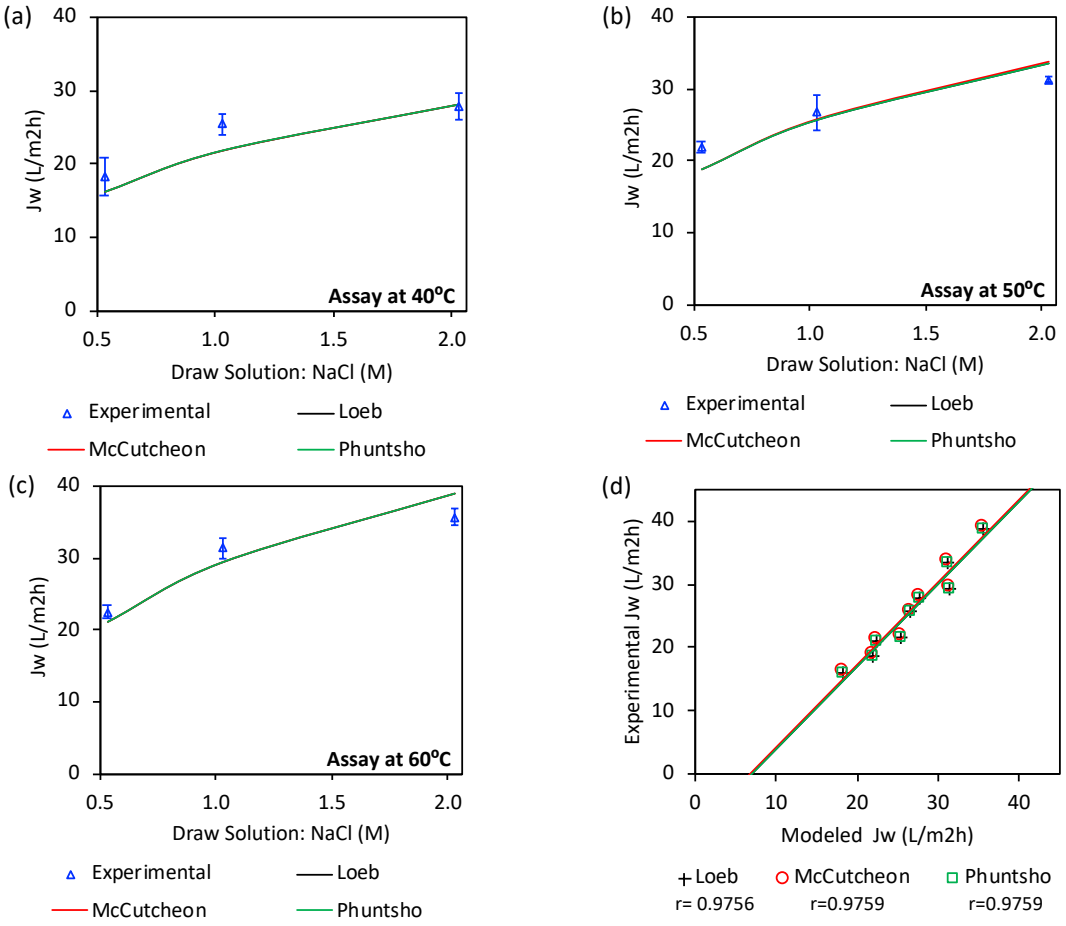

Figure 4. FO water flux modeling results, using tap water as feed and NaCl as draw solution at **a)** 40ºC, **b)** 50ºC, and **c)** 60ºC. **d)** Correlation between experimental Jw and modeled Jw; "r" is Pearson's correlation coefficient. Error bars represent the standard deviation between replicas. All assays were executed for one hour.

An interesting result is the water flux inflection observed at 1.0 M solution of NaCl. Although this behavior is slightly seen in tap-water assays (Figure 5), it is more evident when AMD was used as feed. The observed inflection could be a result of the ECP phenomenon, caused by a high DS concentration (2 M). The higher DS concentration produced a higher flux and a corresponding increase in ECP [47].

Another element that promoted a high ECP was the flow regime inside the module. Module geometry and flow rate used in these assays generated a laminar flow regime inside the cell. As a result of low flow velocity on the membrane surface, a high ECP was able to develop [59].

In Figure 5, there is also appreciable parallelism between Loeb's and the other two models. This different behavior was caused by the non-inclusion of ECP in Loeb's formulation [46]. When tap water was used as feed (Figure 5), a low ECP was developed; this led to overlapping between models. The rich ion composition of AMD generated a high ECP, causing different results between models with and without the inclusion of the ECP phenomenon in their formulation.

The FO model results imply that with the tested conditions it is not possible to performed an accurate water flux prediction behavior when a complex composition feed is used.

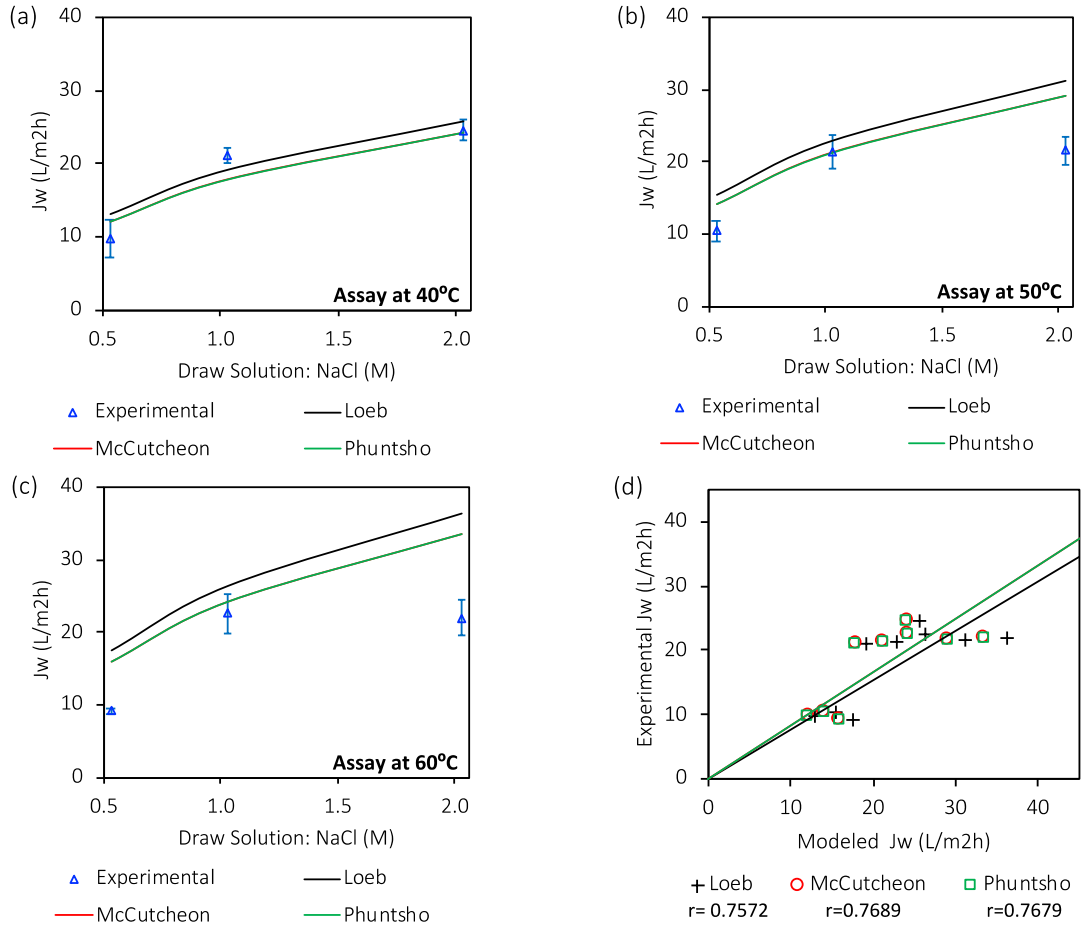

Figure 5. FO water flux modeling results, using AMD as feed and NaCl as draw solution at **a)** 40ºC, **b)** 50ºC, and **c)** 60ºC. **d)** Correlation between experimental Jw and modeled Jw; "r" is Pearson's correlation coefficient. Error bars represent the standard deviation between replicas. All assays were executed for one hour.

3.2. MD baseline assays and modeling results

MD assays were performed using a NaCl solution (FO draw solution) as feed and tap water as permeate (Table 2). Results show a direct relationship between temperature difference (Δt) and membrane flux (Figure 6). As temperature rises, solution vapor pressure increases (Antoine equation), improving the vapor pressure potential, and enhancing the transmembrane flux [60]. Nevertheless, membrane flux decreases when feed concentration rises. This behavior is explained by Raoult's law, where the water vapor pressure is reduced as it becomes more concentrated [60].

MD modeling results are shown in Figure 7a (Equation 4), considering the same conditions as the experimental trials. Overall, the MD model shows a good fit for water flux at different temperatures and feed concentrations. Figure 7b compares measured and predicted flux values, achieving a high correlation coefficient ($r > 0.98$).

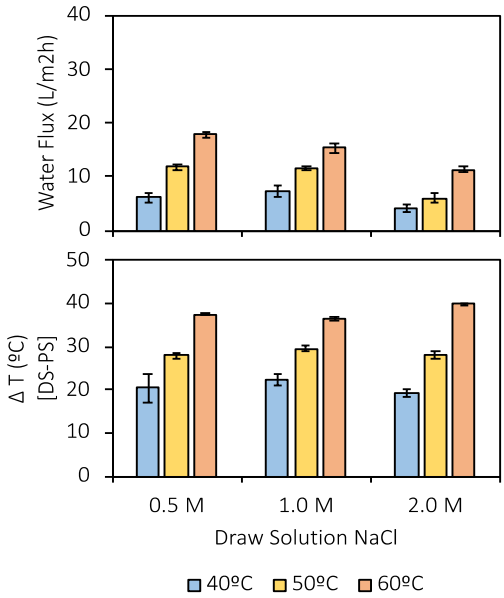

Figure 6. MD experimental results. NaCl as feed solution and tap water as permeate solution. Error bars represent the standard deviation between replicas.

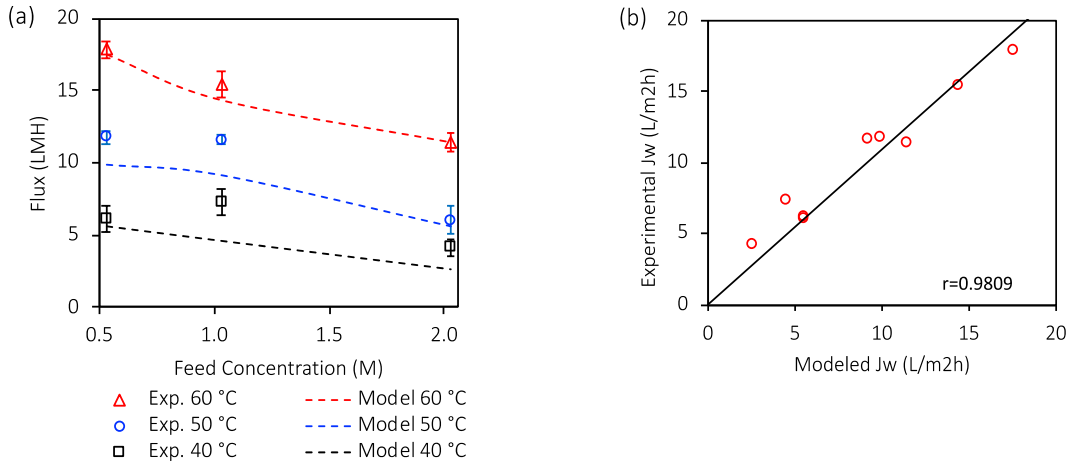

Figure 7. MD water flux modeling comparison. Experimental and modeled data are presented: **a)** MD water flux modeling results, using NaCl as feed solution at 40ºC, 50ºC, and 60ºC. **b)** Correlation between experimental Jw and modeled Jw; "r" is Pearson's correlation coefficient. Error bars represent the standard deviation between replicas. All assays were executed for one hour.

3.3. Continuous FO-AMD assay

Following the results shown in Figure 3b, FO continuous assay was performed using 1.0 M NaCl solution as draw solution at 60°C. The 1.0 M solution was selected since no evident flux improvement was observed when a higher concentration of NaCl was used. The lower FO flux when 2.0 M of NaCl was used could be as a result of the development of a high ECP (Figure 3b). The temperature effect on FO flux was mild. However, it showed a notable effect on MD permeate flux (Figure 4).

The previous selection was validated using a two-way ANOVA analysis (Tukey), which found no significant difference between FO fluxes when using 1.0 M or 2.0 M solutions of NaCl. Besides, the selected condition, 1M NaCl at 60°C, had the lowest significant difference between FO and MD fluxes (ANOVA result). A lower flux difference allows using less membrane area for MD in order to match the FO flux.

A FO continuous assay was performed until a 50% recovery was achieved. Results show an initial flux similar to both baseline and model results (Figure 8a). However, after one hour, a constant decline in flux was observed. This decline could be explained mainly by two phenomena: the decrease of net osmotic potential (between feed side and draw side) and the appearance of membrane fouling. Membrane fouling and osmotic potential reduction caused

a continuous flux decrease until the end of the experiment, reaching up to 64% in total flux reduction.

Throughout the experiment, water permeated from FS through the membrane to the DS, constantly concentrating the feed side while diluting the draw side. The assay was designed to maintain DS below a 5% dilution, so the reduction in osmotic potential was mainly caused by the concentration of the feed solution.

The adverse effects of feed concentration, concentrative ECP, and dilutive ICP on the flux behavior were simulated using the models reported above [46–48] (Figure 8a). Although, FO model's overall correlation coefficient was low (r = 0.77) (Figure 5d), for the chosen operation condition, 1.0 NaCl solution at 60°C, models fitted well with experimental results (Figure 5c).

Loeb's model [46] does not include concentrative ECP, which resulted in a higher flux estimation than the other two models. McCutcheon and Elimelech (2006) [47] and Phuntsho *et al.* (2014) [48] models estimated the initial experimental flux correctly. In this context, it could be assumed that flux reduction observed in the models were results of feed re-concentration and CP.

Overall, the 64% flux reduction observed in the experiment was the result of fouling, feed re-concentration, and CP Models estimated that the effect of feed re-concentration and CP caused around 15% of the overall 64% flux reduction, leaving a 49% impact caused by fouling.

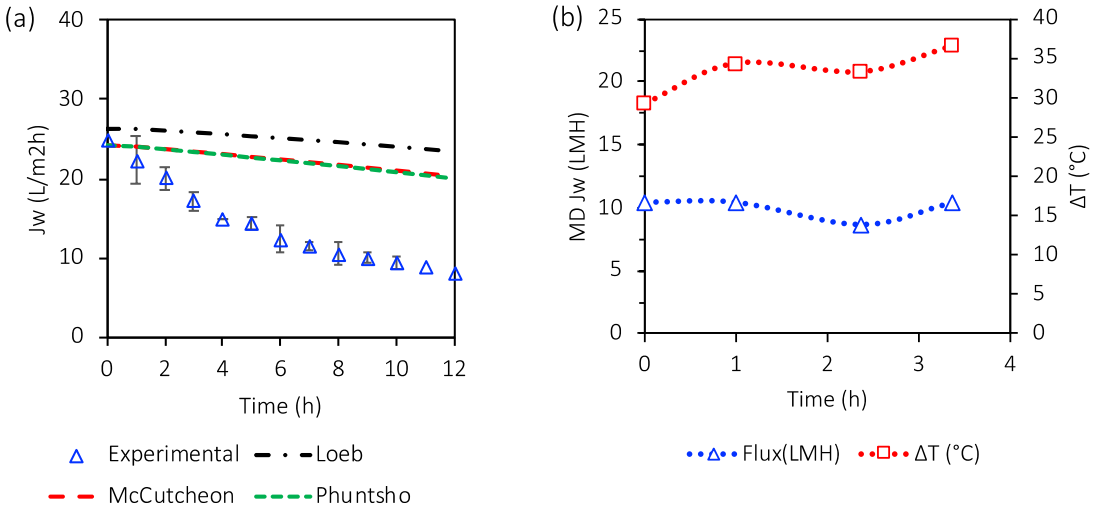

Figure 8. Continuous assay results. **a)** AMD FO assay results using 1.0 M NaCl as draw solution at 60ºC. **b)** MD assay with 1.0 M NaCl as feed. Error bars in the experimental series represent the standard deviation between replicas. Temperatures shown correspond to DS; ΔT in b) is between Draw Solution and Permeate Solution.

An MD continuous assay was performed for three and a half hours (Figure 8b). Results show an initial flux similar to both baseline and model results, around 10.5 LMH. During the experiment's length, the flux was constant at 10.5 LMH, with only a slight decrease at two hours and a half when the flux when around 8.6 LMH. Nevertheless, this decrease was due to a rise in permeate temperature, going from 20 °C to 23°C. The temperature was corrected, and we managed to achieve 10.5 LMH once again.

MD flux behavior was quite different from FO's, where after one hour, we observe a constant flux decline. Because of the operating principle of MD, it was not affected by salt concentration and salt deposition on the membrane. Nonetheless, MD temperatures must be monitored and consistent; otherwise, flux decline will happen.

3.4. Ion rejection analysis

Samples were taken in the feed and draw solutions at the beginning and end of the continuous experiment. The initial concentration of copper and sulfate was 1020 mg/L and 6267 mg/L, respectively. Results show high copper rejection, above 95%, and sulfate rejection of around

88%. The difference between copper and sulfate rejections could be explained by the change of the electric charge (ζ potential) of the membrane due to acid pH.

The zeta potential of the FO membrane is affected by changes in pH. The electric charge of the membrane is usually negative for basic solutions (pH > 7). Nevertheless, as a solution becomes acid, the electric charge moves from negative to an isoelectric point and then to positive [61]. TFC Membranes from Porifera have their isoelectric point around pH=4; for lower pH values, the membrane charge is positive [62,63]. The AMD used in our research had a pH of 3.5, which indicates that our membrane attracted anions from the AMD solution. This affinity with anions could explain the lower sulfate rejection rate of the membrane.

MD systems had shown high flux performance when NaCl and PTFE membrane was used [64–68]. These studies show that MD flux behavior was stable or suffered a slow decline in long-lasting assays. However, other studies have shown high NaCl rejection [64,66] and high rejection of heavy metals and sulfates [69–71] (over 99% for NaCl and sulfate). In our case, preliminary use of FO reduced copper and sulfate levels to 1.6 mg/L and 31 mg/L, respectively. Following the cited studies, our direct contact MD set-up could achieve high permeate quality and high efficiency in draw solution recovery while maintaining a stable flux over time.

3.5. Membrane fouling-scaling analysis

The deposition of foulants on the membrane feed side was observed from the start of the FO assay. This produced a change in membrane coloring, from white to a yellowish-brownish color in those areas with lower than flow velocities. Continuous deposition affected membrane performance by creating a foulant layer that interfered with the normal transmembrane flux. The foulant cake layer covered approximately 50% of the membrane area (Figure 9).

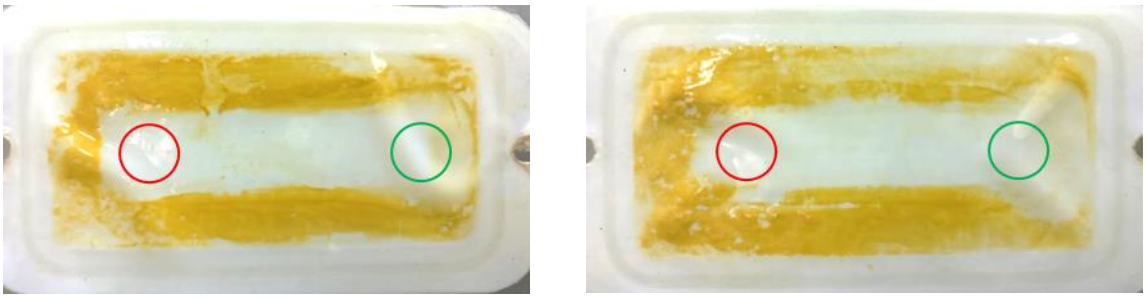

Figure 9. Continuous FO assay membrane after passive washing with water. The green and red circles represent the module inlet and outlet, previously shown in Figure 2.

Vital et al. (2018) [21] studied the fouling and rejection of AMD using the same TFC membrane and draw solution (1.0 M NaCl) as our study. The initial flux was 14 LMH, with a flux decrease of approximately 43% by the end of the experiment (run until 50% recovery). In our research, the initial flux was 25 LMH, with a flux reduction of 64% by the end of the experiment. Flux decay (initial flux minus final flux) between Vital's and this study were numerically similar, 8 and 9 LMH, respectively. Nevertheless, in our study, we achieved a final flux 2.7 times higher than Vital's.

The difference between flux results from Vital´s and our study may be explained by the use of different operation and hydrodynamic conditions. The modules in Vital's set-up had a low flow velocity, and fluids on both sides of the membrane were quasi-static. In contrast, we used crossflow modules where fluid flows continuously with a higher velocity alongside the membrane. This velocity tangential to the membrane created a wall shear stress that improved water flux by reducing ECP effects, which was fully developed in Vital's study. Another significant difference between studies is that Vital et al. (2018) [21] performed every assay at room temperature; while we used the FS at room temperature, but DS was kept at 60°C.

Higher flow velocity and temperature helped to enhance the flux [41] but increased fouling deposition. This high flux, which was 1.8 times higher than reported by Vital´s [21], may have dragged more solutes from feed solution to the membrane surface, causing a high ECP [41]. Since FO modelling estimated a flux reduction around 15% due to re-concentration and CP (Figure 8a), the rest of the observed flux decline could be attributed to the fouling effect.

Figure 9 shows that the module inlet and outlet placement promoted the formation of a linear flow path with high flow velocities (high wall shear stress) between these points. Outside this

flow path, flow velocities were lower, producing a low wall shear stress, which helped the formation of a thick fouling layer. Although fouling cannot be eliminated, its impact could be reduced by improving the hydrodynamic conditions inside the module. Membrane spacers have been used successfully to mitigate fouling by increasing turbulence in the system, which has a self-cleaning effect on the membrane; and also improves mass transfer, producing a significant increase in transmembrane flux [72–74].

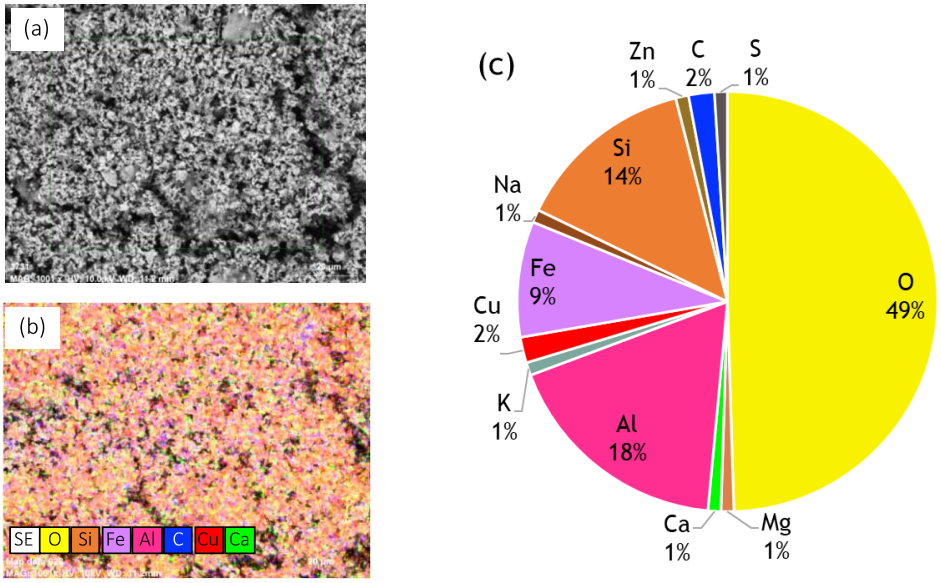

Figure 10. Fouled membrane image from SEM-EDX analysis: **a)** microscope image of membrane surface, **b)** membrane surface image with colored principal elements and **c)** SEM-EDX analysis with every identified ion.

At the end of the long-term experiments, FO membrane sections (Figure 9) were analyzed using SEM-EDX to describe the fouling layer composition. The FO membrane results show a dense layer of foulants on the feed side of the membrane (Figure 10). The thickness of the fouling layer was around 60 µm, comparable with the membrane thickness of 56 µm. This dense layer of precipitates was the main cause of the flux decrease experienced in experimental assays, increasing the ECP effect, and acting as a physical barrier to transmembrane flux.

FO SEM-EDX results indicate a diverse ion composition in the foulant layer (Figure 10a, b), containing all the principal elements present in the AMD sample (**Error! Reference source not found.**1). Nonetheless, copper and sulfate, the ions with the highest concentrations in

AMD, were not found in large quantities in the foulant layer. The FO membrane acted as a successful barrier to these elements, leaving most of its concentration in the concentrated solution. In addition, these results will help decide future cleaning methodologies, focusing on the ions with the highest presence in the fouling layer.

4. Conclusions

This study evaluated the application of FO-MD to a waste stream rich in heavy metals, in this case, AMD. Overall, the results of the study highlighted that:

- As expected, the feed solution temperature (vapor pressure) was the key parameter for achieving high MD fluxes. In the case of FO, the draw solution concentration was the most important parameter.
- Feed solutions with a complex composition, like AMD, present a modeling challenge. The Model inputs did not describe the complex interaction between solution constituents.
- ECP had a significant impact on FO transmembrane flux when ion-rich wastewater (e.g., AMD) was used as feed solution and low wall-shear stress was present.
- Well-distributed wall shear stress throughout the membrane surface is needed to avoid fouling in areas with low flow velocities. Hydrodynamic improvements could be achieved by module redesign or by using membrane spacers.
- Membrane spacers have been used for flow regime enhancement, minimizing the effect of ECP and reducing fouling deposition. The study and design of high-performance membrane spacers will help to ensure the future of FO as an efficient alternative for saline wastewater treatment.

5. Acknowledgments

The authors wish to express their thanks for the financial support provided by CONICYT/FONDECYT project Nº 3160398 and project Nº 1191230, and the scholarship grant of CONICYT Nº 21160046. The authors are grateful for Acid Mine Drainage supplied by CONICYT/FONDAP/15130015

CHAPTER III:

3D printed spacers for fouling mitigation in membrane distillation

Chapter III: 3D printed spacers for fouling mitigation in membrane distillation.

❖ This chapter was published as a research paper in the Journal of Membrane Science. https://doi.org/10.1016/j.memsci.2019.03.040

Abstract

3D printing offers the flexibility to achieve favorable spacer geometrical modification. The role of 3D printed spacers for organic fouling mitigation in direct contact membrane distillation (DCMD) is evaluated. Compared to a commercial spacer, the design of 3D printed triply periodic minimal surfaces spacers (Gyroid and tCLP) - varying filament thickness and smaller hydraulic diameter enhanced DCMD fluxes by 50–65%. The highest DCMD flux was obtained with the 3D tCLP spacer due to its specific geometrical design feature. However, its design characteristics resulted in higher channel pressure drop compared to 3D Gyroid spacer. Moreover, 3D Gyroid spacer exhibited superior fouling mitigation (lower membrane organic mass deposition and reversible membrane hydrophobicity with humic acid solution), attributed to its tortuous design that repelled foulants. 3D Gyroid spacer was effective in achieving high water recovery (85%) while maintaining good quality distillate (10–15 μS/cm, 99% ion rejection) in DCMD with wastewater concentrate that contained high organics, mixed with inorganics. In MD, high organic contents minimally affected MD fluxes but reduced membrane hydrophobicity. Repeated DCMD cycles showed that organic pre-treatment, as well as cleaning-in-place of membrane and spacer, are essential for achieving a high recovery rate while maintaining a stable long-term DCMD operation with wastewater concentrate.

Keywords: *Organic fouling, Membrane distillation, 3D printed spacers, Triply periodic minimal surfaces, wastewater.*

List of abbreviations

CFD	Computational Fluid Dynamics
DCMD	Direct Contact Membrane Distillation
DI	Deionized water
GAC	Granular Activated Carbon
LC-OCD	Liquid Chromatography with Organic Carbon Detection
LMH	$L*m^{-2}*h^{-1}$
LMW	Low Molecular Weight Organics.
MD	Membrane Distillation
MQ	Milli-Q water
PTFE	Polytetrafluoroethylene
RO	Reverse Osmosis
SEM-EDS	Scanning Electron Microscope - Energy-Dispersive Spectroscopy
tCLP	transverse Crossed Layer of Parallel
TDS	Total Dissolved Solids
TOC	Total Organic Carbon
TPMS	Triply Periodic Minimal Surfaces
VCF	Volume Concentration Factor

1. Introduction

Membrane distillation (MD) is a thermal integrated membrane process driven by a vapor pressure gradient across a microporous and hydrophobic membrane [75–77]. As a phase separation process, MD produces high-quality permeate (distillate) with a good recovery due to its insensitivity to osmotic pressure of a highly saline solution [77]. The energy requirement for MD can be met by waste heat from the industry [77]. These factors have led to a focus on the application of MD as an alternative treatment process for wastewater [78], seawater [79] and other saline solutions from the industry [80]. Direct contact MD (DCMD) is the most frequently studied MD configuration due to its simplicity [73,77]. In the DCMD configuration, the hot feed and cold distillate streams are in direct contact with the membrane; thus, heat conduction and temperature polarization are significant factors governing the energy efficiency. Several operational approaches have been explored to reduce the impact of temperature polarization and increase the overall performance of DCMD, such as improving the hydrodynamic conditions at the membrane surface by increasing the circulation flow rate or generating a suction (vacuum) on the distillation side [81,82]. Another noteworthy approach is to improve the design of the membrane spacer. Previous studies have shown that spacers act as static turbulence promoter to enhance the efficiency of transmembrane mass transfer, thereby, increasing permeate fluxes by up to 60% compared to an empty channel [83–86]

1.1. 3D printed spacers for MD.

The effectiveness of spacers is highly dependent on factors such as mesh design, thickness, flow attack angle, and materials. The onset of 3D printing has enabled the fabrication of novel spacers with complex mesh designs, varying thickness and materials without manufacturing restraints. The performance of 3D printed spacers has been previously evaluated in reverse osmosis (RO) and ultrafiltration (UF) processes [87–91]. These studies reported a considerable enhancement in mass transfer with 3D spacers compared to conventional feed spacers. Nevertheless, an invariable trade-off with spacers is pressure drop [90], which increases the energy consumption of the process. Even so, the significant enhancement in water recovery may potentially offset the overall energy consumption. The application of 3D

printed spacers for MD has not been explored in detail thus far. Most studies used computational fluid dynamics (CFD) simulations to evaluate the effect of spacer geometrical parameters such as orientation, filament diameter, and thickness to identify optimal spacers for MD [83,86,92]. For instance, Chang et al. [83] used CFD simulations to study the transmembrane DCMD transfer mechanism using empty and spacer-filled channels. The simulations established the benefits of using spacers in DCMD for enhanced mass flux as well as heat transfer and these enhancement factors depended on both the spacer design as well as the operating parameters such as the Reynolds number. Taamneh and Bataineh [93] used CFD simulations to evaluate the performance of DCMD with thick spacers with varied filament orientation (angle) and reported a positive increase of shear stress and the Nusselt number with spacer filaments oriented at 45° angles to the flow channel. Similarly, based on simulation results, Seo et al. [85] recommended zigzag spacers with symmetric circular designs and relatively high filament numbers as ideal to enhance permeate flux. These simulation studies imply the suitability of 3D spacers for MD application. In another study, Hagedorn et al. [94] highlighted that spacer characteristics such as porosity and spacer and filament thickness attributed to higher hydraulic diameter, which contributed towards turbulence (higher Reynold number) in DCMD. This factor is especially relevant for 3D printed spacers, as they can be fabricated at varied filament and spacer thickness. Thomas et al. [73] analyzed the performance of MD with 3D printed spacers and reported on enhanced permeate flux and overall heat transfer coefficient by up to 60% compared to commercial spacers. The performance enhancement was attributed to the significantly higher turbulence induced by the maze-like interpenetrating design characteristics of triply periodic minimal surfaces (TPMS) used as the spacer topologies.

1.2. Potential of 3D printed spacers for fouling mitigation in MD.

Apart from flux enhancement, spacer design can influence fouling and channel pressure drop in membrane processes. The presence of spacers enhances flow turbulence, which improves the mixing of the solution close to the membrane surface with the bulk solution, preventing the foulant layer build-up on the membrane surface [95,96]. A number of RO studies have established that spacer characteristics such as larger mesh size with varying/irregular filament thickness play a significant role in maintaining reasonable pressure drop, while

creating high shear stress at the membrane surface, which is essential to avoid polarization and fouling issues [89,97,98]. These studies demonstrated the potential for fouling reduction using spacers with specific characteristics. 3D spacers can potentially meet such characteristics, given that the technology has the flexibility to fabricate spacers with complex features.

Organic fouling development in MD was systematically evaluated by a number of studies [99–101]. The severity of fouling in an MD process appears to be significantly lower compared to pressure based membrane processes such as RO [75]. Nevertheless, the long-term operation can still lead to the accumulation of deposits on the membrane surface and pores, causing a decline of membrane permeability and it is a challenge to reverse fouled MD membrane even with chemical cleaning [76]. Further, the gradual membrane surface hydrophobicity reduction due to organic foulants deposition increases its susceptibility to wetting [76,100]. This is especially relevant when MD is used to treat wastewater that contains a significant amount of organics [78,102]. For instance, Wu et al. [102] reported significant membrane wetting when DCMD was used for fermented wastewater with high organic concentrations. Naidu et al. [78] demonstrated the potential of DCMD for wastewater RO concentrate treatment. However, they also showed that the deposition of low molecular weight organics onto the membrane, due to the breakdown of humics at elevated temperature, resulted in a considerable reduction in the membrane hydrophobicity [78]. The presence of spacers may potentially reduce fouling deposition onto the MD membrane. While Thomas et al. [73] indicated that 3D spacers show significant promise for treating brine solutions with high scaling tendency, a detailed evaluation of the implication of 3D spacers on fouling development in MD is still lacking. This study intends to bridge this gap.

Hence, this study aims to evaluate the role of 3D printed spacers (for simplicity referred to as 3D spacers hereafter) in improving the overall performance and mitigating fouling development in DCMD. The influence of 3D spacer-filled channels for enhancing DCMD permeate flux, energy efficiency, as well as the implication on pressure drop, were evaluated. Specifically, in-depth analysis of organic fouling tendency in the presence of 3D spacers in DCMD used to treat wastewater RO concentrate up to high recovery rates (80–85% water

recovery) was carried out. Factors such as accumulation of foulants onto the spacers and fouling reversibility with cleaning were also evaluated in detail.

This chapter was designed to address some serious performance issues from the previous chapter, concerning high fouling deposition on the FO membrane and a low flux performance in the MD stage. Even though this chapter was applied in an MD system, the hydrodynamic improvement and fouling mitigation capabilities of using spacers are regardless of the type of membrane used, meaning that if applied on an FO membrane, the same overall improvement can be expected.

2. Methodology

2.1. Membrane, chemicals, and feed solutions

A commercial polytetrafluoroethylene (PTFE) hydrophobic flat-sheet membrane (General Electric, US) with nominal pore size, porosity, and membrane thickness of 0.22 μm, 70–80% and 179 μm, respectively [78] and total effective area of 40 cm^2 was used for all DCMD experiments.

DI water was used as a feed solution in the baseline tests. Baseline tests were conducted to evaluate the performance of DCMD with empty and spacer-filled channels at varied feed temperatures and flow velocities. The influence of spacers on organic fouling development in DCMD was tested using model humic solution as well as actual wastewater RO concentrate. The latter was obtained from a water reclamation plant of Sydney Olympic Park Authorities. Key characteristics of this wastewater RO concentrate are summarized in Table 1. A model humic solution at a concentration of 20.3 ± 0.7 mg/L was used to represent only the organic contents of the actual wastewater RO concentrate (Table 1) without any inorganic salts. The actual wastewater RO concentrate was used in this study to represent wastewater with both organic contents as well as inorganic salts.

Table 1: Characteristics of wastewater RO concentrate obtained from Sydney Olympic Park water reclamation plant [78].

Parameter	Value	Parameter	Value

Total dissolved solids (TDS)	1500.3 ± 1.4 mg/L
Turbidity	0.2 ± 0.1 NTU
pH	8.0 ± 0.3
Dissolved organic carbon	20.3 ± 0.7 mg/L
Ca	97.0 ± 2.3 mg/L
Mg	69.0 ± 1.6 mg/L
Na	448.5 ± 3.2 mg/L
K	66.9 ± 4.1 mg/L
SO4	184.4 ± 5.7 mg/L
Cl	611.4 ± 3.3 mg/L
Hardness as CaCO3	429.7 ± 6.1 mg/L

Humic acid (Sigma-Aldrich, USA) and citric acid (Sigma-Aldrich, reagent grade) were used to prepare the model feed solution and chemical cleaning solution, respectively. The model humic acid solution was prepared by mixing 500 mg/L humic acid powder in deionized (DI) water with continuous stirring for 24 h. The pH of the final solution was not adjusted to ensure that the natural organic characteristics are unaltered. The humic acid stock solution was filtered (0.45 μm Millipore filter) to remove suspended solids and thereafter, stored at 4 °C.

Furthermore, to critically determine the impact of organic contents in a mixed constituent, a condition of reduced organics with actual wastewater RO concentrate was used in this study. To achieve this condition, granular activated carbon (GAC) (from James Cumming & Sons Pty Ltd, MDW4050CB, particle size range 430–600 μm) was mixed (120 rpm) at 5.0 ± 0.2 g/L with wastewater RO concentrate (24 h) to adsorb the organic contents, following the approach of our previous work [78]. Upon batch adsorption, the wastewater RO concentrate was filtered (0.45 μm millipore filter) to exclude suspended solids. The batch absorption using GAC significantly reduced the organic contents in actual wastewater RO concentrate to less than 2 mg/L while maintaining the inorganic salt contents.

2.2. Spacers

In this study, one commercial spacer and two types of 3D spacers were used. The commercial polypropylene spacer (FILMTEC™) was diamond-shaped (45° filament angle) with porosity and thickness of 0.85 and 0.79 mm, respectively. The 3D spacers were designed based on TPMS resulting in a sheet-based transverse Crossed Layer of Parallel (tCLP) spacer and a skeletal-based Gyroid spacer. More details about TPMS shapes and their governing mathematical equations can be found elsewhere [73,90]. The designs were modeled using computerized design software and then 3D printed by selective laser sintering technique. The unit cell representation of the selected TPMS spacer designs is presented in Fig. 1. The 3D tCLP spacer design consists of protrusions that create microchannels aligned perpendicular to the feed flow direction. This design feature was considered to create maximum flow disruption and resultantly increased turbulence. The specifications of the 3D spacers and their images are presented in Table 2 and Fig. 2, respectively. The adaptation of TPMS is especially beneficial in minimizing the contact area between the membrane and spacer, which is essential to avoid flow restrictions and flow dead zones formation [88].

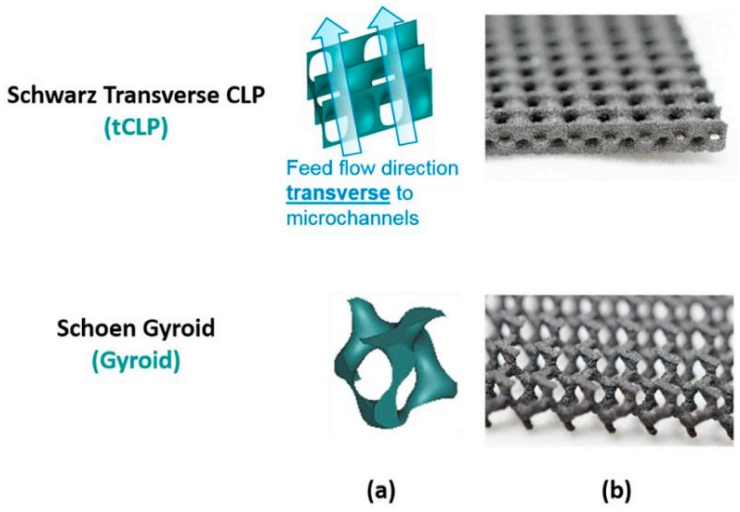

Figure 1. 3D printed TPMS spacer design features presented as **(a)** representative volume element, and **(b)** photographic images (profile view).

Table 2: Characteristics of 3D printed spacers.

Structure design	Surface Area (mm^2)	Volume (mm^3)	Voidage (%)	Hydraulic Diameter (mm)
tCLP	14786	1067	88	1.2

Gyroid	10709	1471	84	1.4

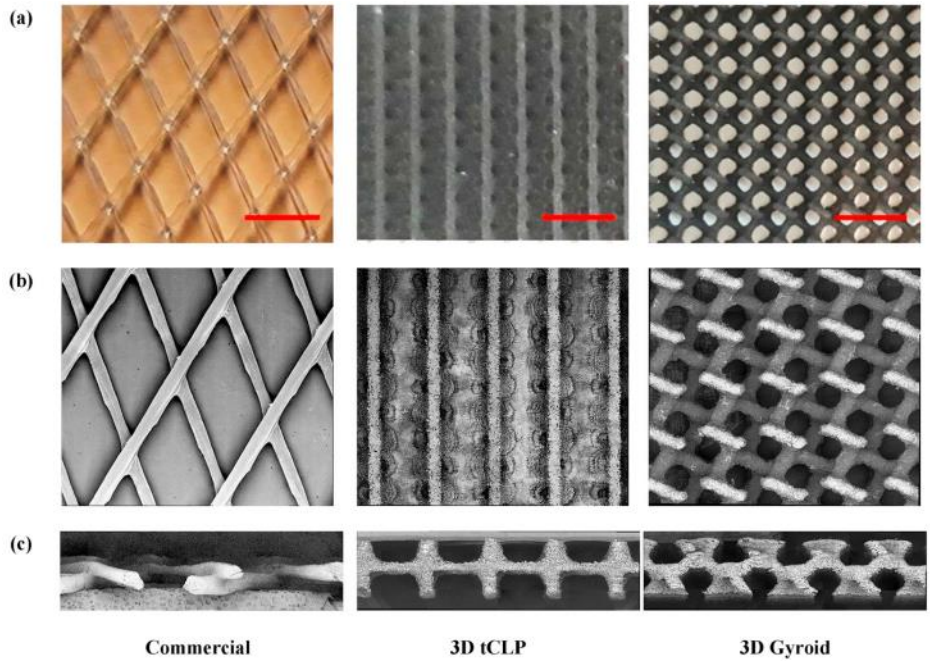

Figure 2. Commercial spacer and 3D printed spacers (tCLP and Gyroid) **(a)** photographic images (image scale bar = 0.5 cm) **(b)** SEM image (top view) **(c)** SEM image (cross section).

2.3. Direct contact membrane distillation (DCMD)

The spacer performance was evaluated in a closed-looped bench scale DCMD system containing an acrylic membrane module (Fig. 3). The module length and width were 8.10 cm × 5.10 cm, respectively, with a channel depth of 0.23 cm. Gear pumps (Cole-Parmer, model 75211-15, United States) were used to direct both the permeate (deionized (DI) water) and feed solution into the membrane channel in countercurrent flow at velocity (v_f and v_p) ranges of 0.1–0.3 m/s. Pressure variation at the feed inlet and outlet were recorded using pressure gauges placed at the feed inlet and outlet channel. A jacketed feed vessel coupled with a heating system was used to vary the feed solution temperature (T_f) from 45.0 ± 2.0 °C to 65.0 ± 2.0 °C while the permeate solution temperature (T_p) was maintained at 22.0 ± 2.0 °C for all experiments. Temperatures at the inlet and outlet of the feed and permeate flow channels close to the membrane module was recorded using temperature sensors. The average feed and permeate membrane surface temperature profiles were obtained through these values. Heat losses on the feed side were determined based on the

feed inlet to outlet temperature difference and as a function of the feed flow rate and constants (specific heat capacity = 4.2 kJ/kg*K; water density = 1000 kg/m^3).

The permeate flux obtained across the active membrane area and latent heat of vaporization (2345.5 kJ/kg) was used to determine the latent heat transferred. The system energy efficiency was calculated based on the latent heat transferred over the heat losses at the feed side. The MD module was thermally isolated using expanded polystyrene (EPS) to prevent heat losses that could affect the energy efficiency measurements.

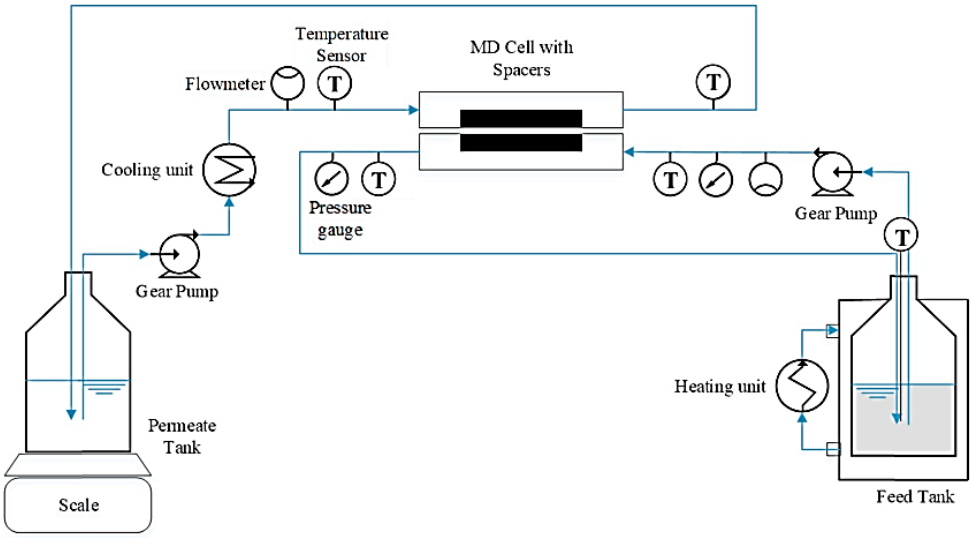

Figure 3. DCMD experimental setup.

DCMD experiments were carried out until 85% water recovery, equivalent to a reduction of the initial feed volume from 1.7 L to approximately 0.25 L or up to the point of significant permeate flux decline. An electronic balance was used for recording the weight changes in the permeate tank throughout the operation duration. The permeate flux computed as the ratio of permeate volume (L) increment over operation duration (h) and unit membrane area (m^2) was reported as L*m^{-2}*h^{-1} (LMH). The permeate flux was represented as a function of the water recovery rate as well as volume concentration factor (VCF). The VCF (defined as the ratio of initial to final feed solution volume) indicates the extent of feed solution volume reduction achieved by DCMD.

DCMD with empty and spacer-filled channels were carried out with a number of feed solutions from DI water for baseline evaluations followed by model humic solution as well

as wastewater RO concentrate for detailed analysis on the influence of spacers on fouling phenomena. The same spacer design was used in both the feed and permeate channels for each DCMD experiment with the spacer-filled channels.

The overall salt removal efficiency of DCMD was determined by measuring the conductivity and pH value of the feed and permeate solution before and after DCMD operation, using a portable multimeter (HQ40d, HACH, US). Inductively coupled plasma-mass spectrometry (ICP-MS, Agilent 7900, US) was used to measure the concentration of each individual cation in the wastewater RO concentrate. For organic removal efficiency, the initial and final permeate and feed solutions (humic acid concentrations and wastewater RO concentrate) upon DCMD operation were analyzed by a total organic carbon (TOC) analyzer (Analytik Jena multi N/C® 3100)

2.4. Fouling reversibility with membrane cleaning

2.4.1. Batch membrane cleaning

The effectiveness of cleaning the membrane as an approach to reverse membrane fouling was evaluated using DI water as well as a chemical solution (0.1% citric acid). For this reason, small portions of the used membranes were places in falcon tubes with 20 ml of cleaning solution. The falcon tubes were stirred in a flat shaker at 120 rpm for 24 h. Upon air drying, the membrane contact angle was analyzed.

2.4.2. Cleaning-in-place

Cleaning-in-place (cleaning the membrane and spacer while in the module) was carried out to emulate membrane maintenance and fouling mitigation in an actual operational scenario, upon wastewater RO concentrate treatment. Cleaning-in-place was carried out with water cleaning (flushing 300 ml of DI water through membrane module using the same operating flow velocity, 0.13 m/s) as well and chemical cleaning (0.1% citric acid with water flushing). Acid cleaning was carried out by recirculating acid (20 min at a low flow velocity of 0.08 m/s to achieve sufficient contact time with the membrane) followed by water flushing (to neutralize the acid residues) (200 ml at 0.13 m/s). Cleaning-in-place is pertinent to establish the reuse capacity of both the membrane as well as the 3D spacer.

2.5. Characterization techniques

2.5.1. Organic characterization

Organic characterization of the feed and permeate solution, as well as membrane foulant, was established using liquid chromatography with organic carbon detection (LC-OCD) [78,103]. To evaluate the organic deposits on the MD membrane, the foulant residues were extracted from the membrane into MQ water based on the procedure of our previous studies [78,100]

2.5.2. Membrane characterization

Changes in membrane characteristics before and after the DCMD experiments were evaluated in terms of surface hydrophobicity and morphology. Membrane surface hydrophobicity was measured using contact angle. Contact angle measurement was carried out at the end of each experiment (upon drying the used membrane) together with a virgin membrane as a control measure for the instrument setting. The contact angle measurements were conducted using a water droplet goniometer (Theta Lite). Further, the surface morphology and element contents of the membranes (virgin and used upon DCMD experiments) were examined using a scanning electron microscope (SEM) integrated with energy-dispersive spectroscopy (EDS) as described in a previous study [78].

3. Results and discussion

3.1. Baseline study

The DCMD performance with and without spacer-filled channels was evaluated. For the baseline study, DI water was used as the feed and permeate solution.

3.1.1. Permeate flux performance

In an empty channel (i.e., no spacer condition), increasing the bulk feed temperature from 45 to 65 °C (at a fixed flow velocity of 0.08 m/s) enhanced the permeate flux by 200% from 7.68 ± 0.92 LMH to 24.26 ± 1.45 LMH (Fig. 4a). In this study, temperature losses at the membrane feed side were evaluated by measuring the temperature difference at the channel inlet and outlet (Section 2). With the increase of bulk feed temperature, a higher feed temperature loss was observed due to the large quantity of heat required for vaporizing liquid

at the feed side of the membrane surface [82]. As a result of the temperature loss, only minimal energy efficiency increment was achieved with the increase of permeate flux (Fig. 4a).

Meanwhile, at similar operating condition (feed temperature of 55 °C and flow velocity of 0.08 m/s), the permeate flux increased significantly by 63% (20.78 ± 1.24 LMH) with commercial spacer-filled channel, and by more than 200% (30.62 ± 1.36 LMH to 36.06 ± 1.09 LMH) with 3D printed spacers as compared to that with empty-channel (12.67 ± 1.87 LMH) (Fig. 4b). More importantly, the scenario of increasing the feed temperature to achieve higher permeate flux invariably resulted in higher feed temperature losses, which compromised the energy efficiency. The approach of spacer-filled channels was especially favorable in achieving both higher permeate fluxes and energy efficiency.

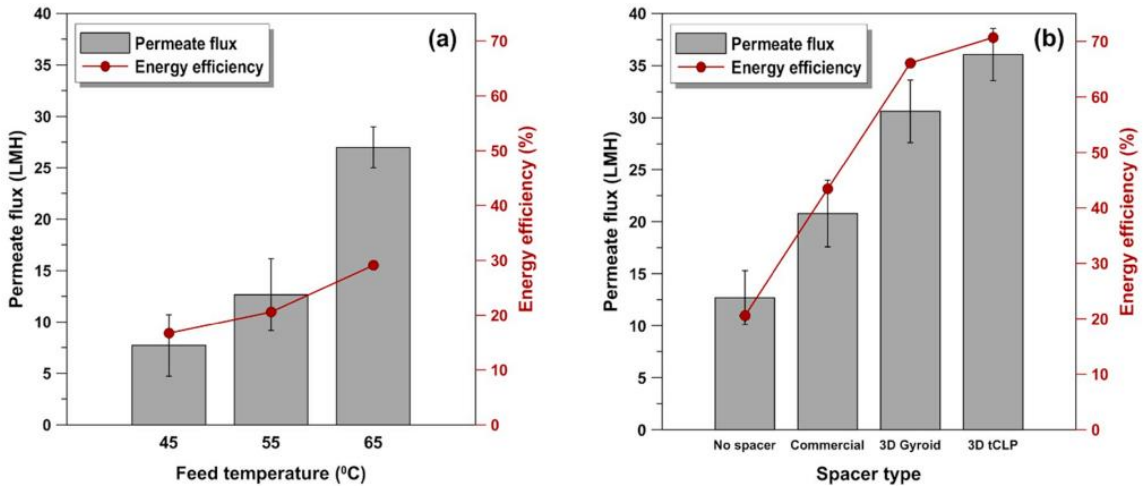

Figure 4. Baseline performance of DCMD with **(a)** empty channel at Tf of 45.0 ± 2.0 to 65.0 ± 2.0 °C **(b)** empty and spacer-filled channels at Tf of 55.0 ± 2.0 °C (vf, vp = 0.08 m/s; Tp = 22.0 ± 1.5 °C)

Upon comparing the performance of DCMD with different spacers, the 3D spacer-filled channels achieved 30–70% higher permeate fluxes compared to commercial spacer-filled channels under similar operating conditions (Fig. 5a). This could be attributed to the smaller hydraulic diameter of the 3D spacers (Table 2) and the channels/protrusions aligned perpendicular to the feed flow, such as in 3D tCLP spacer. A smaller hydraulic diameter increases the flow velocity and Reynolds number. This, in turn, increases turbulence,

resulting in higher mass transfer. Amongst the 3D spacers, tCLP achieved 15–24% higher permeate fluxes compared to that with the Gyroid spacer.

3.1.2. Channel pressure drop

Pressure drop is an inevitable trade-off associated with spacer application. The results of this study showed a trend of channel pressure drop increment in the ranges of 0.02–0.07 bar/m up to 0.13–0.25 bar/m as the flow velocity was increased (represented by Reynolds number) for both empty and spacer filled channels (Fig. 5b). The same trend of increasing pressure drop with flow velocity and Reynolds number was reported in previous MD studies [93,94]. For instance, a previous MD study [94] showed that pressure drop in spacers could range from as low as 0.008 bar/m to over 1.0 bar/m depending on the flow velocity as well as spacer characteristics. A 48–200% increment in channel pressure drop was observed with spacer-filled channels compared to an empty channel. Higher drag force in the presence of spacers is associated with the higher channel pressure drop [85,93,94]. This apart, spacer characteristics such as spacer hydraulic-diameter also influences the degree of channel pressure drop. Hagedorn et al. [94] demonstrated the inverse correlation of channel pressure drop and spacer hydraulic-diameter, in which, reduced flow velocity associated with higher hydraulic-diameter of the spacer resulted in lower channel pressure drop. Likewise, in this study, the channel pressure-drop with the Gyroid spacer (hydraulic diameter of 1.6 mm) was lower compared to the tCLP spacer (hydraulic diameter of 1.4 mm). In addition to the hydraulic diameter, another spacer characteristic that influences the feed channel pressure drop is the flow attack angle [104]. The flow attack angle of the spacer is the angle formed between the spacer strands and the fluid flow direction. In the tCLP design, the microchannels of the spacer are aligned perpendicular to the flow direction creating maximum disruption to the approaching fluid. However, with increasing flow attack angle, the pressure drop also increases. This explains the higher permeate flux and pressure drop observed with the tCLP spacer. Thus, based on the combined effects of flux enhancement and channel pressure drop, the Gyroid spacer demonstrated an overall improved performance over the commercial spacer.

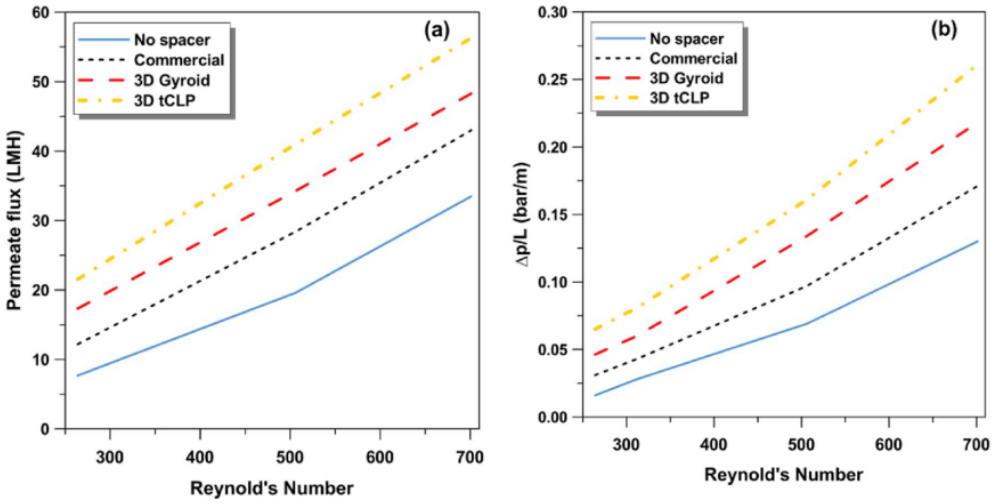

Figure 5. Performance of empty and spacer-filled channel at varying flow velocities based on **(a)** permeate flux **(b)** channel pressure drop (figure trend line derived from experimental data from Table S1).

3.2. Influence of spacer design on organic fouling mitigation

The baseline results established that the incorporation of spacers in DCMD enabled an improvement in permeate flux by maintaining a low temperature polarization. The results also highlighted that at increased flow velocity, a higher permeate flux was achieved. However, at increased flow velocity, a trade-off of channel pressure drop is inevitable, especially in the presence of spacers. Based on all these factors, a DCMD operational setting of 55 °C feed temperature and 0.13 m/s flow velocity was decided upon for the subsequent tests to evaluate the influence of spacers on organic fouling development.

3.2.1. Process performance

DCMD tests were conducted for empty and spacer-filled channels using organic (humic acid) feed solution. Permeate flux results were compared in terms of the normalized flux (J/Jo). The obtained initial permeate fluxes (Jo) of 20.2 ± 2.3 LMH (empty channel), 27.1 ± 1.7 LMH (commercial spacer-filled channel), 37.5 ± 1.3 LMH (3D Gyroid spacer-filled channel) and 44.2 ± 2.4 LMH (3D tCLP spacer-filled channel) were in line with the baseline permeate flux results discussed earlier.

For both empty and spacer-filled channels, the flux performance was relatively consistent over the majority of the experiment duration followed by a marginal decline towards the end of the experiment (Fig. 6). A similar pattern of marginal decline in permeate fluxes was

reported in previous studies [75,99]. In MD, organic foulant tends to predominantly deposit onto the membrane surface and minimally on the membrane pores, due to the vapour pressure driving force rather than applied pressure. As a result, only marginal flux decline was observed. Fig. 6b highlights the improved performance duration achieved with the incorporation of 3D spacers. Owing to the enhanced flux performance, both the 3D spacers were able to achieve the targeted 85% water recovery within a shorter duration of MD operation, i.e., 50–80% of the operational duration needed with that of the commercial spacer. Additionally, the final flux decline with the 3D Gyroid spacer (12%) was slightly lower than the obtained with the commercial spacer (17%) and empty channel (16%).

These results suggest that 3D spacer-filled channels were able to improve MD process performance. Further, in order to ascertain the influence of spacers on organic deposition onto the MD membrane, evaluations were carried out to study the organic mass deposition, characteristic of the organic compounds (LC-OCD analysis) and the condition of the used membranes such as the hydrophobicity and foulant deposition pattern.

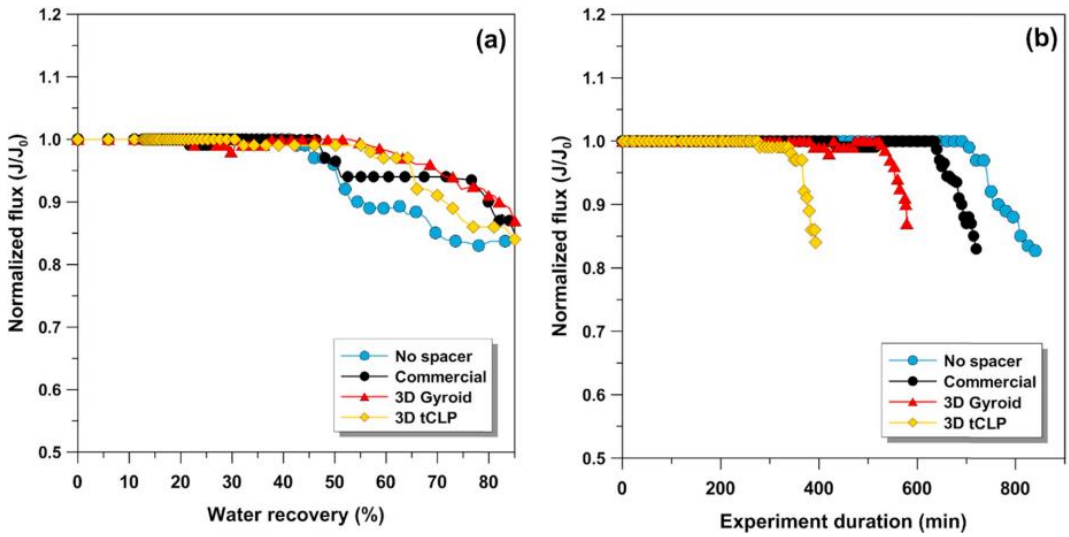

Figure 6. Normalized DCMD permeate flux as a function of **(a)** water recovery and **(b)** experiment duration for both empty and spacer-filled channels. Conditions: Feed: model humic feed solution, T_f = 55.0 ± 2.0 °C, T_p = 22.0 ± 2.0 °C, v_f, = v_p = 0.13 m/s.

3.2.2. Membrane foulant

For all experimental conditions, a high-quality permeate was obtained throughout the experiment duration. The conductivity (10–15 μS/ cm) and organic contents (0.05–0.10 mg/L) in the final permeate solutions were at trace levels and remained lower than that of the initial permeate solutions, corresponding to 98–99% rejection of organics. The results indicated that the organics of the feed solution did not penetrate into the membrane pores, as also supported by the marginal permeate flux decline pattern (Fig. 6).

The dissolved organic content of the initial and final feed solution showed that the total organic mass contents (Table 3) of the final feed solution with the empty channel and commercial spacer-filled channels were 33% and 21% lower, respectively, than the expected value corresponding to a seven-fold volume concentration (85% water recovery, VCF 6.7) of the organic contents in the initial feed solution. On the contrary, the organic mass content of the final feed solutions with the 3D spacer-filled channels was closely similar to the expected value for seven-fold volume concentration (85% water recovery, VCF 6.7) of the organic contents in the initial feed solution. As only trace level of organics was detected in the permeate solutions, the reduced final feed organic contents could presumably be attributed to organics deposition onto the feed channel and adhesion onto the membrane as organic foulants. Considering that the same operating conditions were applied for all the experiments, the organics deposition onto the feed channel would be closely similar between empty and spacer-filled channels. However, based on the relatively lower organic mass reduction of the feed solutions with 3D spacer-filled channels (3–8%), it would be reasonable to infer that organic losses by deposition on the feed channel was minimal. Hence, the significant organic mass losses within the empty channel and commercial spacer-filled channels (21–33%) could most likely be attributed to organic foulant adhesion onto the membrane surface.

Table 3: Feed solution organic mass balance for empty and spacer-filled channel DCMD operated with model humic acid solution (initial feed solution volume -1.70 L; final feed solution volume - 0.25 L).

DCMD Operating condition	Spacer type	Feed solution organic concentration (mg/L)		Feed solution organic mass (mg)		Organic mass reduction (%)
		Initial	Final	Initial	Final	
Empty channel	None	19.50±0.75	87.27±0.62	33.15±0.45	22.08±0.51	33.4
Spacer-filled channel	Commercial	19.50±0.75	102.96±0.71	33.15±0.45	26.05±0.60	21.4
	3D Gyroid	19.50±0.75	127.63±0.60	33.15±0.45	32.29±0.33	2.6
	3D tCLP	19.50±0.75	120.75±0.57	33.15±0.45	30.55±0.41	7.8

Analysis of the organic characteristics of the initial feed solution affirmed that it predominantly consisted of humics (Fig. 7). Meanwhile, the final feed solutions of the empty and spacer-filled channels displayed some variation in organic characteristics. The final feed solution with empty channel showed a pattern of low humic peak with a substantially higher peak of building blocks. On the other hand, the organic characteristics of the final feed solution with spacer-filled channels maintained the same pattern as the initial feed solution, containing major peaks of humics with minor portions of low molecular weight (LMW) organics.

Overall, the organic analyses of the feed solutions indicated that the presence of spacers in MD plays a significant role in organic fouling deposition pattern. Specifically, 3D spacers showed significantly lower organic mass losses compared to commercial spacers. Overall, the organic analyses of the feed solutions strongly indicated that the presence of spacers in MD play a significant role in organic fouling deposition pattern. The 3D spacers, in particular, showed significantly lower organic mass losses compared to commercial spacers. This observation was in line with recent studies that analyzed membrane fouling development with spacer filled channels [105–107]. For instance, Wu et al. [107] explored the role of 3D spacers in membrane fouling mitigation and highlighted that the design and orientation of 3D spacers resulted in lower fouling by 25% compared to 2D spacers. Likewise, a simulation MD study observed that membrane fouling occurs in small isolated regions with spacer-filled channels compared to empty-channel attributed to uniform resident time and induction of the feed solution with the incorporation of spacers [105]. Further, the

feed solution organic characteristics results with LC-OCD imply that spacers play a role in reducing the breakdown of humics to low molecular weight. To further substantiate this observation and to understand the correlations between different spacer types and organic fouling development in MD, organic characteristics of the foulant deposited onto the membrane were analyzed.

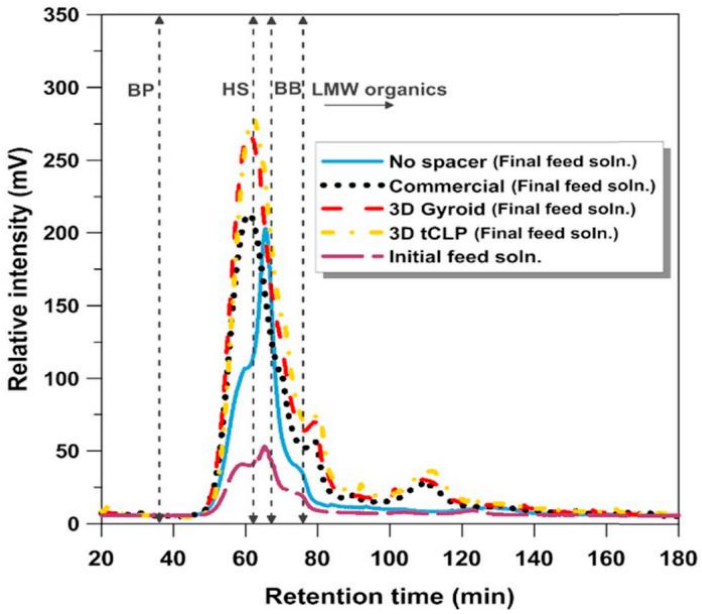

Figure 7. LC-OCD chromatogram of initial and final humic feed solution for empty and spacer-filled channels (*BP- Biopolymers, HS- Humic substances, BB- Building blocks, LMW –Low molecular weight organics*).

Foulant deposition on the surface of the used membrane was visibly different with empty and spacer-filled channels (Fig. 8a). The used membrane in the empty channel, showed significant brown deposition while less deposition was observed in spacer-filled channels, especially with 3D spacers. The SEM images (Fig. 8b) showed the presence of large colloid-like deposits on the used membrane with the empty channel. Comparatively, only small and scattered deposits were observed on the used membrane with spacer-filled channels.

The hydrophobicity of the virgin and used membrane surfaces were measured using water contact angle. The used membrane with empty channels showed the lowest water contact angle (70.2 ± 1.3°), with a 50% hydrophobicity reduction compared to the virgin membrane (139.5 ± 1.7°). Meanwhile, the used membranes with both commercial and 3D tCLP spacers

showed similar hydrophobicity reduction in the range of 33–36%. On the other hand, the used membrane with 3D Gyroid spacer-filled channel retained the highest contact angle (only 13% hydrophobicity reduction) compared to the other used membranes, and its hydrophobicity was restored closely to the original condition with membrane cleaning (batch membrane cleaning). These results suggest that the low foulant deposition with 3D Gyroid spacer-filled channels enabled the membrane hydrophobicity to be restored closely to its original condition, even as the organic concentration in the feed solution was increased by more than 100 mg/L.

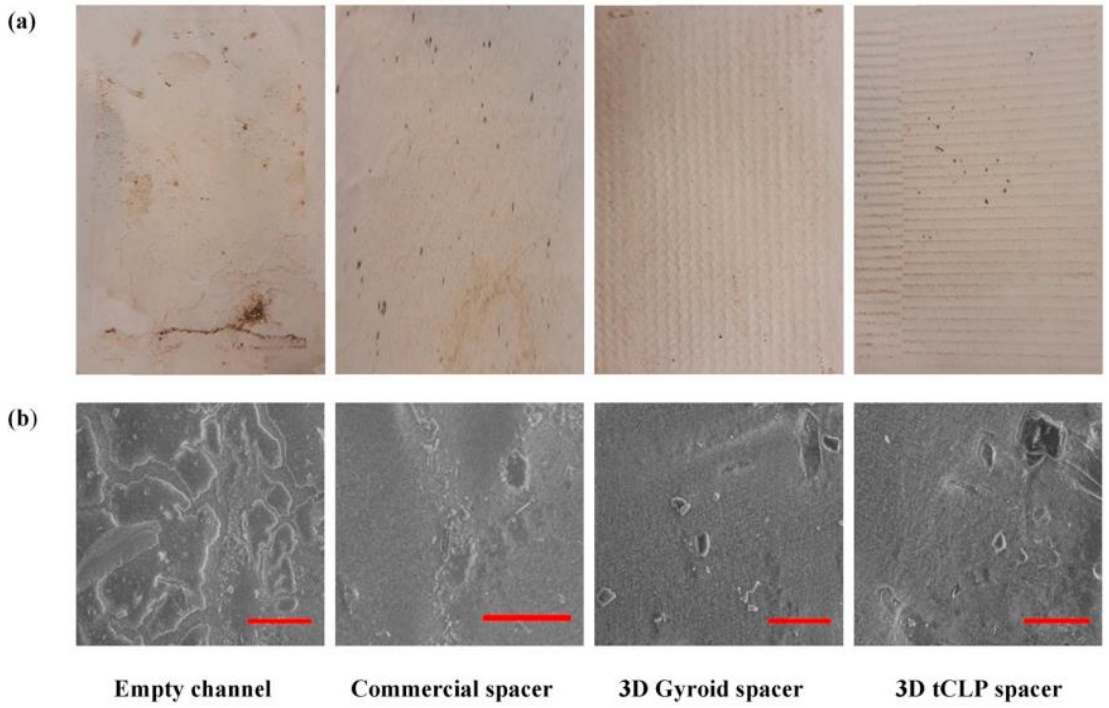

Figure 8. Membrane surface morphology showing **(a)** foulant deposition on the used membranes **(b)** high magnified SEM images of the used membrane upon DCMD operation with empty and spacer-filled channels using model humic acid solution (SEM image scale bar = 100 μm).

LC-OCD chromatograms of the membrane foulant (extracted from the membrane at the end of the experiment) are presented in Fig. 9. The results showed that the foulant deposited on the used membranes predominantly consisted of LMW organics. This was in line with the observation from our previous studies that established the tendency of humics to break down to LMW organics in MD operation and thereafter, for LWM organics to deposit onto the hydrophobic membrane [78,100]. This was attributed to the thermal condition in MD as well

as the hydrophilic-hydrophobic attraction tendency between the foulant and the hydrophobic membrane. Given that the thermal condition was the same for all these four experiments, it is likely that the presence of the spacers may have acted as a barrier that reduced the hydrophilic-hydrophobic attraction between the MD membrane and the foulant. Therefore, the breakdown of humics was reduced in the scenarios with spacer-filled channels. Due to the barrier created by spacers, the tendency of humics breaking down to LMW organics in the feed solution was reduced, as observed with the feed solution organics characteristics analysis (Fig. 7). Hence, less LMW organics are deposited onto the membrane with spacer-filled channels. This tendency was especially apparent with 3D spacers and this could be due to their higher surface area coverage compared to commercial spacers (Table 2). The deposition of LMW organics onto the membrane is associated with membrane hydrophobicity reduction. In line with this, the substantially high LMW organics deposition on the used membrane with the empty channel resulted in significantly higher contact angle reduction (Table 4). The lower deposition of LMW organics on the membrane with spacer-filled channels could be due to the spacers acting as a barrier between the membrane and the concentrated feed solution.

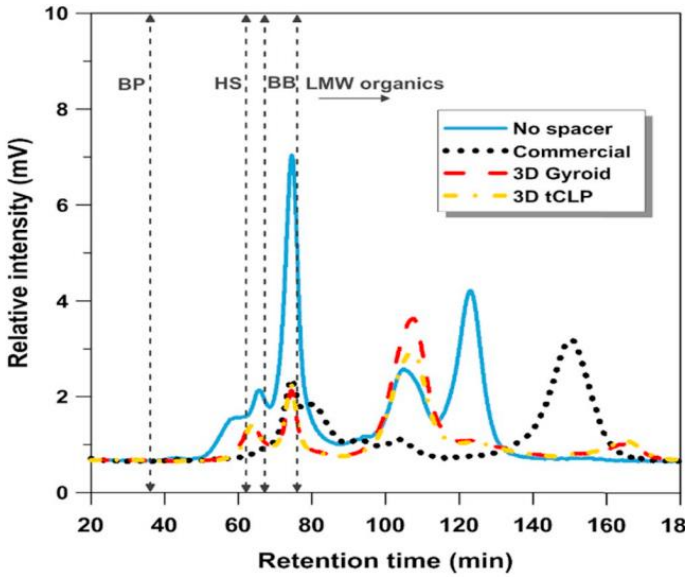

Figure 9. LC-OCD chromatogram representing membrane foulant composition upon operation in empty and spacer-filled channels (*BP- Biopolymers, HS- Humic substances, BB- Building blocks, LMW –Low molecular weight organics*).

Table 4: Water contact angle of MD membrane (virgin, used and DI water cleaned) for empty and spacer-filled channel DCMD operation with model humic acid solution (Contact angle of new/virgin membrane = 139.5 ± 1.7°).

DCMD operating condition	Spacer type	Membrane water contact angle (°)	
		Used membrane (upon 85% water recovery)	[a] Cleaned membrane (DI water)
Empty channel	None	70.2 ± 1.3	115.4 ± 0.8
Spacer-filled channel	Commercial	87.5 ± 1.5	129.7 ± 1.7
	3D Gyroid	119.3 ± 1.0	132.2 ± 2.0
	3D tCLP	91.4 ± 1.7	123.3 ± 1.1

[a] Batch membrane cleaning (method as reported previously).

3.2.3. Effect on fouling deposition patterns

Overall, the results indicated that the application of spacers (both commercial as well as 3D spacers) in MD resulted in lower fouling deposition compared to the empty channel. This could be related to the higher turbulence created by spacers. Higher turbulence disrupts the boundary layer close to the membrane (polarization effect) and enhances shear stress as established by a number of CFD modeling studies [85,93,105]. Higher shear stress is directly associated with reduced fouling deposition onto the membrane [90,108].

Meanwhile, compared to the commercial spacer-filled channel, both the 3D spacers showed reduced fouling intensity, based on the lower foulant deposition on the membrane (Table 3 and Fig. 8) as well as the lower reduction in membrane hydrophobicity (Table 4). This could be attributed to two factors, enhanced turbulence, and reduced dead zones. Firstly, compared to the commercial spacer, 3D spacers resulted in higher turbulence at the same feed velocity as reflected by the higher permeate fluxes achieved (Fig. 5a). The higher turbulence in 3D spacers is attributed to the non-uniform/varying filament thickness and smaller hydraulic diameter characteristics of the 3D spacers. In a simulation study, Taamenh and Bataineh [93] showed that significantly higher average shear stress was achieved by varying the top and bottom filament angle and when the angle of the spacers was closer to 90°. Hagedorn et al. [94] indicated that spacers with irregular filament surface and varying filament thickness contributed to better heat transfer efficiency and flow mixing. The higher turbulence and mixing with enhanced shear stress on the membrane surface with 3D spacers can be

associated with the lower fouling deposition. Secondly, the factor of dead zone (restricted flow area) could likely contribute to higher fouling deposition onto the commercial spacer compared to the 3D spacers. Dead zone occurs when a spacer is in direct contact with the membrane which restricts flow velocity and accumulates deposits close to the membrane [90,92]. Compared to a commercial spacer, 3D spacers are designed with TPMS topographies to generate surfaces (mean curvature of zero) with minimal contact area to the membrane [90]. The lower contact area to the membrane with 3D spacers reduces dead zone and results in lower fouling intensity compared to commercial spacers. Sreedhar et al. [90] observed higher biofouling development on RO membrane incorporated with commercial spacers than 3D spacers and this was attributed to the tendency of biofoulants to adhere especially around the contact area (dead zone) between the commercial spacer and the membrane.

In comparing the fouling performance with 3D spacer-filled channels, lower membrane fouling intensity was observed with Gyroid spacer over tCLP spacer on the basis of lower foulant mass deposition on the membrane (Table 3) as well as restored membrane hydrophobicity (Table 4). The variation in fouling deposition pattern between Gyroid and tCLP spacer could be explained in terms of their different design characteristics. Lower surface area/volume (Table 2) value of Gyroid (7.1 mm^{-1}) compared to tCLP (13.9 mm^{-1}) indicates that for a given channel volume the Gyroid spacer offers a lower surface area for foulant adhesion and entrapment. This translates to reduced dead zone and accumulation of foulants onto the membrane with Gyroid spacer. Spacer voidage (porosity) is also an important characteristic that influences spacer performance. However, in this case, the voidage for both the 3D spacers (Gyroid - 84%, tCLP - 88%) are closely similar. On the other hand, in closely examining the design of both spacers, the skeletal-based structure of the Gyroid spacer resembles a zigzag cubic shape with an infinite smooth surface. This condition most likely creates a wave-like flow mechanism that does not potentially retain the foulant. Comparatively, tCLP is a tetragonal sheet/layer which resembles a ‘pocket’ like shape. In the case of tCLP, the channels or protrusions aligned perpendicular to the feed flow direction creates high turbulence, which results in significantly higher permeate flux compared to Gyroid (Fig. 5a). However, it is highly likely that the combination of this turbulence in the presence of the pocket like shape promotes higher affinity for deposition of foulant onto the membrane as depicted in Fig. 10. Likewise, a recent study evaluating the performance of

vibrating 3D spacers, reported on the superior membrane fouling mitigating by wave-like spacer compared to hill-like spacer (a similar resemblance to the tCLP pocket like shape) [106]. In that study, Tan et al. [106] highlighted that although hill-like spacer does demonstrate higher local velocity, the protrusions of wave like spacers creates large fluid movement, which enhances the overall shear along the membrane, resulting in higher fouling mitigation.

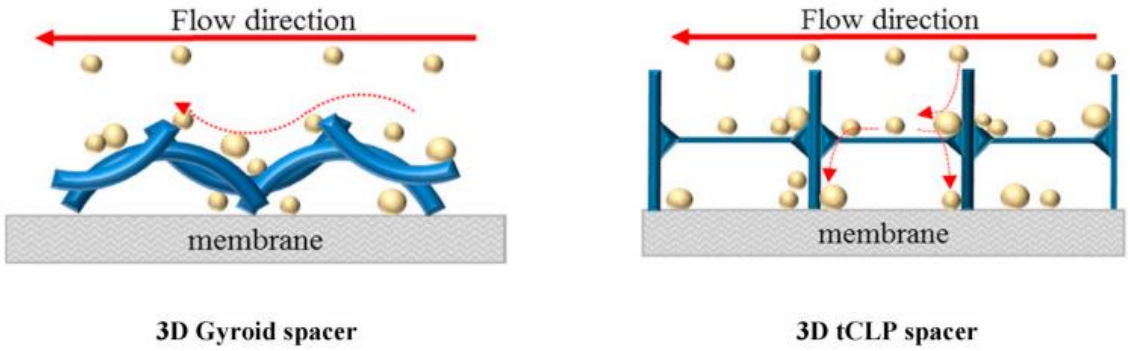

Fig. 10. Depiction of fouling deposition mechanism in DCMD with 3D spacer-filled channel

In summary, although tCLP spacer-filled channel allowed to achieve enhanced permeate fluxes compared to the other spacers, the organic fouling evaluation highlights that the best fouling mitigation capacity was with the 3D Gyroid spacer. Moreover, the lower channel pressure drop of 3D Gyroid spacer is an added advantage over the tCLP spacer.

3.3.Practical spacer application for wastewater treatment in MD.

Based on the above factors, conditions that emulate actual treatment and fouling pattern (high organic contents in the presence of inorganic salts) is necessary to further substantiate and establish the role and practical application of 3D Gyroid spacer-filled channel towards fouling mitigation in MD. For this reason, evaluations were carried out with wastewater RO concentrate that contains high organics (similar to the model organic solutions) in a mixed composition with carbonate based inorganic salts (majorly Na, Ca, Mg) as listed in Table 1. At the same time, low organics wastewater RO concentrate (organic contents reduced through GAC adsorption) while maintaining the same inorganic salt concentration was used to compare and establish the role of organics in wastewater treatment with MD operation. Aspects such as permeate flux and quality and fouling pattern, potential pre-treatment

requirement for enhancing the membrane durability as well as the adhesion of foulant onto the spacer and its reversible and reuse capacity was studied in detail.

3.3.1. Process performance

DCMD experiments with actual wastewater RO concentrate using both empty and Gyroid spacer-filled channels achieved initial permeate fluxes of 19.5 ± 1.7 LMH (empty channel) and 37.0 ± 0.4 LMH (3D Gyroid spacer-filled channel for high and low organics), closely similar to the initial fluxes with model organic solution (as reported previously). However, at 85% water recovery, permeate fluxes declined by 21–27% (Fig. 11), which was almost two times higher compared to the 12–15% permeate flux decline rates with model organic solution (Fig. 6). Further, the low organic wastewater RO concentrate (with 1.5 ± 0.5 mg/L organics) exhibited similar permeate flux trend as the actual wastewater RO concentrate (with 20.3 ± 0.7 mg/L organics) (Fig. 11). These results suggest that, under the selected operating conditions, the inorganic ions at high saturation (concentration) levels in wastewater RO concentrate played a more dominant role in influencing the mass transport mechanism in DCMD rather than the organic contents.

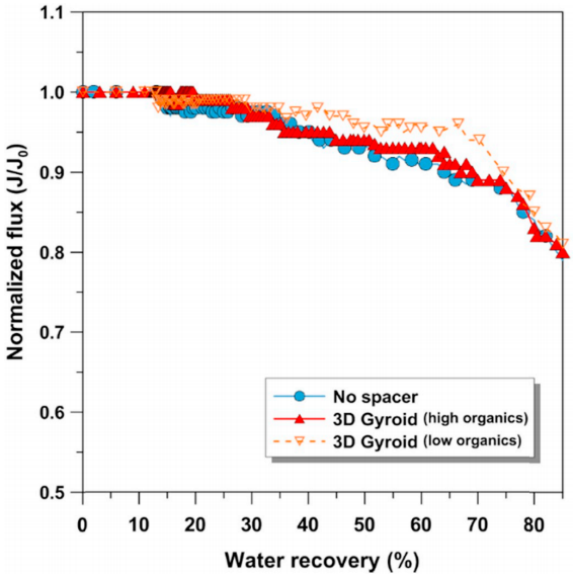

Fig. 11. DCMD permeate fluxes as a function of water recovery rate with empty and 3D Gyroid spacer-filled channels for wastewater RO concentrate treatment (Tf = 55.0 ± 2.0 °C, Tp = 22.0 ± 2.0 °C, vf,vp = 0.13 m/s) (Initial permeate fluxes: 19.5 ± 1.7 LMH (empty channel) and 37.0 ± 0.4 LMH (3D Gyroid spacer-filled channel for high and low organics)).

In terms of permeate quality, the final permeate conductivity (18–22 μS/cm) increased slightly compared to the initial permeate conductivity (10–15 μS/cm) for the case scenario of empty channel. The rise in permeate conductivity reflected that partial wetting may have occurred. On the other hand, the operation with Gyroid spacer-filled channels did not show any increment in permeate conductivity, indicating the stability of the performance up to 85% water recovery rate.

Table 5: Water contact angle of the membranes (virgin, used and cleaned) for empty and 3D Gyroid spacer-filled channels DCMD operation with wastewater RO concentrate (Contact angle of new/virgin membrane = 139.5 ± 1.7°).

DCMD operating condition	Wastewater RO concentrate	Membrane water contact angle (°)		
		Used membrane	[a] Cleaned Membrane	
			DI water	Acid (0.1%)
Empty channel	High organics	5.2 ± 2.7	7.4 ± 0.8	10.4 ± 0.8
3D Gyroid spacer	High organics	50.5 ± 1.3	61.2 ± 1.2	88.4 ± 1.4
	Low organics	66.3 ± 1.1	87.2 ± 1.3	129.7 ± 1.7

[a] Batch membrane cleaning (method as reported previously).

3.3.2. Membrane foulant

The used membrane with empty channel showed large mud colloid like mixture of humics with inorganic salt crystals (Fig. 12a). The crystal shape and EDX element analysis established $CaCO_3$ as the main inorganic scalant. Comparatively, the used membrane with 3D Gyroid spacer displayed only small isolated regions containing colloidal foulant (Fig. 12b). In the case of low organic wastewater RO concentrate, the used membrane with 3D Gyroid spacer showed a different pattern with small scattered foulants that were loosely deposited onto the membrane (Fig. 12c).

In terms of membrane hydrophobicity, the used membrane with empty channel resulted in more than 95–97% contact angle reduction compared to the virgin membrane (Fig. 12a and Table 5). The high hydrophobicity loss could be correlated to the partial wetting phenomena, based on the permeate conductivity increment as reported above. Moreover, membrane cleaning (batch membrane cleaning) with neither water nor acid could restore the membrane, indicating irreversible fouling. It is also worth mentioning that the high humic content as a single solute (Table 4) minimally affected the membrane hydrophobicity and the membrane condition was easily reversed with only water cleaning. These results suggest that treating

and concentrating actual wastewater RO concentrate containing high humics mixed with inorganic ions is a challenge and would detrimentally affect the long-term performance of MD. Compared to the used membrane with empty channel, the incorporation of 3D Gyroid spacer resulted in less membrane hydrophobicity loss (57–60% contact angle reduction to the virgin membrane) (Fig. 12b and Table 5). This highlights the importance of 3D Gyroid spacer as a barrier that improved MD performance for wastewater treatment. Nevertheless, in attaining 85% water recovery (highly concentrated wastewater), reversing the foulant deposition and membrane hydrophobicity was still a challenge. Meanwhile, the combination of low organic wastewater RO concentrate with the incorporation of 3D Gyroid spacer was effective in enabling to achieve high water recovery while restoring the membrane hydrophobicity with acid membrane cleaning. These results clearly indicated the necessity for a simple organic pre-treatment such as GAC filtration [78,109] to maintain a stable MD performance in treating wastewater containing high organics.

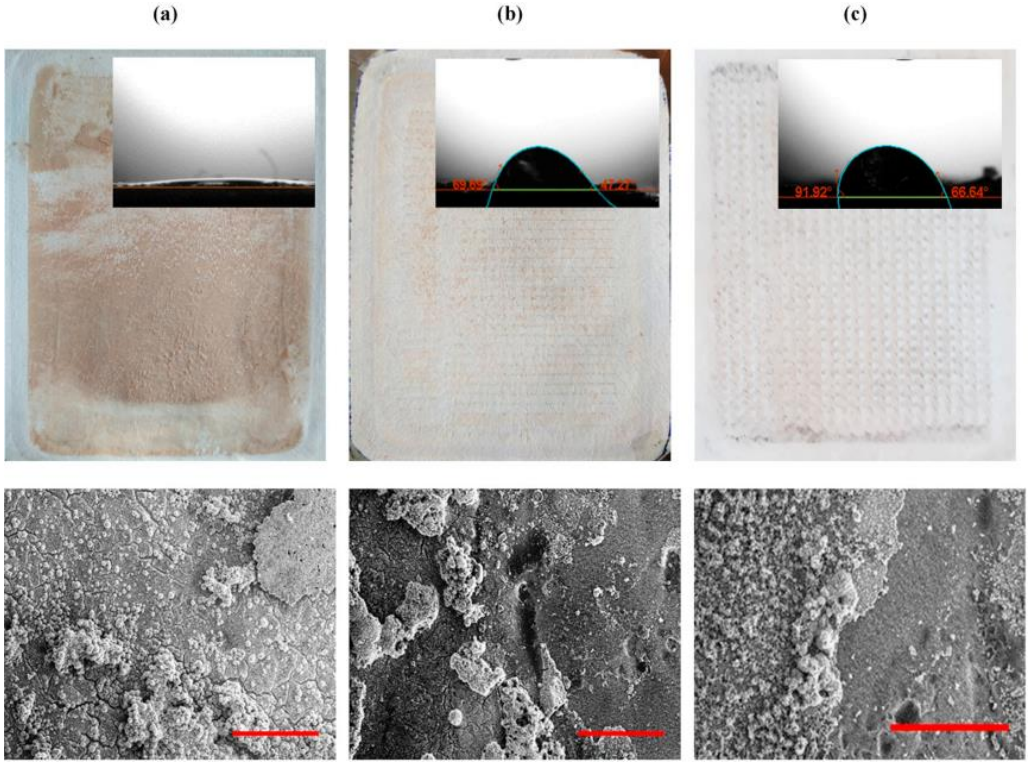

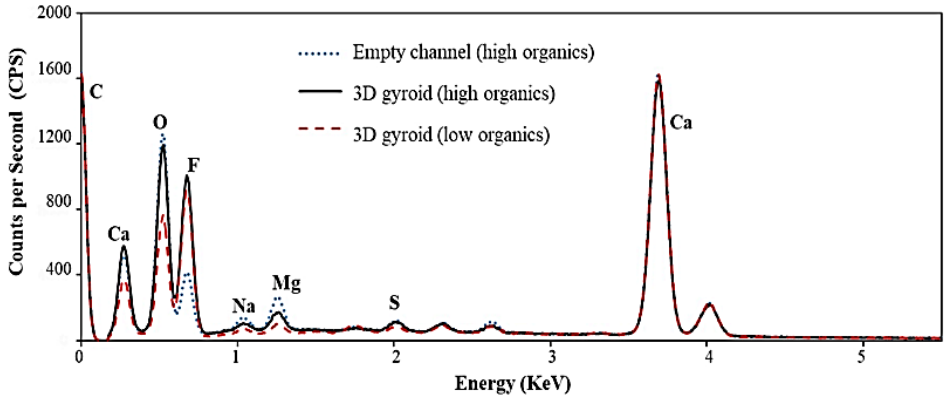

Figure 12. SEM-EDX and contact angle of the used MD membrane using wastewater RO concentrate with **(a)** empty channel (high organics) **(b)** 3D Gyroid spacer-filled channel (high organics) and **(c)** 3D Gyroid spacer-filled channel (low organics) (SEM image scale bar = 300 μm).

Overall, the mentioned evaluation highlighted the capacity of MD to treat wastewater RO concentrate and achieve high water recovery (85%) through a combination of GAC pre-treatment of wastewater (low organics wastewater) and the use of 3D Gyroid spacer-filled channels. Nevertheless, to establish the performance of MD for wastewater treatment, practical aspects such as cleaning-in-place (cleaning the membrane and spacer while it is in the module) as well as evaluation of membrane and spacer reuse capacity must be carried out. These aspects are discussed in the subsequent section.

3.3.3. Membrane and spacer reuse capacity

Three repeated MD cycles with low organic wastewater RO concentrate using the same membrane and 3D Gyroid spacer were carried out to establish the performance of MD for wastewater treatment. At the end of each cycle, cleaning-in-place (cleaning the membrane and spacer while it is the module) with water and chemical (0.1% citric acid with water flushing) was carried out to determine the reuse capacity of both the membrane as well as the spacer.

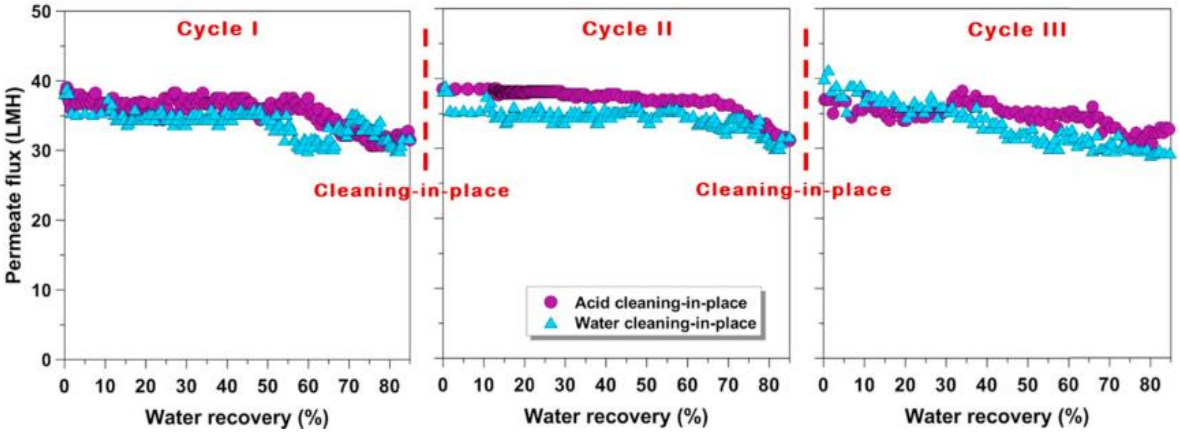

Figure 13. Repeated cycles of DCMD with 3D Gyroid spacer-filled channel using low organics wastewater RO concentrate with cleaning-in-place (DI water and citric acid) at the end of each cycle.

The results showed the capability of MD incorporated with 3D spacers to achieve high water recovery (85%) while maintaining stable permeate fluxes with low organic wastewater RO concentrate in three repeated cycles with cleaning-in-place (Fig. 13). However, compared to the water membrane cleaning (final average contact angle = 87.2 ± 1.7°), acid membrane cleaning was effective in maintaining the membrane hydrophobicity (final average contact angle = 130.7 ± 1.7°) close to the virgin membrane (average contact angle = 139.5 ± 1.7°) (Fig. 14). Likewise, the SEM images showed the presence of visible foulant deposition on the membrane with DI water cleaning.

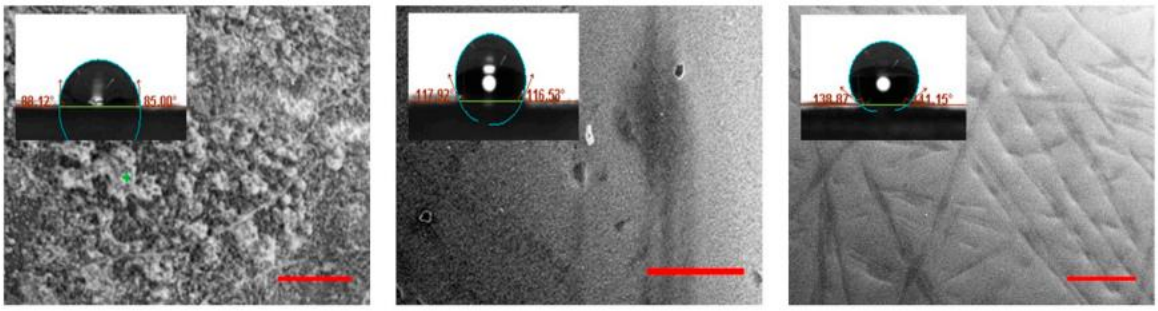

Figure 14. Condition of the used membranes after three repeated DCMD cycles (low organic wastewater RO concentrate treatment feed solution with 3D Gyroid spacer-filled channels) upon cleaning-in-place with water and acid compared to the virgin membrane (SEM image scale bar = 200 μm).

Meanwhile, minimal deposition was visible on the acid cleaned membrane (closely resembling the virgin membrane). It is also worth mentioning that the membrane contact angle results with the cleaning-in-place were closely similar to the batch membrane cleaning (Table 5), indicating the suitability of a simple cleaning-in-place approach for maintaining the membrane in MD operation. Both the cleaning-in-place and batch membrane cleaning results indicated the necessity for a simple acid membrane cleaning for reversing foulant deposition and maintaining the membrane durability to achieve repeated cycles of MD operation for wastewater treatment.

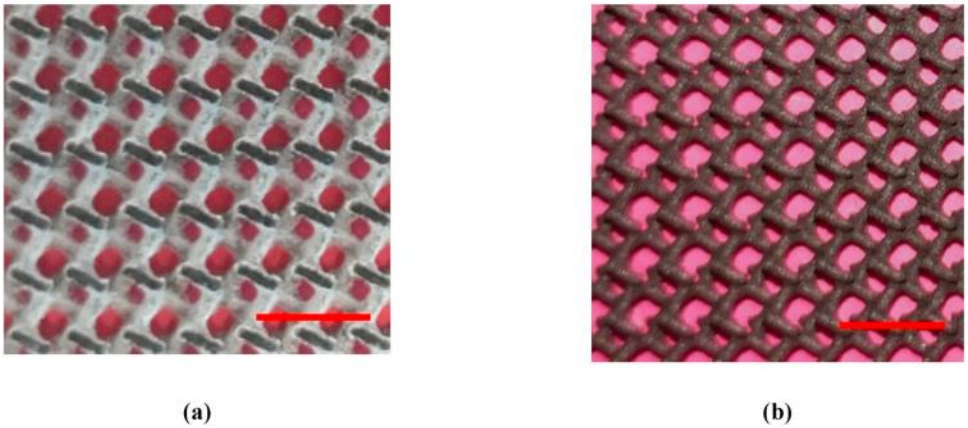

Figure 15. Condition of spacer (a) upon wastewater RO concentrate operation (b) upon cleaning in place in DCMD (image scale bar = 0.5 cm).

Foulant deposition on the 3D Gyroid spacer was evident from its condition observed upon DCMD operation (Fig. 15a). This is because the spacer acts as a barrier between the concentrated feed solution and the membrane, which is favorable in reducing foulant deposition onto the membrane. Nevertheless, inevitably, foulant tends to deposit onto the spacer. Hence, it is highly pertinent to evaluate foulant reversibility and reuse capacity of the spacer. The results of the study showed minimal foulant deposition (Fig. 15b) on the spacer used for three repeated cycles of MD operation. This established the effectiveness of a simple cleaning-in-place for reversing foulants on the spacer. The ease of reversing foulant on the spacer could be attributed to the spacer design and material type that tend to repel foulant from adhering strongly on it. The reverse fouling and reuse capacity of the 3D Gyroid spacer established its suitability to be incorporated in MD for enhancing its performance for wastewater treatment.

4. Conclusions

This study evaluated the influence of 3D printed spacers in improving MD performance and organic fouling development for treating wastewater. Overall, the results of the study highlighted that:

- 3D spacers (Gyroid and tCLP) enabled to significantly enhance the performance of MD (up to 200% increase in permeate flux and energy efficiency) compared to the empty channel and up to 30–70% improved flux performance relative to the commercial spacer. This was attributed to the unique features of 3D spacers that enhanced turbulence and mass transfer. The trade-off of higher channel pressure drop with 3D spacers is inevitable.
- 3D Gyroid spacer showed better organic fouling mitigation capacity (based on the membrane hydrophobicity and lower organic mass deposition) compared to tCLP and this was attributed to the tortuous spacer design that can repel foulants;
- Treating and concentrating actual wastewater RO concentrate using MD without spacer resulted in partial wetting with significant and irreversible foulant deposition onto the membrane. This is attributed to the presence of organics in mixed constituents with inorganic ions, as the membrane foulant with singe solute organics (humics feed solution) was highly reversible;
- Repeated cycle of MD operation with a combination of low organics wastewater RO concentrate with 3D Gyroid spacer and cleaning-inplace established the importance of (i) a simple pretreatment to reduce organic content (ii) 3D spacers as a foulant barrier (ii) cleaning-in-place, for achieving high recovery rate and stable longterm MD operation with wastewater; and
- Cleaning-in-place established the foulant reversibility and reuse capacity of 3D Gyroid spacer in MD.

CHAPTER IV:

Forward Osmosis–Membrane Distillation economic assessment: An application for acid mine drainage

Chapter IV: Forward Osmosis–Membrane Distillation economic assessment: An application for acid mine drainage

- This chapter corresponds to a research paper submitted in the Journal of Membrane Science. Nevertheless, some article results were presented previously in Chapter II; these results will be refenced to avoid repeating information.

Abstract

Contamination of water bodies by concentrated wastewater from the mining industry affects global freshwater availability, especially in arid zones like northern Chile. Acid mine drainage (AMD) is acidic wastewater, rich in dissolved metal sulfates and salts, making it very dangerous if it reaches water resources. A real AMD from a contaminated river in northern Chilean was used in this study. The objective of this work was to evaluate an economic projection of a Forward Osmosis–Membrane Distillation (FO-MD) process versus a Forward Osmosis–Reverse Osmosis (FO-RO) for the treatment of saline wastewater with an emphasis on water recovery. FO-MD continuous assays (12 hours) were performed using AMD solution as feed, achieving an initial flux of 25 LMH with FO. Nevertheless, fouling was observed since early beginnings, decreasing the flux up to 8 LMH after 12 hours. MD was used as a draw solute recovery stage, and the experimental flux remains stable around 10 LMH up to 4 hours without signs of fouling or scaling. Different economic models were developed for FO-MD and FO-RO and using steam and thermal-fluid as MD heat sources. The cost assessment showed that under the studied conditions, the thermal-fluid FO-MD investment could be recovered in 1.7 years. The FO-RO model revealed to be more profitable than FO-MD with a payback period of around a year. Results from the economic assessment revealed that if a waste-heat source is available, the FO-MD operation cost would be lower than FO-RO, even with today's high FO/MD membrane purchase cost.

Keywords*: Reverse osmosis, cost estimation, deterministic analysis.*

List of abbreviations

ACC	Annualized Capital Cost [$/year]
AOC	Annualized Operation Cost [$/year]
AMD	Acid Mine Drainage
CAPEX	Capital Expenditure (cost) [$]
DCC	Direct Capital Cost [$]
DCMD	Direct Contact Membrane Distillation
DEEP	Desalination Economic Evaluation Program
DS	Draw Solution
ERD	Energy Recovery Device
FO	Forward Osmosis
FS	Feed Solution
HX	Heat Exchanger
ICC	Indirect Capital Cost [$]
IRR	Internal Rate of Return [%]
$\mathbf{J_w}$	Membrane water flux [$L*m^{-2}*h^{-1}$ = LMH]
MD	Membrane Distillation
MED	Multi-Effect Distillation
MSF	Multi-Stage Flash distillation
NPV	Net Present Value [$]
OPEX	Operation and maintenance Expenditures (cost) [$/year]
P	Pumping Pressure [bar]
PP	Payback Period [year]
$\mathbf{Q_{perm}}$	Permeate flow rate [L/day]
$\mathbf{Q_{plant}}$	Plant flow rate [L/day]
RHX	Recovery Heat Exchanger
RO	Reverse Osmosis
$\boldsymbol{S_{diffusion}}$	Specific reverse salt diffusion [g/L]
$\mathbf{SEC_{MD}}$	Specific thermal Energy Consumption [kJ/day]
SF	Size correction Factor [-]
TCC	Total Capital Cost [$]
TDS	Total Dissolved Solids [mg/L]
WC	Water production Cost [$/$m^3$]
ΔT	Temperature difference
$\boldsymbol{\eta_p}$	Pump efficiency [%]

1. Introduction

Wastewater production has increased exponentially since the industrial revolution, contaminating water bodies, and reducing freshwater availability [5]. The mining industry is well known for including processes with high water consumption, generating large amounts of acid wastewaters. Acid mine drainage (AMD) is highly acidic wastewater, rich in dissolved ferrous and non-ferrous metal sulfates and salts, produced as a result of mining activities. AMD composition will be subjected to the content of heavy metals and minerals of the original geology (Chapter II, Table 1) [8].

Saline wastewaters, such as AMD, tend to have high concentrations of organic and/or inorganic compounds, making them difficult to treat using conventional treatment methods (Multi-Stage Flash, Multiple-Effect or Vapor-Compression Distillation), which generally have low salt-tolerance [7,110]. Desalinization techniques like membrane separation have reached adequate treatment standards for this kind of wastewater [111]. Depending on their quality, the treated effluents can be reused for industrial applications, irrigation, and even as a source for drinking water [14].

Forward osmosis (FO) is an emerging membrane technology based on the osmosis phenomenon, in which a semipermeable membrane is placed between two solutions of different chemical potentials, a feed (FS) and a draw solution (DS). Concentration difference between solutions drives water from the FS through the membrane to the high concentrated DS [112]. FO is gaining ground against conventional desalination processes like reverse osmosis (RO) because of its lower energy consumption and lower pre and post-treatment costs [15]. FO has been used successfully in a variety of wastewaters, such as municipal sewage [17–20,113] or oil-gas produced water [114]. The evaluation of water recovery from AMD using FO was performed for the first time by Vital *et al.* (2018) [21].

Although FO can achieve high rejection ratios for heavy metals [21], it has a significant drawback: it requires a coupled DS regeneration unit or re-concentration step. The separation and recovery of the DS require an additional processing unit, and its energy demand remains a significant challenge for water treatment applications [35]. At present, some strategies for

DS recovery are Reverse Osmosis [115][116], Thermal Concentration [117–120], and Membrane Distillation [121]. Each one of these alternatives has advantages and disadvantages regarding the energy-demand and fluid's saline concentration level. In this context, Membrane Distillation (MD) may provide an interesting alternative to draw solution recovery. MD involves water evaporation in the pores of a hydrophobic microporous membrane [6]. The water vapor then passes through the membrane from a hot feed solution to cold liquid water, as a result of coupled heat and mass transfer processes [23]. Unlike FO, MD driving force is the vapor pressure gradient (temperature-related), rather than the osmotic pressure gradient [24]. Vapour pressure is only slightly affected by concentrations of dissolved salts [6], making MD a suitable alternative for the recovery of highly concentrated DS from the FO step. MD is a low-temperature distillation process [6], that can operate with a low-temperature gradient (10-15°C). This low-temperature operation condition makes MD a strong contestant against classical thermal systems like Multi-effect distillation (MED) and multi-stage flash (MSF) distillation, which are high energy demanding [122].

The most common MD setups are Direct Contact MD, Air Gap MD, Sweeping Gas MD, and Vacuum MD. Nevertheless, Direct Contact MD (DCMD) setup is the most used configuration, mainly due to its simplicity, lower energy requirements, and higher fluxes [123]. In DCMD, the inlet solution (hot) and the outlet or permeate solution (cold) are in direct contact with the membrane. The DCMD setup was selected for this study.

Among potential configurations involving FO, the FO-MD alternative has been less explored. It consists of a FO module for extracting clean water from the feed solution (wastewater) and an MD module for re-concentration of the FO diluted draw solution, producing high purity water at the same time [124]. The FO-MD configuration combines the strengths of both processes: high element rejection with a low membrane fouling and a high product water quality with high draw solution recovery [25].

The FO-MD setup has been evaluated in a wide variety of wastewaters: oil industry [36–38], landfill leachate [39], municipal wastewater and urine [40,41], seawater/brackish desalination [42,43] and pharmaceutics industry wastewaters [44]. Much of the FO-MD researches are lab-scale, which brings uncertainty to assess a fair comparison with RO based systems. Few economic studies have dealt with FO-MD in recent years [121,125,126].

However, no study was found combining practical experimentation with an economic assessment for an FO-MD setup to reclaim water from AMD.

The objective of this work is to evaluate an economic projection of an FO-MD process, using FO-RO as a comparison baseline, for the treatment of saline wastewater with an emphasis on water recovery. Research involved experimental activities for the determination of FO water flux, using real acid mine drainage as feed, and different NaCl solutions as DS.

2. Materials and methods

2.1. Technological and Economic assessment

A large-scale FO-MD plant was designed for wastewater treatment and water reclamation from an AMD effluent. The AMD was obtained from a northern Chile river that receives the acid leaching from a nearby copper mine (Chapter II, Table 1). The plant design was based on previous experimental flux results and selected operation conditions from Chapter II (1M NaCl at 60°C), and the technical and economic data presented in Tables 1 & 2. The plant capacity used in the FO-MD design was based on the 2018 recovered-water demands data from the Collahuasi mining company [127].

Two FO-MD configurations were proposed, one with a steam boiler and one with a thermal-fluid heater (Figure 1a). Two different heat exchangers (HX) were used for each configuration. A recovery heat exchangers (RHX) coupled with a gas-liquid HX for the steam alternative and an RHX with liquid-liquid HX for the thermal-fluid variant. Figure 1b shows the different temperatures used in the different heat exchanger (HX) designs. The mentioned FO-MD designs were compared with a projected FO-RO plant (Figure 2). The FO stage design was the same for both configurations.

The land cost was not included in this assessment because the designed treatment plant is assumed to be placed inside the property of the mining processing facility. The inputs for the technological and economic models are presented in Tables 1 & 2. Every cost included in this study was in US dollars.

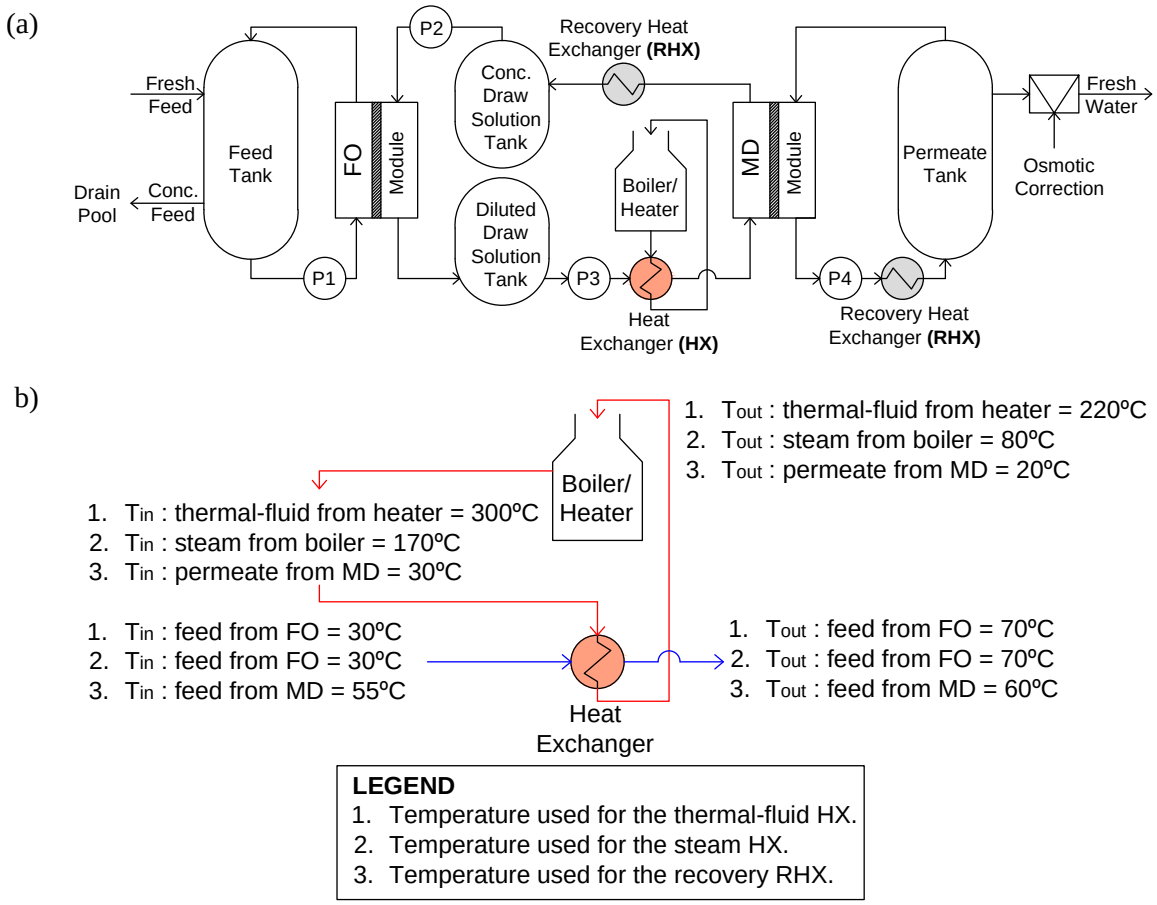

Figure 1. FO-MD proposed setup for economic evaluation: **a)** FO-MD Plant overview, **b)** Temperatures used for the heat exchanger designs.

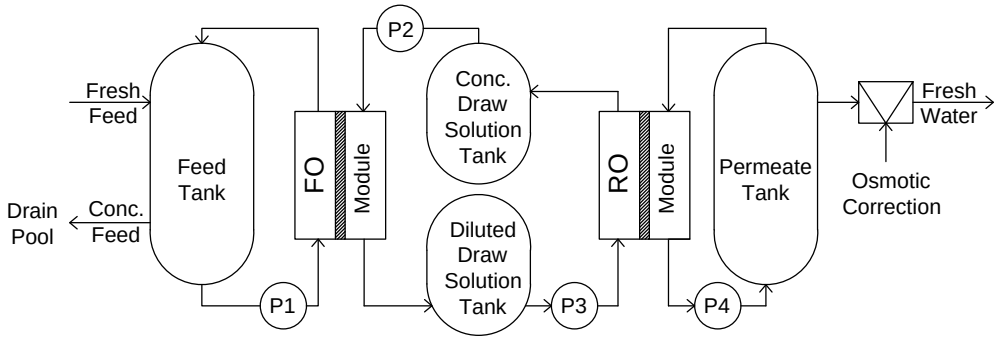

Figure 2. FO-RO proposed setup for economic evaluation.

Table 1. Technical Model Inputs

Parameter	Value	Unit	Reference
Plant feed (Q_{Plant})	29848	m^3/day	[127]
Feed recovery (R)	50	%	This research
Plant permeate (Q_{Perm})	14924	m^3/day	[127]
Plant lifetime ($T_{Plant\ Life}$)	20	years	[128]
Plant availability ($T_{Plant\ Av}$)	90	%	[129]
FO Membrane flux (J_w)	13	LMH	Chapter II
MD Membrane flux (J_w)	10	LMH	Chapter II
NaCl Draw solute concentration (DS)	1	M	Chapter II
Temp. MD Module Feed Inlet ($T_{Feed\ In}$)	60	°C	This research
Temp. MD Module Permeate Outlet ($T_{Perm\ Out}$)	30	°C	This research
Temp. Thermal-fluid HX Inlet (T_{in}) (Figure 2b)	300	°C	This research
Temp. Thermal-fluid HX Outlet (T_{out}) (Figure 2b)	70	°C	This research
Temp. Steam HX Inlet (T_{in}) (Figure 2b)	170	°C	This research
Temp. Steam HX Outlet (T_{out}) (Figure 2b)	70	°C	This research
Temp. Recovery HX Inlet (T_{in}) (Figure 2b)	55	°C	This research
Temp. Recovery HX Outlet (T_{out}) (Figure 2b)	20	°C	This research

Table 2. Model Economic Inputs

Parameter	Value	Unit	Reference
Interest rate	5	%	[129]
Amortization factor	0.065	-	Calculated
Electricity price (C_{Elect})	0.1	$/kWh	[130]
Water price (C_{Water})	5.52	$/$m^3$	[131]
NaCl draw solute cost (C_{Solute})	2.27	$/kg	Bulk purchase
NaCl draw solute cost (C_{Solute})	0.1	$/kg	Lab-scale purchase
FO membrane-module cost ($C_{FO\ Memb}$)	140	$/$m^2$	This research
MD membrane-module cost ($C_{MD\ Memb}$)	120	$/$m^2$	This research
RO membrane-module cost ($C_{RO\ Modules}$)	950	$/unit	[132]
RO vessels cost ($C_{RO\ Vessels}$)	1812	$/unit	[132]
Welded plate exchangers (thermal fluid-liquid)	81	$/$m^2$	[133]
Welded plate exchangers (liquid-liquid)	42	$/$m^2$	[133]
U-tube heat exchanger cost (steam-liquid)	230	$/$m^2$	[133]

For comparing FO-MD and FO-RO, economic parameters were divided into capital expenditure (CAPEX) and operation and maintenance expenditures (OPEX). The CAPEX

assessment divides into direct and indirect costs. Direct cost includes land purchase, infrastructure, pretreatment, equipment, and installation cost. On the other hand, indirect cost includes salaries and wages, insurance, administration costs, and construction overheads [129,134]. Indirect cost was assumed to be 30% of the total direct cost [128].

The OPEX consists of costs of energy (heating and electricity), equipment replacement, chemicals, labor, and routine maintenance [129] and is usually presented as an annual cost.

2.1.1. Capital cost (CAPEX)

The CAPEX are one-time expenses, like the first membrane-module purchases, heat exchangers, pumps, piping, electric installation, and measuring instrumentation.

I. *Membrane and Module*

The membrane area for FO and MD was calculated based on the desired permeate flow rate (Q_{Perm}) and FO and MD experimental membrane flux (J_w) (Table 1). FO and MD membrane representative cost corresponds to the purchase price of an entire module. For FO, the values oscillated between 20 and 1000 \$/m^2 [15,121,132,135–142]. MD purchase prices ranged from 30 to 350 \$/m^2 [121,125,128,134,136,143–150]. The representative membrane-module cost was selected using the mean cost value from all mentioned economic studies (Table 2).

A different approach was applied to estimate the RO membrane capital cost. The number of required elements (membrane modules) and pressure vessels was calculated using different RO design software: IMS Design from Hydranautics [151] CSMPRO 6 by CSM [152], Q+ by LG [153], DS2 by Toray [154], and WinFlows by Suez [155]. Results from RO design software were averaged (Table 3), and these mean values multiplied by their respective purchase cost [132] (Tables 2).

II. *Draw solute*

FO draw solute (NaCl) has to be considered either a capital cost as well as an operational cost (replenish draw solute cost). Replenish draw solute cost was analyzed in the OPEX section. Draw capital cost calculation was determined by multiplying the unitary draw cost by the total volume of the draw solution tank. See Appendix A and Table B1 for further supporting information.

III. *Energy recovery devices: heat exchangers (HX) and pressure exchanger (PX)*

Heat exchangers (HX) are frequently used in thermal processes in order to reduce the external energy supply, decreasing the overall operation cost. For decreasing the system energy consumption, proposed FO-MD plants (Figure 1a) were designed using two different combinations of heat exchangers: a steam HX with recovery RHX, and a thermal-fluid HX with a recovery RHX (Figure 1b). The steam and thermal-fluid HX take heat from a steam boiler or a thermal fluid heater and transmit the heat to the MD feed solution, which is the diluted draw solution from the FO stage. On the other hand, the RHX is meant to recover the latent heat from the MD permeate once it exits the module with a portion of the feed solution temperature. The RHX was designed to decrease the system heat requirement, reducing operation costs. For more details, see Appendix A and Table B1 for supporting information.

IV. *Reverse Osmosis system*

In the case of RO based systems like FO-RO (Figure 2) and single RO, the main cost is the high-pressure pumping electric cost. For this reason, RO systems are usually designed with a pressure exchanger as an energy recovery device to reduce the plant pumping costs (Appendix Table B1).

2.1.2. Operation cost (OPEX)

The OPEX are annualized expenses, which include operation and maintenance, membrane replacement, labor, energy (electricity, thermal or fossil), and consumables like draw solute in an FO driven treatment plant. Other operation cost like labor, chemicals, and maintenance and were estimated based on bibliography costs [129,149] (Table 2 and Appendix Table B2).

I. *Draw replenish and membrane-module replacement cost*

The NaCl draw replenish cost is a significant expense in any FO driven system, and this cost was calculated based on the specific reverse salt diffusion ($S_{diffusion}$). For a hybrid system like FO-MD and FO-RO, the diffusion estimation divides into two groups, the FO and the MD/RO stage. The $S_{diffusion}$ value in the FO stage was retrieved from Achilli, Cath & Childress (2010) [156].

For the RO scheme, the RO permeate concentration was used, previously retrieved from the design programs [151–155]. The MD stage draw solute was estimated using the theoretical rejection of MD (around ≥99.8%) [157,158].

The membrane replacement cost was treated as an amortized cost [159], where *i* is the interest rate, and *n* is the membrane lifetime (Table 2 and Appendix Table B2).

II. Heat sources and Electric demand

Thermal energy cost was based on the specific thermal energy consumption for the operation of the MD module (SEC_{MD}), calculated previously in the CAPEX section (Appendix Table A1). The heat source OPEX was estimated based on electric alternatives of a steam boiler and a thermal-fluid heater to avoid combustible transport cost and its associated expenses (Appendix Table B2). Thermal-fluid heaters have several advantages over a steam-driven system: no corrosion or caking, safer systems as they do not use pressurized fluid, less operation-maintenance cost (up to 75%), higher efficiency, do not require highly qualified operators, amount others [160–163]. Based on this data, a 70% cost reduction was included when using thermal-fluid (Appendix Table B2).

The primary electric consumption in FO and RO setups is the pump power requirement. In Table B2, the P and P_{RO} input represents the pressure pumping; in this case, 1 bar for FO and ~56 bar for RO. The pump efficiency η_p was assumed as 80%. The electricity cost (c_{elect}) presented in Table 4 represents the average price of one kWh for northern Chile [130].

2.1.3. Water Production Cost

The water production cost (WC) could be defined as the cost of producing a certain volume of clean water.

To calculate the WC was necessary to estimate the annualized capital cost (ACC) and annualized operation cost (AOC). The ACC is based on the estimation of system total capital cost (TCC), which is formed by direct capital cost (DCC) and indirect capital cost (ICC) (Appendix Eq. C1 & C2). The ACC was calculated as an amortized capital expenditure with a reasonable interest rate (Table 4) using Eq. C3 and the AOC by the sum of FO-MD and FO-RO OPEX costs (Appendix Eq. C4 & C5).

The WC was calculated based on the plant annualized costs divided by the water flow rate per year for each setup, FO-MDs (Appendix Eq. C6 & C7) and FO-RO (Appendix Eq. C8).

2.1.4. Single AMD RO plant design

In order to include a more robust economic design for a single RO plant, the Desalination Economic Evaluation Program (DEEP) package [164] was used in this study. A single RO plant was projected using DEEP with the total dissolved solids (TDS) from the original AMD sample (Chapter II, Table 1). The estimation of AMD TDS was performed using the IMS Design software capabilities [151].

The DEEP design was compared with two existing studies, Chong and Krantz (2018) and Linares *et al.* (2016), respectively [165,166] (Figure 3). Nevertheless, to compare studies with different capacities, it was necessary to adjust these CAPEX and OPEX costs. Large-scale costs could be estimated using the capacity method or size correction factor (SF) (Appendix Eq. C9), which allows projecting a new plant cost based on an existing study or design [129].

The SF method is applicable for downsizing or scaling. In this study, the reference designs were Linares *et al.* (2016) and Chong and Krantz (2018) [165,166], with a plant capacity of 100,000 m^3/d and 10,000 m^3/day, respectively.

2.1.5. Deterministic economic assessment

A deterministic economic assessment was performed based on CAPEX and OPEX results to determine the viability of projected plants. This assessment consisted of calculating the Net Present Value (NPV), the Internal Rate of Return (IRR), and the Payback Period (PP) based on the plants' cash flow for its 20 years' lifetime. For this analysis, some assumptions were made:

- The project is entirely self-financed.
- As wastewater plants usually do not have tangible cash income, the financial income was estimated as the savings of using reclaimed water instead of paying for freshwater.

In northern Chile, the water price is very high, up to 5.52 $/m^3 (Table 2), which will allow recovering the investment in a short period as no water has to be purchase.

- Another estimated income was the saving of treating the recovered AMD by a standard method like limestone [167,168].
- The discount rate was defined as 12% to represent a moderate investment risk.
- An annual increase of 2.5% for water price and a 7.3% annual increase in electricity price was considered for the analysis [130,131].
- An increasing future water demand was calculated using a tendency equation from the last reported water demands of Collahuasi mining plant (2016, 2017, and 2018) [127].

2.1.6. Probabilistic risk assessment

Additionally, to assess the uncertainty of some parameters, an aleatory Montecarlo model was developed (Appendix Table B3). This model was constructed using a free risk assessment software called ModelRisk from VOSE [169]. The boundary conditions of uncertain parameters are listed in Appendix Table B3. The FO and MD membrane prices were selected based on bibliography data, as mention in the CAPEX section. Draw solute boundaries correspond to the price-range of bulk NaCl purchase. Electricity values represent the variability in electric consumption prices in northern Chile.

3. Results and discussion

3.1. FO and MD performance with real AMD

In Chapter II, it was presented a series of experiments for FO and MD for short and long-term operation using AMD and NaCl as draw solution. Baseline assays were performed to evaluate the permeate flux and for choosing future operating conditions. These conditions were selected as 1M of NaCl at 60 °C (Chapter II, Section 3.1 & 3.2). With the operation conditions elucidated, continuous assays were performed for FO and MD, resulting in similar initial fluxes to baseline assays, around 23 LMH for FO and 10.5 LMH for MD (Chapter II, Section 3.3). Nevertheless, a constant water flux decline was observed throughout the FO

experiment, reaching around 6 LMH at the end of the assay. In the case of MD, no significant flux decline was observed during the experiment.

For further economic assessment, a mean FO flux of 13 LMH and 10 LMH for the MD stage were selected as design parameters. The selected FO flux value corresponds to the point when measured flux reduced to 50% (Chapter II, Figure 8a). As no significant flux reduction was observed during MD continuous assay (Chapter II, Figure 8b), the selected value was similar to the experimental result (10 LMH).

3.2. Technological and Economic assessment

A large-scale FO-MD and FO-RO plants were design based on previously presented experimental data. The FO stage design was equivalent for both configurations, FO-MD and FO-RO. The MD step was conceived and projected with a steam boiler and a thermal-fluid heater (Appendix Table B1 & B2). The RO stage was also designed using the CAPEX and OPEX procedures (Table B1 & B2); however, some parameters were estimated with the assistance of different RO design software (Table 3).

Table 3 presents the RO step design results from the FO-RO setup. The mean value of every calculated parameter was used to describe a representative RO plant, regardless of the different characteristics and design aspects of every company.

Table 3. Design parameters retrieve from different RO design software.

Parameter	IMS Design [151]	CSMPRO [152]	Q+ [153]	Winflows [155]	DS2 [154]	Mean Value
N. Membrane Modules ($n_{modules}$)	8	8	8	8	8	8
N. Pressure Vessels ($n_{vessels}$)	187	100	105	125	125	128
N. Elements ($n_{elements} = n_{modules} * n_{vessels}$)	1122	800	840	1000	1000	1024

3.3. Overall Economic Assessment

Both hybrid FO-RO and FO-MD systems were compared in terms of total capital cost and total operation cost. Alongside these simulated hybrid designs, two RO plants reported in the literature [165,166] were included, as well as a RO design using DEEP [164] (Figure 3).

Figure 3 shows interesting results, where hybrid configurations had similar capital costs to single RO based systems (between 22-26 MM $). Nevertheless, in the case of the FO-RO setup, the capital cost was even lower than single RO plants. This cost behavior could be explained as single RO plants require an intense pretreatment stage, typically formed by chemical addition, conventional granular media filtration, a micro/ultrafiltration step, or a combination thereof [170]. Linares *et al.* (2016) [166] based on the design of Shafer *et al.* (2012) [170], which included a pretreatment stage with membrane filtration.

On the other hand, Chong and Krantz (2018) [165] did not mention if the pretreatment stage had a membrane filtration step. Nonetheless, they estimated that pretreatment associated costs were more than 12% of the total CAPEX. This high percentage could be due to a micro/ultrafiltration step. Another example is the Collahuasi mine wastewater treatment plant, which includes sedimentation, dissolved air flotation, media filtration, activated carbon filtration, ultrafiltration, and reverse osmosis [171].

Opposite to the RO intense pretreatment stage, the FO-RO design of this study had only a standard granular media filtration before the FO step. Due to the high resistance to fouling of FO membranes, there is no need for a micro/ultrafiltration step, which helped to achieve a lower CAPEX than single RO setups (Figure 3). This result demonstrates the potential of using hybrid configurations for reclaiming water from concentrated waste solutions from the capital cost perspective.

Nonetheless, a significant disadvantage arises when comparing hybrid setups with single RO systems in terms of operation cost (Figure 3). The hybrid configurations OPEX was more than ten times the OPEX of single RO designs in some cases. The FO-MD setups had the highest cost of all setups, due to the steam boiler and thermal-fluid heater operation cost. In the case of FO-RO, results showed an operation cost less than FO-MDs but higher than single RO plants. This difference in OPEX between FO-RO and single RO could be explained by a

higher FO membrane replacement cost and the FO draw solute replenish cost. These aspects will be discussed in the OPEX section.

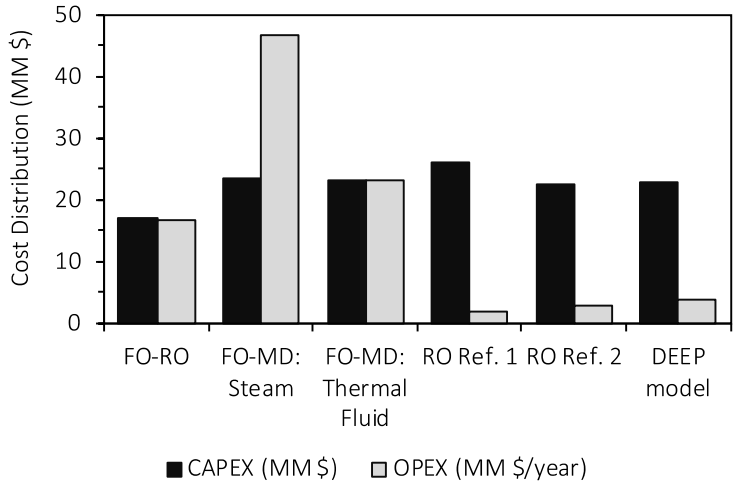

Figure 3. Cost distribution of projected membrane setups and single RO plants. RO Reference 1 & 2 are Chong and Krantz (2018) and Linares *et al.* (2016), respectively [165,166]. The FO-MD and FO-RO plant capacity was 29848 m^3/day [127].

3.4. Capital Expense (CAPEX) and Operation expense (OPEX)

Figure 4a shows the CAPEX distribution results of the projected wastewater plants, where the main capital cost was the FO and MD membrane purchase cost. Since FO and MD are not fully commercialized technologies, this causes the price of membranes and modules to be very high, especially in the plate and frame setup (our design).

Other relevant capital costs like site-development and indirect costs were estimated as a percentage of the total CAPEX. As these technologies become more attractive to the wastewater industry, membrane and module prices will decrease and with them the site-development and indirect costs of the project.

Operation cost distribution (Figure 4b) shows a predictable result with the main expense in MD-based plants been the energy used for heat production, using either a steam boiler or a thermal-fluid heater. The heat production cost has not much room for improvement since the system was based on high-efficiency electric systems. Another solution to the high heat

demand would be the use of low-grade waste heat; however, there is not any available waste heat source near the location of the projected plants (mining processing sites).

The economic assessment revealed an interesting outcome with FO solute replenishment cost been the second-highest cost for MD-based plants and first for the FO-RO setup. In order to reduce the draw replenishment cost, it is essential to understand that this cost is directly related to the solute molecular diffusion. The projected plant uses NaCl as its draw solute, which has a molecular diffusion of 1.485×10^{-9} m^2/s [172]. Other potential draw solutes like $CaCl_2$, $MgCl_2$, and $MgSO_4$ have lower molecular diffusion than NaCl; however, their associated cost could be more than double the cost of NaCl [156]. According to Achilli *et al.* (2010) [156], the best draw solute should have a balance of high flux, low molecular diffusion, and low purchase cost. Achilli *et al.* (2010) [156] analyzed 12 different salts (including NaCl) and concluded that $MgCl_2$ is the best draw solute alternative. The other characteristic that makes $MgCl_2$ most suitable for most FO applications is its low membrane scaling as magnesium scales can be formed only at high pH>9 [156].

(a)

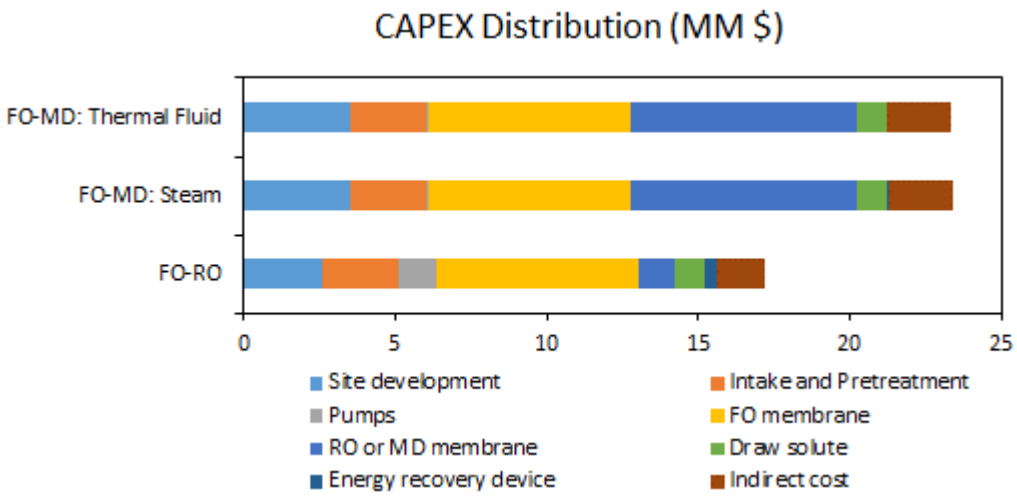

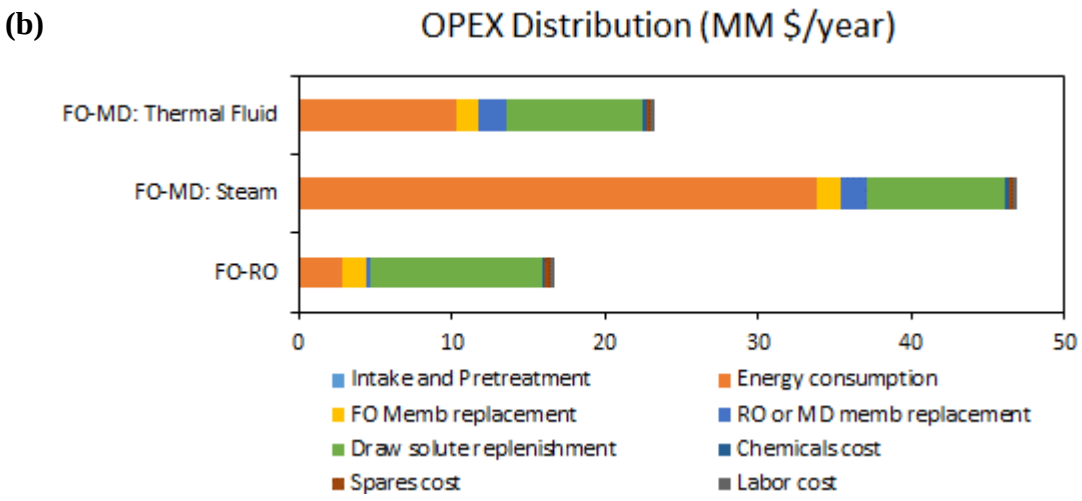

Figure 4. Cost distributions between FO-RO, steam FO-MD, and thermal-fluid FO-MD: **a)** Capital Costs and **b)** Operation and Maintenance Costs. The FO-MD and FO-RO plant capacity was 29848 m^3/day [127].

For the FO-RO setup, the electric consumption by high-pressure pumping was the second-highest operation expense, follow by FO replacement cost. Nonetheless, only small energetic improvements could be achieved for the RO stage since it was designed with a pressure exchanger as the energy recovery device (ERD).

MD and FO membrane replacement costs were similar in magnitude and represented between 3-4% of the total OPEX for FO-MD setups. Although the FO membrane price was higher than MD's (Table 2), a higher MD membrane area was required to match FO water production due to its lower flux (Table 1). Nevertheless, the FO replacement was six times more expensive than RO's and signified 9% of the total operation cost for the FO-RO design. Furthermore, some FO manufactures like Porifera sell the membrane and module as a single compact element, which makes it extremely expensive (up to 7000 $ per module) [132]. The main disadvantage of this compact design is that every time the membrane needs to be replaced, a whole new module has to be purchased. In the case of MD, membranes and modules are sold separately, which reduces the cost of replacements since modules have a longer lifetime than membranes.

As mentioned before, for FO or MD to become competitive against RO, the purchase prices have to decrease; unless these systems are applied in cases where RO is not suitable.

3.5. Total Water Cost

Economical FO-RO studies have shown that production cost could range around 0.4-1.32 $/m^3 depending on the feed solution, the membrane used, draw solution concentration [132,138,173]. The water production cost of the projected FO-RO plant was 1.467 $/m^3, similar to the upper boundary from the mentioned range, 0.4-1.32 $/m^3 [132,138,173]. Nonetheless, the continuous experiment was performed using raw sample AMD, which decrease the FO flux due to fouling. This low FO flux and the plant high capacity of 14924 m^3/day, could explain the increase in cost per volume of reclaimed water.

On the other hand, reclaimed water cost from FO-MD was 9.941 $/m^3 when using steam and 5.118 $/m^3 for thermal-fluid. FO-MD is a low-energy demand system. Nevertheless, when large volumes of fluid are required to be heated, the heat production cost became significant. Although production cost using FO-MD seems high comparing to FO-RO, some authors achieved even higher cost results. Aydiner *et al.* (2014) [125] performed an economic model analysis for treating food industry wastewater and achieve costs around 11.25 and 17.33 $/m^3, using heat recovery and without heat recovery, respectively. In addition, a complete economic study by Toy *et al.* (2017) [174] projected a high TDS (59,442 mg/L) FO-MD plant system, with costs of 9.06 $/m^3 with waste heat recovery of 40% and 14.53 $/m^3 without waste heat (paid heat/cool).

3.6. Deterministic sensibility economic assessment

As mentioned before, three economic parameters (NPV, IRR and PP) were calculated for the projected hybrid plants with cash flow for 20 years' lifetime. These parameters were estimated using two conditions for the NaCl cost; a lab-scale price and the price for bulk purchases (Table 4). Results shown in Table 4 revealed that the high operation-maintenance cost of using a steam boiler ended, making the project noon profitable. On the other hand, when using a thermal-fluid system, the project became profitable, and the investment is paid between around one and a half years and three and a half years, depending on the draw solute cost. Three studies have reported the PP of an FO-MD plant, and these PP values range from 0.68-2.35 years [125,175,176]; however, the lower values of this range correspond to the use of a waste-heat source.

Table 4. Economic indicators for FO-MD

Economic Parameter	FO-MD with steam		FO-MD with thermal-fluid	
	NaCl: lab price (2.27 $/kg)	NaCl: bulk price (0.1 $/kg)	NaCl: lab price (2.27 $/kg)	NaCl: bulk price (0.1 $/kg)
Net present value (NPV)	-3.19×10^8 $	-2.46×10^8 $	2.05×10^7 $	9.42×10^7 $
Internal Rate of Return (IRR)	-	-	29%	71%
Payback Period (PP)	-	-	3.5 years	1.7 years

Nonetheless, when comparing to FO-RO (Table 5), the FO-MD setup is a less profitable alternative with more than double the value of IRR. This profitability is also reflected in the Investment PP with around one year for the FO-RO invested capital to be paid-off. Other studies have reached similar FO-RO results of a one-year PP threshold [125,175,177].

An interesting result was the low PP achieved by both configurations. This behavior could be explained by the significant saving of using reclaim water instead of buying large volumes of expensive freshwater (5.52 $/m^3) for the mining operation.

The FO-MD design has two main advantages over the FO-RO plant. The first possible advantage is the use of a low-grade waste heat source to reduce the heat generation cost, which is the main expense in an MD driven technology. The other advantage of using MD over RO is the capacity to achieve very high recovery rates with simple in-place plant modifications. While RO usual ranges from 35-60% recovery rate [15,116,178], MD can reduce the discharge rate by up to 90% [121,126,179].

Table 5. Economic indicators for FO-RO.

Economic Parameter	NaCl: lab price (2.27 $/kg)	NaCl: bulk price (0.1 $/kg)
Net present value (NPV)	2.57×10^8 $	4.86×10^8 $
Internal Rate of Return (IRR)	89%	161%
Payback Period (IPP)	1.4	1

Opposite to RO, which is a well-established technology with very defined cost range, FO and MD are less explored in terms of pilot-scale or full-scale exploitation. Based on this premise,

a Montecarlo model was developed to address the uncertainty of some critical parameters like; membrane-module cost or draw solute bulk cost.

3.7. Probabilistic risk assessment

As mentioned before, an aleatory Monte Carlo model (VOSE's ModelRisk [169]) was developed to assess the uncertainty of some parameters (Appendix Table B3). The simulation ran with 100,000 iterations, which guaranteed good quality in the results. Model results show there is a 95% probability that the thermal fluid project has a positive NPV and up to $12x10^7$ $ (Figure 5), which is 1.3 times the revenue calculated by deterministic methods (Table 4). There is a 76% probability of achieving the deterministic NPV results ($9.42x10^7$ $) presented in Table 4. The thermal fluid setup had only a 5% probability of becoming unprofitable (Figure 6). On the other hand, the probabilistic risk modeling reinforces the unprofitability of using steam as heat-source for this project.

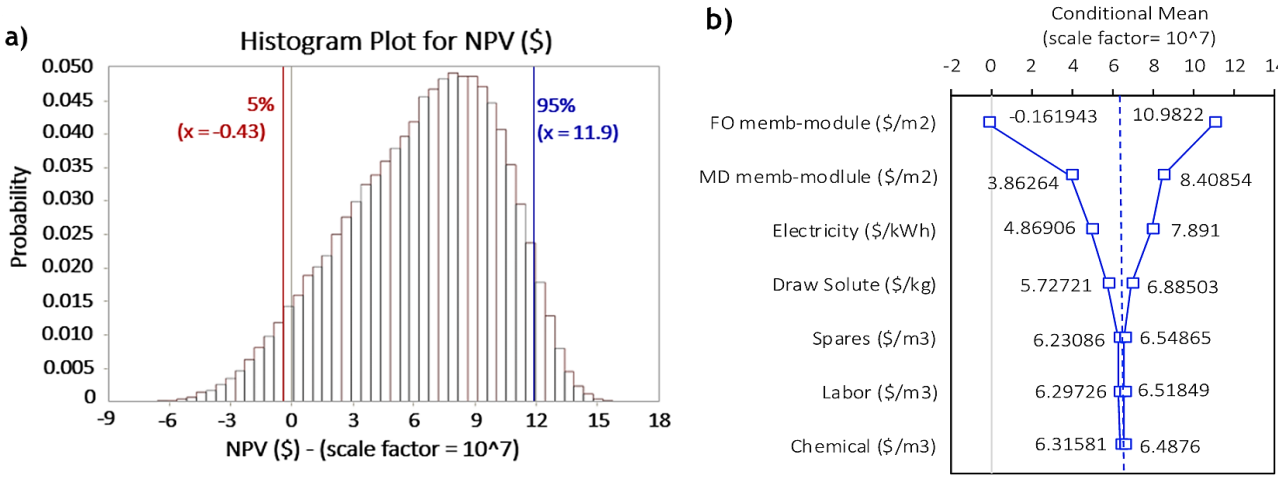

Figure 5. Monte Carlo model results. **a)** Net present value histogram plot of the FO-MD setup with thermal-fluid as heat-source. **b)** Net present value tornado plot of the FO-MD setup with thermal-fluid as heat-source.

A sensibility tornado plot (Figure 5b) was created to address which uncertain parameter from Table 6 had the highest impact on the economic model. This tool revealed that the FO and MD memb-module parameters had the most substantial impact on the model results. The Monte Carlo model identified from a wide range of possible costs (Appendix Table B3) the cost of FO and MD as 795 $/m^2 and 295 $/m^2, respectively, as the most likely cost values after 100,000 iterations. Another interesting outcome was that the stochastic model identified

that if the FO membrane-module cost increases up to 900 $/m^2, the thermal-fluid FO-MD setup could become unprofitable.

4. Conclusions

Alternative technologies like FO and MD have a considerable potential against traditional desalination processes like RO. FO and MD setups achieved similar flux performance, around 14 and 10 LMH, respectively. Nevertheless, this performance could be significantly improved by membrane spacers, which enhance the transmembrane flux and reduce fouling. As mentioned previously, another possible improvement will be replacing NaCl for $MgCl_2$, a draw solute with a low predisposition to membrane scaling. Further studies must be completed to assess the impact of membrane spacer and $MgCl_2$ draw solute on the system's economics and continuous performance.

Nonetheless, these technologies need to be established in the industry and be embraced by more membrane manufacturers, which will reduce the current high purchase cost of FO and MD membranes. In order for FO and MD to become competitive in the water reclamation industry, membrane cost should decrease to the cost range of RO membranes, between 30-50 $/m^2.

The economic assessment showed that using thermal-fluids is a cost-effective alternative against traditional steam boilers. Nevertheless, if a low-grade waste heat or a renewable energy source is available, the operating cost could be lowered to the point where FO-MD setups are a fair competitor to RO systems, even with the actual membrane cost.

5. Acknowledgment

The authors wish to express their thanks for the financial support provided by CONICYT/FONDECYT project Nº 3160398, FONDECYT project Nº 1191230 and for the scholarship grant of CONICYT Nº 21160046. Authors also thanks the support provided by CRHIAM center (ANID/FONDAP/15130015).

CHAPTER V:

General Discussion

Chapter V: General discussion.

The feasibility of using hybrid membrane setups for reclaiming water from acid mine drainage (AMD) was performed in this study, through a series of steps and chapters.

In Chapter II, it was presented an FO-MD design for water reclamation from acid mine drainage wastewater. The FO-MD design performs as a dual membrane filtration system, achieving high rejections ratios (98-99%). Here the FO membrane is in direct contact with a raw AMD solution and MD acts as a high purity water production step while keeping the initial FO draw solution concentration.

Tap-water assays were performed with both FO and MD membranes using different draw solute (NaCl) concentrations and temperatures, to identify the highest achievable fluxes with the current lab setup. Later, AMD was used as feed solution to assess the real initial flux performance of the FO step. In both assays, tap-water and AMD, results were similar, with FO fluxes increasing with higher concentrations of NaCl as well as a slight flux improvement with higher temperatures. Nevertheless, AMD flux results had a flux reduction of 35% compared to tap-water. This outcome was related to the smaller osmotic pressure potential between NaCl draw solution and AMD, as well as the external concentration polarization effect, caused by the accumulation of AMD ions on the active layer of the membrane.

FO and MD mathematical models were designed and validated with tap-water results, showing a high correlation coefficient. Nevertheless, when using AMD as feed solution, the FO modeling failed to predict the experimental fluxes, caused mainly by the external concentration polarization phenomenon. In the case of the MD model, it showed good results for every concentration and temperature of the NaCl solution, achieving a high correlation value.

To performed a continuous test run with AMD, it was necessary to select operation conditions that promoted the highest flux with the lowest NaCl concentration and temperature. Analyzing baseline AMD experimental results, a concentration of 1M NaCl at 60°C was selected as the optimal operation condition for this setup. Continuous AMD assay achieved a high initial flux (~25 LMH), but after one hour, the fouling and external polarization effect

was evident. These phenomena cause the membrane flux to decrease until the end of the assay at 50% water recovery.

At the end of the experiment, it was found that the fouling layer occupied around 50% of the membrane area, which explains the high flux reduction experienced in the assay. The fouling cake was analyzed using SEM-EDX, and results showed a thick precipitate layer around the same thickness of the membrane, which acted as a physical barrier to transmembrane flux. All major elements present in the AMD sample were found in the membrane. Nevertheless, this was not the case for copper and sulfate, where only low quantities were present on the membrane. The FO membrane acted as a successful barrier to these elements, leaving most of them in the concentrated solution and showing a high rejection ratio at the end of the experiment (~90% for sulfate and ~95% for cooper). At the end of this chapter, two main issues were found, a low MD flux performance and a critical fouling deposition on the FO membrane. The next chapter was designed to study a simple solution to overcome these drawbacks; this solution was the use of membrane spacers.

Chapter III presented a new kind of 3D printed membrane spacer for flat sheet modules. These spacers were tested in a membrane distillation configuration; however, the flux and fouling resistance improvements shown in this chapter could be translated for FO membranes as well. In this chapter study, the goal was to reduce the volume of a RO concentrate obtained from the Sydney Olympic Park water reclamation plant. This RO concentrate had a high inorganic and organic content, which limited the recovery rate for the RO plant. The 3D printed spacers were compared with a net commercial spacer and using no spacer in terms of flux and fouling improvement.

MD assay results showed a significant flux enhancement (around 2.7 times) when using the 3D printed spacers. Nevertheless, a higher pressure drop was unavoidable due to the unique shape of the 3D spacers. These spacers also showed better organic fouling mitigation capacity, which was measure through the membrane hydrophobicity and the organic mass deposition. When treating the RO concentrate, the standard configuration (no spacer) lost around 96% of the membrane hydrophobicity, mainly due to the high organic content of the feed solution. On the other hand, this hydrophobicity loss was reduced by 60% when the 3D spacers were used instead. Nevertheless, in order to reduce the organing content of the RO

concentrate and achieve higher concentration rates, a pretreatment by activated-carbon was implemented. Once lowered the organic content, it was possible to achieve a high recovery rate (85%).

Three cycles of MD operation was tested to assess the long-term performance of this setup. All three cycles achieved an 85% recovery rate with a low flux decrease between cycles. Using the 3D printed spacer mitigate the fouling formation, and experimental flux during each cycle was reduced by only 25%, which allow recovering the initial flux after a cleaning procedure. Results showed that in-place cleaning between cycles with a 0.1% citric acid had the best flux recovery.

In Chapter IV, two different hybrid setups, FO-RO and FO-MD, were designed and compared with single RO systems. The plant designs were based on the continuous-assays flux results presented in Chapter II, and the water volume required for the Collahuasi mining company operation. An economic model and assessment were performed in order to compare each configuration and technology.

The economic model highlighted that in terms of capital costs, all systems were similar; however, the FO-RO setup had the lowest CAPEX of all. Mainly because it does not need and intense pretreatment step like single RO plants, and does not need heat exchangers like FO-MD. Another reason for the lower CAPEX is that when comparing FO-RO with FO-MD, the RO membranes are considerably cheaper than MD membranes.

The OPEX results showed that the FO-MD design had de highest operation cost, mainly attributed to the heat production cost for the functioning of the MD stage. Of the two proposed FO-MD designs, the steam variant had a higher thermal production cost comparing with the thermal-fluid alternative. An interesting outcome resulted from the OPEX modeling, where the draw solute replenish cost was the second-highest expense for FO-MD and the first in the case of FO-RO. This highlights the necessity of choosing a draw solute with a low reverse salt diffusion to prevent mayor expenses in replenishing this substance.

Results from a deterministic economic assessment showed that when comparing steam and thermal-fluid as heat sources for the MD stage, the steam setup was not a cost-effective alternative. The steam solution yielded a negative net present value (NPV), which from an

investor point of view, this investment becomes unprofitable. On the other hand, the FO-MD using thermal-fluid as heat source showed a positive NPV and a payback period (PP) of around two years. Nonetheless, this result fell short when compared with the FO-RO configuration. This assembly had a PP of only one year, becoming the more cost-effective hybrid design of the study.

Lastly, an aleatory Monte Carlo model was developed to assess the uncertainty of some parameters in the model. This simulation showed that the purchase cost of FO and MD membranes had the highest impact in the economic model. This behavior was due to the extensive price range found in the literature for FO and MD purchase cost, which is caused by the fact that these technologies are not fully commercialized and implemented.

Results from the present thesis revealed the potentiality of using FO-MD to treat and reclaiming water from AMD. Nevertheless, during experimental assays, a severe fouling deposition was found on the FO membrane, which provoke more than 50% flux reduction in 12 hours in continuous mode (Chapter II, Figure 8). The membrane fouling found on FO assays was attributable to the lack of high turbulence inside the module, which produced low wall-shear stress, allowing the severe deposition of foulant particles (Chapter II, Figure 9) and the development of high external concentration polarization. In the case of MD, it was not found any flux reduction due to fouling; however, the overall flux performance was lower compared to FO´s. The lower flux performance of the MD membrane was due to the presence of a high temperature polarization caused by the absence of high turbulence inside the module, which is explained in Chapter III when comparing flux improvement using spacer-filled and non-filled modules (Chapter III, Figure 4).

The results of the membrane spacer studies reveal that the using spacers improved either the membrane flux and the membrane fouling defense significantly, even when using a complex feed solution like a municipal wastewater treatment byproduct (RO concentrate). The hydrodynamic improvement and fouling mitigation capabilities of using spacers are regardless of the type of membrane used, meaning that if applied to any membrane system, the same overall improvement can be expected. Extrapolating these results to a system using AMD as feed, it is expected to have even better improvement results due to the composition

of AMD, high presence of inorganic element but no significant presence of organic compounds (most recalcitrant fouling type).

During the FO-MD economic assessment section (Chapter IV) it was identified the membrane purchase cost and the thermal energy expense as the elements with the highest impact on the economic indicators (Chapter IV, Figure 4). The flux improvement and foiling mitigation of using spacers will allow extending the lifetime of the FO and MD membranes in a full-scale application, decreasing the membrane replacement ratio and associated cost. In addition, with a higher flux per membrane, a lower permeation area will be required, which will decrease the overall membrane purchase cost. Applying high-performance spacers could be a solution to mitigate the effect of purchasing expensive FO and MD membranes. If spacers are combined with an energy solution like using a renewable energy source or a waste-heat source, the FO-MD system cost could be decreased to the operation cost range of the FO-RO and RO system, allowing positioning the FO-MD alternative as a viable solution to address high concentrated industrial wastewaters.

CHAPTER VI:

General Conclusions

Chapter VI: General Conclusions

This thesis research has shown the vast potential of FO-MD for recovering water from highly concentrated wastewaters. Nevertheless, some improvements could be applied to the FO-MD setup in order to match or surpass the outcomes of RO based systems. Experimental assays showed that the system flux performance was limited due to the appearance of a fouling layer in the FO membrane. MD flux results were not affected by fouling; however, the achieved flux was half the initial value of FO. To overcome the difference between FO and MD fluxes, a higher MD membrane area was required to match the FO permeate volume. This higher membrane area is directly related to a higher membrane capital (CAPEX) and operation (OPEX) cost due to a higher membrane replacement expense.

Two high-performance membrane spacers were presented in this study as a simple solution to enhance the MD flux (to reduce membrane area) and avoiding critical fouling in long-term FO and MD applications. These cutting-edge designs for membrane spacers could increase the membrane flux up to 200% if applied under the right conditions. Although these spacers were studied in an MD setup, the same flux improvement and fouling mitigation capabilities will apply in any membrane system, like FO for example. This improvement is directly translated in a reduction of the required membrane area for FO and MD, lowering the overall plant CAPEX and OPEX associated costs.

The selection of the draw solution also plays a crucial role in the performance of an FO system. Choosing a solute that generates a high osmotic pressure, with a low solute diffusion, will ensure higher membrane fluxes while minimizing the draw solute replenish cost. In this study, the replenish expense was identified as the highest FO associated cost alongside the FO membrane purchase cost.

Another significant improvement will be the use of a low or high-grade waste-heat source from a closeby industry or an indoor thermal process. The use of waste-heat will remove partially or entirely the heat production cost from the equation, which is the highest operation cost in an MD based system. If there is no nearby waste heat available, a renewable energy source could be used instead. Since the FO-MD setup was projected in a northern Chile

location where solar radiation values are one of the highest worldwide, solar energy could be used to fulfill the energy requirement of the MD stage.

By implementing all or some of these solutions, the FO-MD capital and operating cost could be lowered to the point where this setup can become a fair competitor to RO systems, even with actual membrane costs. With the increasing application of these technologies worldwide, the purchase membrane cost will be reduced as the market will regulate the price of these membranes. Taking into consideration the mentioned suggestions in the study, FO-MD could become a leading technology in the desalination and water reclamation industry.

CHAPTER VII:

Appendices

Appendices:

Chapter I Appendix:

Table A1. Coefficients and expressions used in FO and MD models.

N.	Model coefficients	Expression
1	Water permeability coefficient, A	Constant
2	Solute permeability coefficient, B	Constant
3	Draw solution osmotic pressure, π_{draw}	Van't Hoff's equation
4	Feed solution osmotic pressure, π_{feed}	Van't Hoff's equation
5	Mass transfer coefficient, Km	$K_m = \frac{D_d}{S}$
6	Draw solute diffusion coefficient, D_d	Constant
7	Membrane structural parameter, S	$S = \frac{\tau * l}{\varepsilon}$
8	Tortuosity, τ	Constant
9	Actual thickness, l	Constant
10	Porosity of the porous support layer, ε	Constant
11	Solute resistivity for diffusion within the porous support layer, K	$K = \frac{1}{K_m}$
12	Mass transfer coefficient, k	$k = \frac{Sh * D_f}{d_h}$
13	Feed solute diffusion coefficient (copper sulfate diffusion value was used for the AMD), D_f	Constant
14	Hydraulic diameter of the channel, d_h	Constant
15	Sherwood number (For laminar flow), Sh	$Sh = 1.85\left(Re * Sc\frac{d_h}{L}\right)^{0.33}$
16	Sherwood number (For turbulent flow), Sh	$Sh = 0.04 * Re^{0.75} * Sc^{0.33}$
17	Reynolds number, Re	Constant
18	Length of the channel, L	Constant
19	Schmidt number, S_c	$Sc = \frac{\mu}{\rho * D_f}$
20	Feed solution viscosity (water values were used), μ	Constant
21	Feed solution density (water values were used), ρ	Constant
22	Activity coefficient, γ_w	$\gamma_w = 1 - 0.5x_{NaCl} - 10x_{NaCl}^2$
23	Water vapor pressure by Antoine Equation [60]	$P_{w.p}^0 = \exp\left(23.1964 - \frac{3816.44}{-46.13 - T}\right)$
24	Feed vapor pressure based on Raoult's law [60,180]	$P_{w.f}^0 = (1 - 2 * x_{NaCl}) * 1000 * exp\left(16.3872 - \frac{3885.2}{T - 42.96}\right)$

Chapter III Appendices:

1.1. Appendix A: Supplementary information

Membrane Properties

For the FO process, a thin-film composite (TFC) membrane from Porifera Inc. (FOMEM-0415 – Hayward, CA, USA) was used. The water (A_0) and salt (B_0) permeabilities of the membrane are 2.1 LMH*bar and $1.2x10^{-7}$ m/s, respectively. The structural parameter (S_0) was 334 µm, and the zeta potential (ζ) was −13.7±1.9 mV.

For the MD process, a Hydrophobic Polytetrafluoroethylene and Polypropylene (PTFE/PP) membrane was used in this study. The membrane was provided by Membrane Solutions (2202, No.1759 North Zhongshan Road, Shanghai 200061). Properties of the membrane are thickness 140-190 µm, pore size 0.22 µm and bubble point in a range of 0.04-0.05 MPa.

Draw solute

In the draw unitary cost expression, the M represents the molarity of NaCl solution (in this design one mol), *m* is the molecular mass of NaCl (58.44 g/mol). In the Table B1, the c_{solute} value corresponds to a lab-scale price, which costs will be reduced when purchasing bulk quantities of NaCl (Table 5).

Energy recovery devices: heat exchangers (HX) and pressure exchanger (PX)

For designing the steam HX, it was necessary to calculate the MD specific heat consumption (SEC_{MD}) [181–183] (Table B1), where T_{out} and T_{in} are the outlet and inlet temperature of the module, respectively (Table 4 & Figure 2b). In SEC_{MD} expression, the Cp_{water} is the water specific heat capacity (4.185 kJ/kg*C), ρ_w is the water density (997 kg/m^3). These values were used since only water vapor permeates through the MD membrane.

With SEC calculated, an HX area was define based on the temperature difference between the steam coming from a boiler and the MD feed (FO draw solution), respectively (Table B1 & Table 4). The $U_{gas\text{-}liquid}$ is the overall heat transfer coefficient, which value is 300 W/m^2*C for a tubular HX with gas at high pressure inside and liquid outside tubes.

The thermal-fluid HX design was based on the same methodology as for steam HX [181–183]. Nevertheless, the thermal-fluid heater works at higher temperatures than the steam

boiler (Table 4 & Figure 2b). The $U_{liquid\text{-}liquid}$ is the overall heat transfer coefficient, 3500 W/m^2*C for a liquid-liquid plate HX.

For the recovery HX, T_{out} and T_{in} are the outlet and inlet temperature of the liquid-liquid HX itself, respectively (Table 4 & Figure 2b). The $U_{liquid\text{-}liquid}$ was estimated in 3000 W/m^2*C, due to a lower heat transfer between water-water than water and thermal-fluid (3500 W/m^2*C). The cost of the three heat exchangers was calculated using the exchange areas as inputs [133].

1.2. Appendix B: Supplementary Tables

Table B1. Capital expenses modeling expressions.

CAPEX Parameters	Expression	Ref.
Intake and pretreatment (all systems)	$CC_{I\&P}(\$) = 658 * {Q_{Plant}}^{0.8}$	[149]
Feed pumps (FO-MD and FO-RO)	$CC_{Pump}(\$) = 4.78 \times 10^{-6} * Q_{Plant} * 120000$	[128,149]
High-pressure pumps (FO-RO and single RO)	$CC_{HP\ pump}(\$) = \frac{Q_{plant} * (393000 + 10710 * P_{RO})}{30000}$	[128]
FO and MD membranes and modules	$A_{Memb}(m^2) = \frac{Q_{perm}}{J_W}$ $CC_{Mem}(\$) = A_{Mem} * (C_{Mem} + C_{Module})$	
RO membranes and vessels	$CC_{RO\ mem}(\$) = (n_{elemts} * c_{RO\ mem} + n_{vessel}) * c_{vessel}$	
Draw solute (FO-RO and FO-MD)	$c_{unit\ draw}(\$/l) = M * m * c_{solute}$ $CC_{draw}(\$) = c_{unit\ draw} * Q_{perm} * T_{storage}$	
Heat exchangers (FO-MD)	$SEC_{MD}(kJ/day) = (Q_{Plant}/\rho_w) * Cp_{water} * (T_{out} - T_{in})$ $A_{HX}(m^2) = \frac{SEC_i}{U_i * \Delta T_m}$ $CC_{HX_i}(\$) = A_{HX_i} * C_{HX_i}$	[149]
Pressure exchanger (for RO)	$CC_{PX}(\$) = \frac{(Q_{plant} - Q_{perm}) * (393000 + 10710 * P_{RO})}{40000}$	[128]
Equipment	$CC_{Equip}(\$) = \Sigma CC_i$	[128]
Site development	$CC_{Site\ Dev}(\$) = CC_{Equip} * 0.2$	[128]
Direct capital cost	$DCC = CC_{Equip} + CC_{Site\ Dev}$	[128]
Indirect capital cost	$ICC = DCC * 0.1$	[149]

Table B2. Operation expenses modeling expressions.

OPEX Parameters	Expression	Ref.
Intake pump (all systems)	$OC_{I\&P}(\$/y) = \frac{0.028 * P * Q_{plant} * c_{elect}}{0.8} * T_{Plant\ Av} * 365$	[128]
Feed pumps (FO-MD and FO-RO)	$OC_{Pump}(\$/y) = \frac{0.028 * P * Q_{plant} * c_{elect}}{0.8} * T_{Plant\ Av} * 365$	[128]
High-pressure pumps (FO-RO)	$OC_{HP\ pump}(\$/y) = \frac{0.028 * P_{RO} * Q_{plant} * c_{elect}}{0.8} * T_{Plant\ Av}$	[128]
Booster Pump (FO-RO)	$OC_{Pump}(\$/y) = \frac{0.028 * (P_{RO} - P) * 0.95 * (Q_{plant} - Q_{perm}) * c_{elect}}{0.8} * T_{Plant\ Av} * 365$	[128]
Membrane replacement	$OC_{Mem}\ (\$/y) = \frac{i * (1+i)^n}{(1+i)^n - 1} * CC_{Mem}$	[159]
Draw solute replenishment (FO-RO and FO-MD)	$OC_{Draw}\ (\$/y) = S_{diffusion} * c_{draw} * Q_{FO_{perm}} * 365$	[156]
Steam boiler (for FO-MD)	$OC_{Boiler}\ (\$/y) = SEC_{MD} * c_{elect} * T_{Plant\ Av} * 24 * 365$	
Thermal fluid heater (for FO-MD)	$OC_{Heater}\ (\$/y) = SEC_{MD} * c_{elect} * T_{Plant\ Av} * 24 * 365 * 0.3$	
Chemical cost	$OC_{Chem} = c_{chem} * Q_{Perm} * T_{Plant\ Av} * 365$	[129,149]
Spares cost	$OC_{Spares} = c_{Spares} * Q_{Perm} * T_{Plant\ Av} * 365$	[129,149]
Labor cost	$OC_{Labor} = c_{labor} * Q_{Perm} * T_{Plant\ Av} * 365$	[129,149]

Table B3: Probabilistic distributions of uncertain parameters.

Parameter	Distribution	Boundaries
FO membrane price ($/m^2)	Triangular	Lower bound: 20 Most likely: 140 Upper bound: 1000
MD membrane price ($/m^2)	Triangular	Lower bound: 30 Most likely: 120 Upper bound: 350
Draw solute price ($/kg)	Triangular	Lower bound: 0.01 Most likely: 0.1 Upper bound: 0.5
Electricity price ($/kWh)	Triangular	Lower bound: 0.071 Most likely: 0.084 Upper bound: 0.099
Labor cost ($/m3)	Triangular	Lower bound: 0.01 Most likely: 0.03 Upper bound: 0.04
Spares cost ($/m3)	Triangular	Lower bound: 0.01 Most likely: 0.033 Upper bound: 0.04
Chemical cost ($/m3)	Triangular	Lower bound: 0.01 Most likely: 0.018 Upper bound: 0.03

1.3. Appendix C: Supplementary Equations

The following expressions were used to describe the total capital cost (TCC), which is formed by direct capital cost (DCC) and indirect capital cost (ICC).

$$TCC_{FO-MD}(\$) = DCC_{FO-MD} + ICC_{FO-MD} \quad \text{(C1)}$$

$$TCC_{FO-RO}(\$) = DCC_{FO-RO} + ICC_{FO-RO} \quad \text{(C2)}$$

The ACC was calculated as follow:

$$ACC_i(\$/y) = TCC_i * \frac{i*(1+i)^{T_{Plant}}}{(1+i)^{T_{Plant}}-1} \quad \text{(C3)}$$

The AOC was formed by the sum of FO-MD and FO-RO OPEX costs.

$$AOC_{FO-MD}(\$/y) = \Sigma OC_{FO} + \Sigma OC_{MD} \quad \text{(C4)}$$

$$AOC_{FO-RO}(\$/y) = \Sigma OC_{FO} + \Sigma OC_{RO} \quad \text{(C5)}$$

The WC was estimated with the following expressions:

$$WC_{\substack{FO-MD \\ steam}}(\$/m^3) = \frac{ACC_{FO-MD} + AOC_{FO-MD}}{365 * Q_{Perm} * T_{Plant\ Av}} \quad \text{(C6)}$$

$$WC_{\substack{FO-MD \\ thermal\ fluid}}(\$/m^3) = \frac{ACC_{FO-MD} + AOC_{FO-MD} - OC_{steam}}{365 * Q_{Perm} * T_{Plant\ Av}} \quad \text{(C7)}$$

$$WC_{FO-RO}(\$/m^3) = \frac{ACC_{FO-RO} + AOC_{FO-RO}}{365 * Q_{Perm} * T_{Plant\ Av}} \quad \text{(C8)}$$

The capacity method or size correction factor (SF) was estimated by:

$$SF = C_{Ref} * \left(\frac{Q_{Plant}}{Q_{Ref}}\right)^K \quad (9)$$

Where C_{ref} is the reference cost from the bibliography, Q_{plant} is the design plant capacity, Q_{ref} is the reference plant capacity.

Bibliography

[1] Al Fry, Facts and Trends: Water, 2006. doi:10.1080/0379772780030302.

[2] V. Lazarova, B. Levine, J. Sack, G. Cirelli, P. Jeffrey, H. Muntau, M. Salgot, F. Brissaud, Role of water reuse for enhancing integrated water management in Europe and Mediterranean countries, Water Sci. Technol. 43 (2001).

[3] P.A. Davies, Wave-powered desalination: resource assessment and review of technology, Desalination. 186 (2005) 97–109. doi:10.1016/j.desal.2005.03.093.

[4] Y. Liang, H. Zhu, G. Bã Nuelos, B. Yan, Q. Zhou, X. Yu, X. Cheng, Constructed wetlands for saline wastewater treatment: A review, Ecol. Eng. 98 (2016) 275–285. doi:10.1016/j.ecoleng.2016.11.005.

[5] S. Gössling, P. Peeters, C.M. Hall, J.P. Ceron, G. Dubois, L.V. Lehmann, D. Scott, Tourism and water use: Supply, demand, and security. An international review, Tour. Manag. 33 (2012) 1–15. doi:10.1016/j.tourman.2011.03.015.

[6] C.R. Martinetti, A.E. Childress, T.Y. Cath, High recovery of concentrated RO brines using forward osmosis and membrane distillation, J. Memb. Sci. 331 (2009) 31–39. doi:10.1016/j.memsci.2009.01.003.

[7] P. Zhao, B. Gao, Q. Yue, S. Liu, H.K. Shon, The performance of forward osmosis in treating high-salinity wastewater containing heavy metal Ni2+, Chem. Eng. J. 288 (2016) 569–576. doi:10.1016/j.cej.2015.12.038.

[8] Y. Nleya, G.S. Simate, S. Ndlovu, Sustainability assessment of the recovery and utilisation of acid from acid mine drainage, J. Clean. Prod. 113 (2016) 17–27. doi:10.1016/j.jclepro.2015.11.005.

[9] K.K. Kefeni, T.A.M. Msagati, B.B. Mamba, Acid mine drainage: Prevention, treatment options, and resource recovery: A review, J. Clean. Prod. 151 (2017) 475–493. doi:10.1016/J.JCLEPRO.2017.03.082.

[10] P. Meller, A.M. Simpasa, Role of copper in the Chilean & Zambian economies: main economic and policy issues, (2011).

[11] J. Oyarzún, R. Oyarzún, Sustainable development threats, inter-sector conflicts and environmental policy requirements in the arid, mining rich, northern Chile territory, Sustain. Dev. 19 (2011) 263–274.

[12] E.J. Lam, M. Cánovas, M.E. Gálvez, Í.L. Montofré, B.F. Keith, Á. Faz, Evaluation of the phytoremediation potential of native plants growing on a copper mine tailing in northern Chile, J. Geochemical Explor. 182 (2017) 210–217. doi:10.1016/j.gexplo.2017.06.015.

[13] COCHILCO, Chilean Copper Production by Product Type (Yearly and Monthly), 2017.

[14] N.P. Hankins, R. Singh, J. Buchheim, R.M. Wyss, C.-M. Kim, M. Deng, H.G. Park, Emerging Membrane Technology for Sustainable Water Treatment, 2016. doi:10.1016/B978-0-444-63312-5.00015-2.

[15] G. Blandin, A.R.D. Verliefde, J. Comas, I. Rodriguez-Roda, P. Le-Clech, Efficiently combining water reuse and desalination through forward osmosis-reverse osmosis (FO-RO) hybrids: A critical review, Membranes (Basel). 6 (2016) 37. doi:10.3390/membranes6030037.

[16] K.L. Hickenbottom, N.T. Hancock, N.R. Hutchings, E.W. Appleton, E.G. Beaudry, P. Xu, T.Y. Cath, Forward osmosis treatment of drilling mud and fracturing wastewater from oil and gas operations, Desalination. 312 (2013) 60–66. doi:10.1016/j.desal.2012.05.037.

[17] S. Zhang, P. Wang, X. Fu, T.S. Chung, Sustainable water recovery from oily wastewater via forward osmosis-membrane distillation (FO-MD), Water Res. 52 (2014) 112–121. doi:10.1016/j.watres.2013.12.044.

[18] K. Saito, M. Irie, S. Zaitsu, H. Sakai, H. Hayashi, A. Tanioka, Power generation with salinity gradient by pressure retarded osmosis using concentrated brine from SWRO system and treated sewage as pure water, Desalin. Water Treat. 41 (2012) 114–121. doi:10.1080/19443994.2012.664696.

[19] K. Lutchmiah, E.R. Cornelissen, D.J.H. Harmsen, J.W. Post, K. Lampi, H. Ramaekers, L.C. Rietveld, K. Roest, Water recovery from sewage using forward osmosis, Water Sci. Technol. 64 (2011) 1443–1449. doi:10.2166/wst.2011.773.

[20] J.C. Ortega-Bravo, G. Ruiz-Filippi, A. Donoso-Bravo, I.E. Reyes-Caniupán, D. Jeison, Forward osmosis: Evaluation thin-film-composite membrane for municipal sewage concentration, Chem. Eng. J. 306 (2016) 531–537. doi:10.1016/j.cej.2016.07.085.

[21] B. Vital, J. Bartacek, J.C. Ortega-Bravo, D. Jeison, Treatment of acid mine drainage by forward osmosis: Heavy metal rejection and reverse flux of draw solution constituents, Chem. Eng. J. 332 (2018) 85–91. doi:10.1016/j.cej.2017.09.034.

[22] B.D. Coday, C. Hoppe-Jones, D. Wandera, J. Shethji, J. Herron, K. Lampi, S.A. Snyder, T.Y. Cath, Evaluation of the transport parameters and physiochemical properties of forward osmosis membranes after treatment of produced water, J. Memb. Sci. 499 (2016) 491–502. doi:10.1016/j.memsci.2015.09.031.

[23] K.Y. Wang, M.M. Teoh, A. Nugroho, T.-S. Chung, Integrated forward osmosis–membrane distillation (FO–MD) hybrid system for the concentration of protein solutions, Chem. Eng. Sci. 66 (2011) 2421–2430. doi:10.1016/j.ces.2011.03.001.

[24] T.Y. Cath, D. Adams, A.E. Childress, Membrane contactor processes for wastewater reclamation in space: II. Combined direct osmosis, osmotic distillation, and membrane distillation for treatment of metabolic wastewater, J. Memb. Sci. 257 (2005) 111–119. doi:10.1016/j.memsci.2004.07.039.

[25] Q. Ge, P. Wang, C. Wan, T.S. Chung, Polyelectrolyte-promoted Forward Osmosis-Membrane Distillation (FO-MD) hybrid process for dye wastewater treatment, Environ. Sci. Technol. 46 (2012) 6236–6243. doi:10.1021/es300784h.

[26] P.M. Visakh, O. Nazarenko, Nanostructured Polymer Membranes, Volume 2: Applications, John Wiley & Sons, 2016.

[27] Y. Kim, S. Lee, H.K. Shon, S. Hong, Organic fouling mechanisms in forward osmosis membrane process under elevated feed and draw solution temperatures, Desalination. 355 (2015) 169–177. doi:10.1016/j.desal.2014.10.041.

[28] Chilean Mining Council, Anual Report, (2019). https://consejominero.cl/wp-content/uploads/2020/04/Reporte-Anual-CM-2019.pdf.

[29] Chilean Copper Commission (COCHILCO), COBRE Y OTROS MINERALE S YEARBOOK: COPPER AND OTHER MINERAL STATISTICS, 2019. https://www.cochilco.cl/Lists/Anuario/Attachments/20/AE2019avance.pdf (accessed September 19, 2020).

[30] F.D. Ardejani, G.H. Karami, A.B. Assadi, R.A. Dehghan, Hydrogeochemical Investigations of the Shour River and Groundwater Affected by Acid Mine

Drainage in Sarcheshmeh Porphyry Copper Mine, in: Proc. 10th Int. Congr. Mine Water Environ., Karlovy Vary, Czech Republic, 2008: pp. 2–5.

[31] D.K. Nordstrom, C.N. Alpers, C.J. Ptacek, D.W. Blowes, Negative pH and extremely acidic mine waters from Iron Mountain, California, Environ. Sci. Technol. 34 (2000) 254–258. doi:10.1021/es990646v.

[32] V. Milu, J.L. Leroy, C. Peiffert, Water contamination downstream from a copper mine in the Apuseni Mountains, Romania, Environ. Geol. 42 (2002) 773–782. doi:10.1007/s00254-002-0580-5.

[33] H. Al-Zoubi, A. Rieger, P. Steinberger, W. Pelz, R. Haseneder, G. Härtel, Nanofiltration of Acid Mine Drainage, Desalin. Water Treat. 21 (2010) 148–161. doi:10.5004/dwt.2010.1316.

[34] D. Aitken, D. Rivera, A. Godoy-Faúndez, E. Holzapfel, Water Scarcity and the Impact of the Mining and Agricultural Sectors in Chile, Sustainability. 8 (2016) 128. doi:10.3390/su8020128.

[35] L. Chekli, S. Phuntsho, J.E. Kim, J. Kim, J.Y. Choi, J.S. Choi, S. Kim, J.H. Kim, S. Hong, J. Sohn, H.K. Shon, A comprehensive review of hybrid forward osmosis systems: Performance, applications and future prospects, J. Memb. Sci. 497 (2016) 430–449. doi:10.1016/j.memsci.2015.09.041.

[36] D. Lu, Q. Liu, Y. Zhao, H. Liu, J. Ma, Treatment and energy utilization of oily water via integrated ultrafiltration-forward osmosis–membrane distillation (UF-FO-MD) system, J. Memb. Sci. 548 (2018) 275–287. doi:10.1016/J.MEMSCI.2017.11.004.

[37] M.S. Islam, K. Touati, M.S. Rahaman, Feasibility of a hybrid membrane-based process (MF-FO-MD) for fracking wastewater treatment, Sep. Purif. Technol. 229 (2019) 115802. doi:10.1016/J.SEPPUR.2019.115802.

[38] K. Sardari, P. Fyfe, S. Ranil Wickramasinghe, Integrated electrocoagulation – Forward osmosis – Membrane distillation for sustainable water recovery from hydraulic fracturing produced water, J. Memb. Sci. 574 (2019) 325–337. doi:10.1016/J.MEMSCI.2018.12.075.

[39] Y. Zhou, M. Huang, Q. Deng, T. Cai, Combination and performance of forward osmosis and membrane distillation (FO-MD) for treatment of high salinity landfill

leachate, Desalination. 420 (2017) 99–105. doi:10.1016/J.DESAL.2017.06.027.

[40] F. Volpin, L. Chekli, S. Phuntsho, N. Ghaffour, J.S. Vrouwenvelder, H.K. Shon, Optimisation of a forward osmosis and membrane distillation hybrid system for the treatment of source-separated urine, Sep. Purif. Technol. 212 (2019) 368–375. doi:10.1016/J.SEPPUR.2018.11.003.

[41] B.C. Ricci, B. Skibinski, K. Koch, C. Mancel, C.Q. Celestino, I.L.C. Cunha, M.R. Silva, C.B. Alvim, C.V. Faria, L.H. Andrade, L.C. Lange, M.C.S. Amaral, Critical performance assessment of a submerged hybrid forward osmosis - membrane distillation system, Desalination. 468 (2019) 114082. doi:10.1016/J.DESAL.2019.114082.

[42] P. Wang, Y. Cui, Q. Ge, T. Fern Tew, T.-S. Chung, Evaluation of hydroacid complex in the forward osmosis–membrane distillation (FO–MD) system for desalination, J. Memb. Sci. 494 (2015) 1–7. doi:10.1016/J.MEMSCI.2015.07.022.

[43] W. Suwaileh, D. Johnson, D. Jones, N. Hilal, An integrated fertilizer driven forward osmosis- renewables powered membrane distillation system for brackish water desalination: A combined experimental and theoretical approach, Desalination. 471 (2019) 114126. doi:10.1016/J.DESAL.2019.114126.

[44] S.-F. Pan, M.-P. Zhu, J.P. Chen, Z.-H. Yuan, L.-B. Zhong, Y.-M. Zheng, Separation of tetracycline from wastewater using forward osmosis process with thin film composite membrane – Implications for antibiotics recovery, Sep. Purif. Technol. 153 (2015) 76–83. doi:10.1016/J.SEPPUR.2015.08.034.

[45] G. Blandin, H. Vervoort, P. Le-Clech, A.R.D. Verliefde, Fouling and cleaning of high permeability forward osmosis membranes, J. Water Process Eng. 9 (2016) 161–169. doi:10.1016/j.jwpe.2015.12.007.

[46] S. Loeb, L. Titelman, E. Korngold, J. Freiman, Effect of porous support fabric on osmosis through a Loeb-Sourirajan type asymmetric membrane, J. Memb. Sci. 129 (1997) 243–249. doi:10.1016/S0376-7388(96)00354-7.

[47] J.R. McCutcheon, M. Elimelech, Influence of concentrative and dilutive internal concentration polarization on flux behavior in forward osmosis, J. Memb. Sci. 284 (2006) 237–247. doi:10.1016/j.memsci.2006.07.049.

[48] S. Phuntsho, S. Hong, M. Elimelech, H.K. Shon, Osmotic equilibrium in the

forward osmosis process: Modelling, experiments and implications for process performance, J. Memb. Sci. 453 (2014) 240–252. doi:10.1016/j.memsci.2013.11.009.

[49] T.Y. Cath, A. Childress, M. Elimelech, Forward osmosis: Principles, applications, and recent developments, J. Memb. Sci. 281 (2006) 70–87. doi:10.1016/j.memsci.2006.05.048.

[50] N. Akther, A. Sodiq, A. Giwa, S. Daer, H.A. Arafat, S.W. Hasan, Recent advancements in forward osmosis desalination: A review, Chem. Eng. J. 281 (2015) 502–522. doi:10.1016/j.cej.2015.05.080.

[51] H.K. Shon, S. Phuntsho, T.C. Zhang, R.Y. Surampalli, Forward Osmosis - Fundamentals and Applications, American Society of Civil Engineers, 2015. doi:10.1061/9780784414071.

[52] A. Basile, A. Figoli, M. Khayet, Pervaporation, Vapour Permeation and Membrane Distillation. Principles and Applications, Elsevier, 2015.

[53] B.B. Ashoor, S. Mansour, A. Giwa, V. Dufour, S.W. Hasan, Principles and applications of direct contact membrane distillation (DCMD): A comprehensive review, Desalination. 398 (2016) 222–246. doi:10.1016/j.desal.2016.07.043.

[54] R. Valladares Linares, Z. Li, S. Sarp, S.S. Bucs, G. Amy, J.S. Vrouwenvelder, Forward osmosis niches in seawater desalination and wastewater reuse, Water Res. 66 (2014) 122–139. doi:10.1016/j.watres.2014.08.021.

[55] M. Peleg, M.D. Normand, M.G. Corradini, The Arrhenius equation revisited., Crit. Rev. Food Sci. Nutr. 52 (2012) 830–851. doi:10.1080/10408398.2012.667460.

[56] M. Xie, W.E. Price, L.D. Nghiem, M. Elimelech, Effects of feed and draw solution temperature and transmembrane temperature difference on the rejection of trace organic contaminants by forward osmosis, J. Memb. Sci. 438 (2013) 57–64. doi:10.1016/j.memsci.2013.03.031.

[57] S. Phuntsho, S. Vigneswaran, J. Kandasamy, S. Hong, S. Lee, H.K. Shon, Influence of temperature and temperature difference in the performance of forward osmosis desalination process, J. Memb. Sci. 415–416 (2012) 734–744. doi:10.1016/j.memsci.2012.05.065.

[58] S. Shin, A.S. Kim, Temperature Effect on Forward Osmosis, in: Osmotically

Driven Membr. Process. - Approach, Dev. Curr. Status, 2018: pp. 87–110. doi:10.5772/intechopen.72044.

[59] C. Suh, S. Lee, Modeling reverse draw solute flux in forward osmosis with external concentration polarization in both sides of the draw and feed solution, J. Memb. Sci. 427 (2013) 365–374. doi:10.1016/j.memsci.2012.08.033.

[60] J.M. Smith, H.C. Van Ness, M. Abbott, H. Van Ness, Vapor/Liquid Equilibrium: Introduction, in: Introd. to Chem. Eng. Thermodyn., Sixth Edit, McGraw-Hill, 2010: p. 749.

[61] M. Kamali, D.P. Suhas, M.E. Costa, I. Capela, T.M. Aminabhavi, Sustainability considerations in membrane-based technologies for industrial effluents treatment, Chem. Eng. J. 368 (2019) 474–494. doi:10.1016/j.cej.2019.02.075.

[62] S. Lee, Y. Kim, J. Park, H.K. Shon, S. Hong, Treatment of medical radioactive liquid waste using Forward Osmosis (FO) membrane process, J. Memb. Sci. 556 (2018) 238–247. doi:10.1016/j.memsci.2018.04.008.

[63] X. Zhang, J. Tian, S. Gao, W. Shi, Z. Zhang, F. Cui, S. Zhang, S. Guo, X. Yang, H. Xie, D. Liu, Surface functionalization of TFC FO membranes with zwitterionic polymers: Improvement of antifouling and salt-responsive cleaning properties, J. Memb. Sci. 544 (2017) 368–377. doi:10.1016/j.memsci.2017.09.044.

[64] M.M.A. Shirazi, A. Kargari, M. Tabatabaei, Evaluation of commercial PTFE membranes in desalination by direct contact membrane distillation, Chem. Eng. Process. Process Intensif. 76 (2014) 16–25. doi:10.1016/j.cep.2013.11.010.

[65] S.T. Hsu, K.T. Cheng, J.S. Chiou, Seawater desalination by direct contact membrane distillation, Desalination. 143 (2002) 279–287. doi:10.1016/S0011-9164(02)00266-7.

[66] K. He, H.J. Hwang, M.W. Woo, I.S. Moon, Production of drinking water from saline water by direct contact membrane distillation (DCMD), J. Ind. Eng. Chem. 17 (2011) 41–48. doi:10.1016/j.jiec.2010.10.007.

[67] A. Rastegarpanah, H.R. Mortaheb, Surface treatment of polyethersulfone membranes for applying in desalination by direct contact membrane distillation, Desalination. 377 (2016) 99–107. doi:10.1016/j.desal.2015.09.008.

[68] Y. Huang, Q.L. Huang, H. Liu, C.X. Zhang, Y.W. You, N.N. Li, C.F. Xiao,

Preparation, characterization, and applications of electrospun ultrafine fibrous PTFE porous membranes, J. Memb. Sci. 523 (2017) 317–326. doi:10.1016/j.memsci.2016.10.019.

[69] S. Ryu, G. Naidu, A. Hasan, Y. Choi, S. Jeong, S. Vigneswaran, Chemosphere Acid mine drainage treatment by integrated submerged membrane distillation e sorption system, Chemosphere. 218 (2019) 955–965. doi:10.1016/j.chemosphere.2018.11.153.

[70] U.K. Kesieme, H. Aral, Application of membrane distillation and solvent extraction for water and acid recovery from acidic mining waste and process solutions, J. Environ. Chem. Eng. 3 (2015) 2050–2056. doi:10.1016/j.jece.2015.07.008.

[71] E.J. Hull, K.R. Zodrow, Acid Rock Drainage Treatment Using Membrane Distillation: Impacts of Chemical-Free Pretreatment on Scale Formation, Pore Wetting, and Product Water Quality, Environ. Sci. Technol. 51 (2017) 11928–11934. doi:10.1021/acs.est.7b02957.

[72] N. Sreedhar, N. Thomas, O. Al-Ketan, R. Rowshan, H. Hernandez, R.K. Abu Al-Rub, H.A. Arafat, 3D printed feed spacers based on triply periodic minimal surfaces for flux enhancement and biofouling mitigation in RO and UF, Desalination. 425 (2018) 12–21. doi:10.1016/j.desal.2017.10.010.

[73] N. Thomas, N. Sreedhar, O. Al-Ketan, R. Rowshan, R.K. Abu Al-Rub, H. Arafat, 3D printed triply periodic minimal surfaces as spacers for enhanced heat and mass transfer in membrane distillation, Desalination. 443 (2018) 256–271. doi:10.1016/j.desal.2018.06.009.

[74] E.H. Cabrera-Castillo, N. Thomas, O. Al-Ketan, R. Rowshan, R.K. Abu Al-Rub, L.D. Nghiem, S. Vigneswaran, H.A. Arafat, G. Naidu, 3D printed spacers for organic fouling mitigation in membrane distillation, J. Memb. Sci. 581 (2019) 331–343. doi:10.1016/j.memsci.2019.03.040.

[75] G. Naidu, S. Jeong, S. Vigneswaran, T.-M. Hwang, Y.-J. Choi, S.-H. Kim, A review on fouling of membrane distillation, Desalin. Water Treat. 57 (2016) 10052–10076. doi:10.1080/19443994.2015.1040271.

[76] D.M. Warsinger, J. Swaminathan, E. Guillen-Burrieza, H.A. Arafat, J.H. Lienhard

V, Scaling and fouling in membrane distillation for desalination applications: A review, Desalination. 356 (2015) 294–313. doi:10.1016/j.desal.2014.06.031.

[77] N. Thomas, M.O. Mavukkandy, S. Loutatidou, H.A. Arafat, Membrane distillation research & implementation: Lessons from the past five decades, Sep. Purif. Technol. 189 (2017) 108–127. doi:10.1016/J.SEPPUR.2017.07.069.

[78] G. Naidu, S. Jeong, Y. Choi, S. Vigneswaran, Membrane distillation for wastewater reverse osmosis concentrate treatment with water reuse potential, J. Memb. Sci. (2017). doi:10.1016/j.memsci.2016.11.068.

[79] G. Naidu, S. Jeong, M.A.H. Johir, A.G. Fane, J. Kandasamy, S. Vigneswaran, Rubidium extraction from seawater brine by an integrated membrane distillation-selective sorption system, Water Res. (2017). doi:10.1016/j.watres.2017.06.078.

[80] H.C. Duong, A.R. Chivas, B. Nelemans, M. Duke, S. Gray, T.Y. Cath, L.D. Nghiem, Treatment of RO brine from CSG produced water by spiral-wound air gap membrane distillation - A pilot study, Desalination. 366 (2015) 121–129. doi:10.1016/j.desal.2014.10.026.

[81] T.Y. Cath, V.D. Adams, A.E. Childress, Experimental study of desalination using direct contact membrane distillation: a new approach to flux enhancement, J. Memb. Sci. 228 (2004) 5–16. doi:10.1016/J.MEMSCI.2003.09.006.

[82] G. Naidu, W.G. Shim, S. Jeong, Y. Choi, N. Ghaffour, S. Vigneswaran, Transport phenomena and fouling in vacuum enhanced direct contact membrane distillation: experimental and modelling, Sep. Purif. Technol. 172 (2017) 285–295.

[83] H. Chang, J.A. Hsu, C.L. Chang, C.D. Ho, T.W. Cheng, Simulation study of transfer characteristics for spacer-filled membrane distillation desalination modules, Appl. Energy. 185 (2017) 2045–2057. doi:10.1016/j.apenergy.2015.12.030.

[84] J. Phattaranawik, R. Jiraratananon, A.G. Fane, Effects of net-type spacers on heat and mass transfer in direct contact membrane distillation and comparison with ultrafiltration studies, J. Memb. Sci. 217 (2003) 193–206. doi:10.1016/S0376-7388(03)00130-3.

[85] J. Seo, Y.M. Kim, J.H. Kim, Spacer optimization strategy for direct contact membrane distillation: Shapes, configurations, diameters, and numbers of spacer

filaments, Desalination. 417 (2017) 9–18. doi:10.1016/j.desal.2017.05.009.

[86] H. Yu, X. Yang, R. Wang, A.G. Fane, Analysis of heat and mass transfer by CFD for performance enhancement in direct contact membrane distillation, J. Memb. Sci. 405–406 (2012) 38–47. doi:10.1016/j.memsci.2012.02.035.

[87] C. Fritzmann, M. Wiese, T. Melin, M. Wessling, Helically microstructured spacers improve mass transfer and fractionation selectivity in ultrafiltration, J. Memb. Sci. 463 (2014) 41–48. doi:10.1016/J.MEMSCI.2014.03.059.

[88] J.-Y. Lee, W.S. Tan, J. An, C.K. Chua, C.Y. Tang, A.G. Fane, T.H. Chong, The potential to enhance membrane module design with 3D printing technology, J. Memb. Sci. 499 (2016) 480–490. doi:10.1016/J.MEMSCI.2015.11.008.

[89] A. Siddiqui, S. Lehmann, S.S. Bucs, M. Fresquet, L. Fel, E.I.E.C. Prest, J. Ogier, C. Schellenberg, M.C.M. van Loosdrecht, J.C. Kruithof, J.S. Vrouwenvelder, Predicting the impact of feed spacer modification on biofouling by hydraulic characterization and biofouling studies in membrane fouling simulators, Water Res. 110 (2017) 281–287. doi:10.1016/j.watres.2016.12.034.

[90] N. Sreedhar, N. Thomas, O. Al-Ketan, R. Rowshan, H. Hernandez, R.K. Abu Al-Rub, H.A. Arafat, 3D printed feed spacers based on triply periodic minimal surfaces for flux enhancement and biofouling mitigation in RO and UF, Desalination. 425 (2018) 12–21. doi:10.1016/j.desal.2017.10.010.

[91] W.S. Tan, S.R. Suwarno, J. An, C.K. Chua, A.G. Fane, T.H. Chong, Comparison of solid, liquid and powder forms of 3D printing techniques in membrane spacer fabrication, J. Memb. Sci. 537 (2017) 283–296. doi:10.1016/j.memsci.2017.05.037.

[92] M. Shakaib, S.M.F. Hasani, I. Ahmed, R.M. Yunus, A CFD study on the effect of spacer orientation on temperature polarization in membrane distillation modules, Desalination. 284 (2012) 332–340. doi:10.1016/j.desal.2011.09.020.

[93] Y. Taamneh, K. Bataineh, Improving the performance of direct contact membrane distillation utilizing spacer-filled channel, Desalination. 408 (2017) 25–35. doi:10.1016/j.desal.2017.01.004.

[94] A. Hagedorn, G. Fieg, D. Winter, J. Koschikowski, A. Grabowski, T. Mann, Membrane and spacer evaluation with respect to future module design in

membrane distillation, Desalination. 413 (2017) 154–167. doi:10.1016/j.desal.2017.03.016.

[95] L. Fortunato, Y. Jang, J.-G. Lee, S. Jeong, S. Lee, T. Leiknes, N. Ghaffour, Fouling development in direct contact membrane distillation: Non-invasive monitoring and destructive analysis, Water Res. 132 (2018) 34–41. doi:10.1016/J.WATRES.2017.12.059.

[96] S. West, M. Wagner, C. Engelke, H. Horn, Optical coherence tomography for the in situ three-dimensional visualization and quantification of feed spacer channel fouling in reverse osmosis membrane modules, J. Memb. Sci. 498 (2016) 345–352. doi:10.1016/J.MEMSCI.2015.09.047.

[97] Y. Gao, S. Haavisto, C.Y. Tang, J. Salmela, W. Li, Characterization of fluid dynamics in spacer-filled channels for membrane filtration using Doppler optical coherence tomography, J. Memb. Sci. 448 (2013) 198–208. doi:10.1016/j.memsci.2013.08.011.

[98] H.G. Park, S.G. Cho, K.J. Kim, Y.N. Kwon, Effect of feed spacer thickness on the fouling behavior in reverse osmosis process - A pilot scale study, Desalination. 379 (2016) 155–163. doi:10.1016/j.desal.2015.11.011.

[99] M. Khayet, A. Velázquez, J.I. Mengual, Direct contact membrane distillation of humic acid solutions, J. Memb. Sci. 240 (2004) 123–128. doi:10.1016/j.memsci.2004.04.018.

[100] G. Naidu, S. Jeong, S.J. Kim, I.S. Kim, S. Vigneswaran, Organic fouling behavior in direct contact membrane distillation, Desalination. 347 (2014) 230–239. doi:10.1016/j.desal.2014.05.045.

[101] S. Srisurichan, R. Jiraratananon, A.G. Fane, Humic acid fouling in the membrane distillation process, Desalination. 174 (2005) 63–72. doi:10.1016/j.desal.2004.09.003.

[102] Y. Wu, Y. Kang, L. Zhang, D. Qu, X. Cheng, L. Feng, Performance and fouling mechanism of direct contact membrane distillation (DCMD) treating fermentation wastewater with high organic concentrations, J. Environ. Sci. (China). 65 (2018) 253–261. doi:10.1016/j.jes.2017.01.015.

[103] S.A. Huber, A. Balz, M. Abert, W. Pronk, Characterisation of aquatic humic and

non-humic matter with size-exclusion chromatography - organic carbon detection - organic nitrogen detection (LC-OCD-OND), Water Res. 45 (2011) 879–885. doi:10.1016/j.watres.2010.09.023.

[104] A.R. Da Costa, A.G. Fane, D.E. Wiley, Spacer characterization and pressure drop modelling in spacer-filled channels for ultrafiltration, J. Memb. Sci. 87 (1994) 79–98. doi:10.1016/0376-7388(93)E0076-P.

[105] J. Amigo, R. Urtubia, F. Suárez, Exploring the interactions between hydrodynamics and fouling in membrane distillation systems – A multiscale approach using CFD, Desalination. 444 (2018) 63–74. doi:10.1016/j.desal.2018.07.009.

[106] Y.Z. Tan, Z. Mao, Y. Zhang, W.S. Tan, T.H. Chong, B. Wu, J.W. Chew, Enhancing fouling mitigation of submerged flat-sheet membranes by vibrating 3D-spacers, Sep. Purif. Technol. (2019). doi:10.1016/j.seppur.2018.12.085.

[107] B. Wu, Y. Zhang, Z. Mao, W.S. Tan, Y.Z. Tan, J.W. Chew, T.H. Chong, A.G. Fane, Spacer vibration for fouling control of submerged flat sheet membranes, Sep. Purif. Technol. (2019). doi:10.1016/j.seppur.2018.08.062.

[108] H.S. Abid, D.J. Johnson, R. Hashaikeh, N. Hilal, A review of efforts to reduce membrane fouling by control of feed spacer characteristics, Desalination. 420 (2017) 384–402. doi:10.1016/j.desal.2017.07.019.

[109] S. Jeong, H. Bae, G. Naidu, D. Jeong, S. Lee, S. Vigneswaran, Bacterial community structure in a biofilter used as a pretreatment for seawater desalination, Ecol. Eng. (2013). doi:10.1016/j.ecoleng.2013.09.005.

[110] B.D. Coday, T.Y. Cath, Forward osmosis: Novel desalination of produced water and fracturing flowback, J. Am. Water Works Assoc. 106 (2014) 37–38. doi:10.5942/jawwa.2014.106.0016.

[111] B.D. Coday, P. Xu, E.G. Beaudry, J. Herron, K. Lampi, N.T. Hancock, T.Y. Cath, The sweet spot of forward osmosis: Treatment of produced water, drilling wastewater, and other complex and difficult liquid streams, Desalination. 333 (2014) 23–35. doi:10.1016/j.desal.2013.11.014.

[112] L.A. Hoover, W.A. Phillip, A. Tiraferri, N.Y. Yip, M. Elimelech, Forward with osmosis: Emerging applications for greater sustainability, Environ. Sci. Technol.

45 (2011) 9824–9830. doi:10.1021/es202576h.

[113] E.R. Cornelissen, D. Harmsen, K.F. de Korte, C.J. Ruiken, J.J. Qin, H. Oo, L.P. Wessels, Membrane fouling and process performance of forward osmosis membranes on activated sludge, J. Memb. Sci. 319 (2008) 158–168. doi:10.1016/j.memsci.2008.03.048.

[114] B.D. Coday, J. Regnery, E. Bell, T. Poynor, R. Maltos, S. Fox, T.Y. Cath, Forward Osmosis Desalination in Upstream Oil and Gas: lmpacts of Produced Water Exposure on Membrane Physiochemical Properties and Contaminant Transport, Proc. Water Environ. Fed. 2016 (2016) 962–972. doi:10.2175/193864716819712962.

[115] R. Thiruvenkatachari, S. Su, M. Cunnington, FO-RO for mining wastewater treatment, in: Curr. Trends Futur. Dev. Membr., Elsevier, 2020: pp. 325–336. doi:10.1016/B978-0-12-816777-9.00014-9.

[116] B.G. Choi, M. Zhan, K. Shin, S. Lee, S. Hong, Pilot-scale evaluation of FO-RO osmotic dilution process for treating wastewater from coal-fired power plant integrated with seawater desalination, J. Memb. Sci. 540 (2017) 78–87. doi:10.1016/j.memsci.2017.06.036.

[117] A. Altaee, G. Zaragoza, A conceptual design of low fouling and high recovery FO-MSF desalination plant, Desalination. 343 (2014) 2–7. doi:10.1016/j.desal.2013.09.025.

[118] A. Altaee, A. Mabrouk, K. Bourouni, P. Palenzuela, Forward osmosis pretreatment of seawater to thermal desalination: High temperature FO-MSF/MED hybrid system, Desalination. 339 (2014) 18–25. doi:10.1016/j.desal.2014.02.006.

[119] J. Kim, J. Kim, J. Lim, S. Hong, Evaluation of ethanol as draw solute for forward osmosis (FO) process of highly saline (waste)water, Desalination. 456 (2019) 23–31. doi:10.1016/j.desal.2019.01.012.

[120] M.S. Thabit, A.H. Hawari, M.H. Ammar, S. Zaidi, G. Zaragoza, A. Altaee, Evaluation of forward osmosis as a pretreatment process for multi stage flash seawater desalination, Desalination. 461 (2019) 22–29. doi:10.1016/j.desal.2019.03.015.

[121] M. Li, K. Li, L. Wang, X. Zhang, Feasibility of concentrating textile wastewater

using a hybrid forward osmosis-membrane distillation (FO-MD) process: Performance and economic evaluation, Water Res. 172 (2020) 115488. doi:10.1016/j.watres.2020.115488.

[122] M.R. Massoudinejad, E. Aghayani, K. Arman, F. Gohari, H. Mohamadi, Investigation of saline and brackish waters desalination by carbon aerogel technology, J Appl. Environ. Biol. Sci. 4 (2014) 145–149.

[123] M.T. Ali, H.E.S. Fath, P.R. Armstrong, A comprehensive techno-economical review of indirect solar desalination, Renew. Sustain. Energy Rev. 15 (2011) 4187–4199. doi:10.1016/j.rser.2011.05.012.

[124] H.H. Salih, S.A. Dastgheib, Treatment of a hypersaline brine, extracted from a potential CO 2 sequestration site, and an industrial wastewater by membrane distillation and forward osmosis, Chem. Eng. J. 325 (2017) 415–423. doi:10.1016/j.cej.2017.05.075.

[125] C. Aydiner, U. Sen, S. Topcu, D. Ekinci, A.D. Altinay, D.Y. Koseoglu-Imer, B. Keskinler, Techno-economic viability of innovative membrane systems in water and mass recovery from dairy wastewater, J. Memb. Sci. (2014). doi:10.1016/j.memsci.2014.01.058.

[126] L. Toy, Y.C. Choi, Z. Hendren, G.D. Kim, Advanced, Energy-Efficient Hybrid Membrane System for Industrial Water Reuse, Golden, CO (United States), 2017. doi:10.2172/1375009.

[127] Collahuasi, Collahuasi - Mucho más que Cobre | Sustentabilidad en Collahuasi, (2020). http://www.collahuasi.cl/sustentabilidad/sustentabilidad-en-collahuasi/ (accessed June 14, 2020).

[128] Y.-J. Choi, S. Lee, J. Koo, S.-H. Kim, Evaluation of economic feasibility of reverse osmosis and membrane distillation hybrid system for desalination, Desalin. Water Treat. 57 (2016) 24662–24673. doi:10.1080/19443994.2016.1152648.

[129] S. Tavakkoli, O.R. Lokare, R.D. Vidic, V. Khanna, A techno-economic assessment of membrane distillation for treatment of Marcellus shale produced water, Desalination. 416 (2017) 24–34. doi:10.1016/j.desal.2017.04.014.

[130] Revista Electricidad, Energía: clientes libres pagan 44% más que las mineras,

(2019). https://www.revistaei.cl/2019/10/10/energia-clientes-libres-pagan-44-mas-que-las-mineras/ (accessed May 7, 2020).

[131] SISS, Aguas Antofagasta, 2020. http://www.siss.gob.cl/appsiss/historico/articles-4497_Aguas_Antofagasta_G1_dic_2017.pdf (accessed May 7, 2020).

[132] S.J. Im, S. Jeong, S. Jeong, A. Jang, Techno-economic evaluation of an element-scale forward osmosis-reverse osmosis hybrid process for seawater desalination, Desalination. 476 (2020) 114240. doi:10.1016/j.desal.2019.114240.

[133] M.S. Peters, K.D. Timmerhaus, R.E. West, Equipment Costs for Plant Design and Economics for Chemical Engineers - 5th Edition, (2020). http://www.mhhe.com/engcs/chemical/peters/data/ (accessed June 11, 2020).

[134] R. Schwantes, K. Chavan, D. Winter, C. Felsmann, J. Pfafferott, Techno-economic comparison of membrane distillation and MVC in a zero liquid discharge application, Desalination. 428 (2018) 50–68. doi:10.1016/j.desal.2017.11.026.

[135] N.H. Ab Hamid, S. Smart, D.K. Wang, K.W.J. Koh, K.J.C. Ng, L. Ye, Economic, energy and carbon footprint assessment of integrated forward osmosis membrane bioreactor (FOMBR) process in urban wastewater treatment, Environ. Sci. Water Res. Technol. 6 (2020) 153–165. doi:10.1039/c9ew00608g.

[136] S.R. Osipi, A.R. Secchi, C.P. Borges, Cost assessment and retro-techno-economic analysis of desalination technologies in onshore produced water treatment, Desalination. 430 (2018) 107–119. doi:10.1016/j.desal.2017.12.015.

[137] Z. Li, R.V. Linares, S. Sarp, G. Amy, Direct and indirect seawater desalination by forward osmosis, in: Membr. Salin. Gradient Process. Water Treat. Power Gener., Elsevier, 2018: pp. 245–272. doi:10.1016/B978-0-444-63961-5.00009-2.

[138] S. Vinardell, S. Astals, J. Mata-Alvarez, J. Dosta, Techno-economic analysis of combining forward osmosis-reverse osmosis and anaerobic membrane bioreactor technologies for municipal wastewater treatment and water production, Bioresour. Technol. 297 (2020) 122395. doi:10.1016/j.biortech.2019.122395.

[139] A. Altaee, A. Sharif, G. Zaragoza, A.F. Ismail, Evaluation of FO-RO and PRO-RO designs for power generation and seawater desalination using impaired water feeds, Desalination. 368 (2014) 27–35. doi:10.1016/j.desal.2014.06.022.

[140] T.N. Bitaw, K. Park, D.R. Yang, Optimization on a new hybrid Forward osmosis-

Electrodialysis-Reverse osmosis seawater desalination process, Desalination. 398 (2016) 265–281. doi:10.1016/j.desal.2016.07.032.

[141] S.R. Osipi, A.R. Secchi, C.P. Borges, Cost analysis of forward osmosis and reverse osmosis in a case study, in: Curr. Trends Futur. Dev. Membr., Elsevier, 2020: pp. 305–324. doi:10.1016/b978-0-12-816777-9.00013-7.

[142] L. Chekli, J.E. Kim, I. El Saliby, Y. Kim, S. Phuntsho, S. Li, N. Ghaffour, T.O. Leiknes, H. Kyong Shon, Fertilizer drawn forward osmosis process for sustainable water reuse to grow hydroponic lettuce using commercial nutrient solution, Sep. Purif. Technol. 181 (2017) 18–28. doi:10.1016/j.seppur.2017.03.008.

[143] I. Hitsov, K. De Sitter, C. Dotremont, I. Nopens, Economic modelling and model-based process optimization of membrane distillation, Desalination. 436 (2018) 125–143. doi:10.1016/j.desal.2018.01.038.

[144] J. Swaminathan, K.G. Nayar, J.H. Lienhard V, Mechanical vapor compression—Membrane distillation hybrids for reduced specific energy consumption, Desalin. Water Treat. 57 (2016) 26507–26517. doi:10.1080/19443994.2016.1168579.

[145] V. Karanikola, S.E. Moore, A. Deshmukh, R.G. Arnold, M. Elimelech, A.E. Sáez, Economic performance of membrane distillation configurations in optimal solar thermal desalination systems, Desalination. 472 (2019) 114164. doi:10.1016/j.desal.2019.114164.

[146] R. Creusen, J. van Medevoort, M. Roelands, A. van Renesse van Duivenbode, J.H. Hanemaaijer, R. van Leerdam, Integrated membrane distillation-crystallization: Process design and cost estimations for seawater treatment and fluxes of single salt solutions, Desalination. 323 (2013) 8–16. doi:10.1016/j.desal.2013.02.013.

[147] M.I. Ali, E.K. Summers, H.A. Arafat, J.H. Lienhard V, Effects of membrane properties on water production cost in small scale membrane distillation systems, Desalination. 306 (2012) 60–71. doi:10.1016/j.desal.2012.07.043.

[148] C.A. Quist-Jensen, M.K. Jørgensen, M.L. Christensen, Treated seawater as a magnesium source for phosphorous recovery from wastewater—A feasibility and cost analysis, Membranes (Basel). 6 (2016). doi:10.3390/membranes6040054.

[149] S. Al-Obaidani, E. Curcio, F. Macedonio, G. Di Profio, H. Al-Hinai, E. Drioli, Potential of membrane distillation in seawater desalination: Thermal efficiency,

sensitivity study and cost estimation, J. Memb. Sci. 323 (2008) 85–98. doi:10.1016/j.memsci.2008.06.006.

[150] M. Baghbanzadeh, D. Rana, C.Q. Lan, T. Matsuura, Zero thermal input membrane distillation, a zero-waste and sustainable solution for freshwater shortage, Appl. Energy. 187 (2017) 910–928. doi:10.1016/j.apenergy.2016.10.142.

[151] Hydranautics, IMS Design, (2020). https://membranes.com/solutions/software/.

[152] CSM, CSMPRO, (2020). www.csmfilter.com.

[153] LG, Q+ Projection Software, (2018). http://www.lgwatersolutions.com/en/tools/software.

[154] Toray, Toray DS2, (2019). https://ap3.toray.co.jp/toraywater/.

[155] SUEZ, Winflows, (2019). https://www.suezwatertechnologies.com/resources/winflows.

[156] A. Achilli, T.Y. Cath, A.E. Childress, Selection of inorganic-based draw solutions for forward osmosis applications, J. Memb. Sci. 364 (2010) 233–241. doi:10.1016/j.memsci.2010.08.010.

[157] D. Qu, J. Wang, D. Hou, Z. Luan, B. Fan, C. Zhao, Experimental study of arsenic removal by direct contact membrane distillation, J. Hazard. Mater. 163 (2009) 874–879. doi:10.1016/j.jhazmat.2008.07.042.

[158] J.A. Bush, J. Vanneste, T.Y. Cath, Membrane distillation for concentration of hypersaline brines from the Great Salt Lake: Effects of scaling and fouling on performance, efficiency, and salt rejection, Sep. Purif. Technol. 170 (2016) 78–91. doi:10.1016/j.seppur.2016.06.028.

[159] D. Woldemariam, A. Kullab, U. Fortkamp, J. Magner, H. Royen, A. Martin, Membrane distillation pilot plant trials with pharmaceutical residues and energy demand analysis, Chem. Eng. J. 306 (2016) 471–483. doi:10.1016/j.cej.2016.07.082.

[160] Raghunathan G, THERMIC FLUID VS. STEAM SYSTEMS – Thermic-Fluid.com, (2018). http://thermic-fluid.com/2018/01/03/thermic-fluid-vs-steam-systems/ (accessed June 14, 2020).

[161] Tulsa Heaters Midstream, Hot Oil vs Steam - 3 Reasons Why Hot Oil Wins, (2020). http://blog.tulsaheatersmidstream.com/hot-oil-vs-steam-3-reasons-why-

hot-oil-wins (accessed June 14, 2020).

[162] Process Engineering Magazine, Plant Equipment: how efficient are thermal fluid systems? | Process Engineering, (2017). http://processengineering.co.uk/article/2022931/plant-equipment-how-efficient-are-thermal-fluid-systems (accessed June 14, 2020).

[163] Paratherm, Thermal Fluid vs. Steam - Comparison | Paratherm Heat Transfer Fluids, (2016). https://www.paratherm.com/thermal-fluid-vs-steam/ (accessed June 14, 2020).

[164] IAEA, Desalination Economic Evaluation Program (DEEP), (2014). https://www.iaea.org/topics/non-electric-applications/nuclear-desalination.

[165] T.H. Chong, W.B. Krantz, Process economics and operating strategy for the energy-efficient reverse osmosis (EERO) process, Desalination. 443 (2018) 70–84. doi:10.1016/j.desal.2018.05.007.

[166] R.V. Linares, Z. Li, V. Yangali-Quintanilla, N. Ghaffour, G. Amy, T. Leiknes, J.S. Vrouwenvelder, Life cycle cost of a hybrid forward osmosis–low pressure reverse osmosis system for seawater desalination and wastewater recovery, Water Res. 88 (2016) 225–234.

[167] J.G. Skousen, P.F. Ziemkiewicz, L.M. McDonald, Acid mine drainage formation, control and treatment: Approaches and strategies, Extr. Ind. Soc. 6 (2019) 241–249. doi:10.1016/j.exis.2018.09.008.

[168] Y.C. Sharma, P. Aggarwal, T.N. Singh, Economic liabilities of environmental pollution by coal mining: Indian scenario, Environ. Dev. Sustain. 11 (2009) 589–599. doi:10.1007/s10668-007-9131-2.

[169] VOSE Software, Risk Analysis Software for Excel, (2020). https://www.vosesoftware.com/products/modelrisk/ (accessed June 15, 2020).

[170] D.L. Shaffer, N.Y. Yip, J. Gilron, M. Elimelech, Seawater desalination for agriculture by integrated forward and reverse osmosis: Improved product water quality for potentially less energy, J. Memb. Sci. 415–416 (2012) 1–8. doi:10.1016/j.memsci.2012.05.016.

[171] Fluence Corporation, What Is Zero Liquid Discharge (ZLD)?, (2020). https://www.fluencecorp.com/what-is-zero-liquid-discharge/ (accessed August 15,

2020).

[172] V. Vitagliano, P.A. Lyons, Diffusion Coefficients for Aqueous Solutions of Sodium Chloride and Barium Chloride, J. Am. Chem. Soc. 78 (1956) 1549–1552. doi:10.1021/ja01589a011.

[173] J. Korenak, C. Hélix-Nielsen, H. Bukšek, I. Petrinić, Efficiency and economic feasibility of forward osmosis in textile wastewater treatment, J. Clean. Prod. 210 (2019) 1483–1495. doi:10.1016/j.jclepro.2018.11.130.

[174] L. Toy, Y.C. Choi, Z. Hendren, G.D. Kim, Advanced, Energy-Efficient Hybrid Membrane System for Industrial Water Reuse, RTI International, Research Triangle Park, NC (United States), 2017.

[175] C. Aydiner, U. Sen, D.Y. Koseoglu-Imer, E. Can Dogan, Hierarchical prioritization of innovative treatment systems for sustainable dairy wastewater management, J. Clean. Prod. 112 (2016) 4605–4617. doi:10.1016/j.jclepro.2015.08.107.

[176] D. Topaloglu, Y.M. Tilki, S. Aksu, T.N. Yilmaz, E.E. Celebi, S. Oncel, C. Aydiner, Novel technological solutions for eco-protective water supply by economical and sustainable seawater desalination, Chem. Eng. Res. Des. 136 (2018) 177–198. doi:10.1016/j.cherd.2018.04.022.

[177] C. Aydiner, U. Sen, S. Topcu, D. Sesli, D. Ekinci, A.D. Altinay, B. Ozbey, D.Y. Koseoglu-Imer, B. Keskinler, Techno-economic investigation of water recovery and whey powder production from whey using UF/RO and FO/RO integrated membrane systems, Desalin. Water Treat. 52 (2014) 123–133. doi:10.1080/19443994.2013.786655.

[178] G. Blandin, A.R.D. Verliefde, C.Y. Tang, P. Le-Clech, Opportunities to reach economic sustainability in forward osmosis-reverse osmosis hybrids for seawater desalination, Desalination. 363 (2015) 26–36. doi:10.1016/j.desal.2014.12.011.

[179] Z. Triki, M.N. Bouaziz, M. Boumaza, Performance and cost evaluation of an autonomous solar vacuum membrane distillation desalination plant, Desalin. Water Treat. 73 (2017) 107–120. doi:10.5004/dwt.2017.20596.

[180] H. Hayer, O. Bakhtiari, T. Mohammadi, Simulation of momentum, heat and mass transfer in direct contact membrane distillation: A computational fluid dynamics

approach, J. Ind. Eng. Chem. 21 (2015) 1379–1382. doi:10.1016/j.jiec.2014.06.009.

[181] H.C. Duong, P. Cooper, B. Nelemans, T.Y. Cath, L.D. Nghiem, Optimising thermal efficiency of direct contact membrane distillation by brine recycling for small-scale seawater desalination, Desalination. 374 (2015) 1–9. doi:10.1016/j.desal.2015.07.009.

[182] E.U. Khan, P. Hansson, H. Jönsson, Å. Nordberg, Small-scale polygeneration integrated with membrane distillation for Swedish community, (2017).

[183] N. Dow, J. Villalobos García, L. Niadoo, N. Milne, J. Zhang, S. Gray, M. Duke, Demonstration of membrane distillation on textile waste water assessment of long term performance, membrane cleaning and waste heat integration, Environ. Sci. Water Res. Technol. 3 (2017) 433–449. doi:10.1039/c6ew00290k.